SOME PROBLEMS IN OCEANIC RADIATIVE TRANSFER

Submitted by

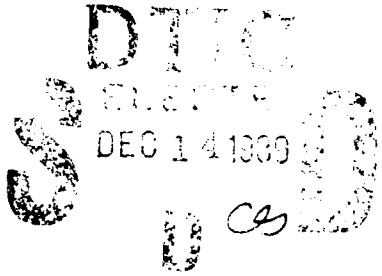

Howard R. Gordon

Principal Investigator

FINAL REPORT

for

OFFICE OF NAVAL RESEARCH

Contract No. **N00014-84-K-0451**

University of Miami
Department of Physics
Coral Gables, FL 33124

May 1989

Foreward

This report describes work performed under ONR Contract N00014-84-K-0451. The author wishes to thank Dr. Eric O. Hartwig and Dr. Richard W. Spinrad of ONR for their encouragement during the coarse of the investigation, and ONR for financial support.

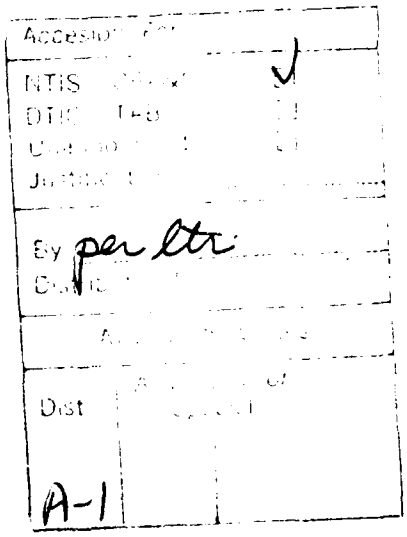

Introduction

The research described in this report constitutes a part of the long-term scientific goal of the Principal Investigator, i.e., to better understand the distribution of phytoplankton in the world's oceans through their influence on the optical properties of the water. Optically, phytoplankton reveal their presence through the absorption of light by their photosynthetic (chlorophyll a) and accessory pigments. However, this absorption is seldom directly observed outside a laboratory setting. Instead, it is usually indirectly inferred by virtue of its effect on the apparent optical properties: the diffuse reflectance of the water, e.g., the color of the water, or the downwelling irradiance attenuation coefficient. Thus, an understanding of the relationship between the inherent and apparent optical properties is fundamental to the interpretation of field observations. Although ultimately our understanding of such relationships must be based on field experiments, the approach taken here — the construction of mathematical models which simulate as closely as possible the physical processes — can make a very valuable contribution because the various parameters, many of which may be either difficult to measure or highly variable in space and time, are known and carefully controlled in the models.

There were two specific interrelated goals for the present research: (1) to understand the influence of the optical properties of the ocean as determined by the concentration of constituents in Case 1 waters, e.g., phytoplankton, detrital particles, dissolved organic material, etc., on the transport of light from a point source in the ocean to the sea surface, for possible application to the remote (surface) detection of bioluminescence; and (2) to understand the dependence of the classical apparent optical properties (the irradiance attenuation coefficient and the diffuse reflectance) on the inherent optical properties (absorption and scattering coefficient and the volume scattering function). The interrelationship between these goals is threefold: first, the propagation of the radiant energy in both cases is governed by the radiative transfer equation; next, the same inherent optical properties (and their dependence on the constituent concentrations) are required in

both problems; and finally, a useful approximate solution to (1) requires results from the solution to (2).

Summary of Research Performed

The main problem of concern in this research was the transport of radiant energy from a point source in the ocean, e.g., a flash of light emitted by a bioluminescent organism, to the surface. The goal was to determine a way of predicting the horizontal distribution of irradiance on the surface from the spatial distribution and power of extended sources in the ocean and from the optical properties of the medium. To this end it was necessary to model the inherent optical properties of the water in terms of easily measured quantities such as the phytoplankton pigment concentration, [a] as well as to solve the radiative transfer equation in the given geometry.

Briefly (Gordon 1987), a model of the optical properties of the ocean was developed providing the absorption and scattering coefficients of the medium as nonlinear functions of the concentration of pigments associated with phytoplankton and their immediate detrital material. Monte Carlo computations of the attenuation coefficient of downwelling irradiance, K_d, for an ocean-atmosphere system illuminated by the sun at zenith, were found to agree well with experimental data, and thus demonstrated the validity of the bio-optical model for studying the influence of phytoplankton biomass on the propagation to the surface of light generated through bioluminescence. The radiative transfer equation for the irradiance at the sea surface resulting from illumination by a point source imbedded in a *homogeneous* ocean was then solved by Monte Carlo techniques. The solution technique

[a] By the term pigment concentration (C) we mean the concentration (mg/m^3) of chlorophyll a and all chlorophyll-like pigments, which absorb in the same spectral bands as chlorophyll a, such as phaeophytin a, and which are contained in phytoplankton or in their detrital materials. The sum of the concentrations of chlorophyll a and phaeophytin a is frequently used as an indicator of plankton biomass.

was validated through comparison with an asymptotic analytic solution for isotropic scattering. The computations reveal that the irradiance distribution just beneath the surface as a function of R, the distance measured along the surface from a point vertically above the source, is described by two regimes: (1) a regime in which the irradiance is governed mostly by absorption and by geometry, with scattering playing a negligible role — the *near* field; and (2) a regime in which the light field at the surface is very diffuse and the irradiance decays approximately exponentially with R and is a very weak function of the source depth — the *diffusion* regime. The near field is of primary interest because it contains most of the power reaching the sea surface. An analytical model of the irradiance distribution just beneath the surface as a function of R, the source depth, and the pigment concentration for the near field was developed. This model is based on the observation that at most scattering events the change in the photon's direction is slight and, therefore, scattering is rather ineffective in attenuating the irradiance. The analytic solution for the irradiance from the point source was first carried out ignoring scattering altogether; however, recognizing that backscattering *will* attenuate the irradiance, the absorption coefficient was replaced by an effective attenuation coefficient, k. This effective attenuation coefficient was then determined by fitting the total power just beneath the surface determined from the Monte Carlo computations to the analytical model. The resulting k was found to be closely related to K_d, and the Monte Carlo irradiance as a function of R and source depth in the near field regime could be approximated with high accuracy using the analytical model. These results also indicated that K_d can be estimated at night by releasing a point source in the water, measuring the irradiance at the surface as it sinks, and fitting the measurements to the relationships developed during the course of the research to determine k. Finally, the analytic model can also be inverted, enabling the remote estimation of the source depth and power from the irradiance distribution just beneath the surface. Gordon (1987), provided the details of these results, is reproduced as Appendix 1.

The solution to the point source problem above was incomplete to the extent that the medium was taken to be homogeneous, i.e., the optical properties were *independent of depth.* To remedy this, we posed the following question: is it possible to estimate the

point source-generated irradiance in a *stratified* ocean given the vertical distribution of the pigment concentration ($C(z)$) and the source depth? It was found (Gordon 1988) that the vertical stratification was *unimportant* in determining the horizontal distribution of irradiance on the surface — the results of the homogeneous ocean model could be extended to the stratified ocean if a constant effective pigment concentration $\langle C \rangle$, defined to be the value of C for a homogeneous ocean that would yield the same source *optical depth* as the stratified ocean, was used in place of the pigment concentration in the homogeneous ocean model. The details of this this observation are presented in Appendix 2.

The point source problem described above required the downwelling irradiance attenuation coefficient just beneath the surface (K_d) expressed as a function of the inherent optical properties. To determine this, and to extend our understanding of the relationship between the inherent and apparent optical properties to include the details of the scattering phase function (volume scattering function normalized to the total scattering coefficient) as well as environmental factors such as the solar zenith angle, the presence of a scattering atmosphere, and sea surface roughness, approximately 450 simulations of radiative transfer in the ocean-atmosphere system were carried out. Such simulations provide the distribution of radiation in the entire system. The radiation field is treated as experimental data, albeit data collected under carefully controlled conditions: a cloud free sky and a homogeneous ocean of precisely known inherent optical properties. The irradiances, K_d, etc., can be derived from this radiation field as a function of the inherent optical properties of the ocean and ultimately as a function of the constituent concentrations. Although the results of the Monte Carlo simulations are still under analysis, two completed works have been submitted to *Limnology and Oceanography* for publication.

In the first (Gordon 1989a) it was shown that the that the downwelling irradiance attenuation coefficient just beneath the surface (K) and the mean irradiance attenuation coefficient from the surface to the depth where the irradiance falls to 10% of its value at the surface ($\langle K \rangle$) can be corrected for the geometric structure of the in-water light field to yield quantities that are, to a high degree of accuracy, inherent optical properties. This

geometric correction is effected simply by dividing the experimental irradiance attenuation coefficient by D_0, the downwelling distribution function for a *totally absorbing ocean* with the same surface illumination, i.e., $D_0 = E_{0d}(0)/E_d(0)$, where $E_d(0)$ is the downwelling irradiance and $E_{0d}(0)$ is the downwelling *scalar* irradiance just beneath the surface. An accurate scheme for estimating D_0 from simple irradiance and wind speed measurements was suggested. The geometry-corrected quantities were then shown to satisfy the Lambert-Beer law, i.e., that K_d can be linearly resolved into constituent components, to a reasonable degree of accuracy, with the largest error ($\approx 15\%$) in the case of $\langle K \rangle$ arising from mixing nonabsorbing particles, e.g., white sand, with strongly absorbing water (wavelengths $>$ 600 nm). This near-validity of the Lambert-Beer law, when there are compelling reasons to believe that it should fail, is shown to result from three *independent* facts: (1) the dependence of the diffuse attenuation coefficients on the geometric structure of the light field can be removed; (2) pure sea water is a much better absorber than scatterer at optical frequencies; and (3) the phase functions for particles suspended in the ocean differs significantly from that of pure sea water. Finally, it is shown that extrapolation of the corrected diffuse attenuation coefficients to the limit $c \rightarrow c_w$, where c is the total beam attenuation coefficient and c_w is the beam attenuation coefficient of pure sea water, yields quantities that are within 2% of the corresponding quantities that would be measured for an ocean consisting of pure sea water with the sun at the zenith and the atmosphere removed. The details of the analysis of K_d are presented in Appendix 3.

In the second (Gordon 1989b, and Appendix 4), the variation of the diffuse reflectance of natural waters with sun angle was studied is found to be dependent on the shape of the volume scattering function (VSF) of the medium. It was also found that single scattering theory can be used to estimate the reflectance – sun angle variation given the VSF, and conversely, the VSF can be retrieved from measurements of the variation of the reflectance with sun angle. The complex variation of reflectance with the incident illumination and surface roughness was found to be reducible to the variation of a single parameter: $R(D_0) = kD_0R(1)$, where k is a constant, and $R(1)$ is the reflectance the ocean would have with the atmosphere removed and the sun at the zenith, i.e., the variation of

R with the incident illumination and the surface roughness can be completely explained through their effect on D_0, which was defined in the preceeding paragraph. The parameter k depends mostly on the scattering phase function, and for $\omega_0 \lesssim 0.9$, where ω_0 is the ratio of the scattering coefficient to the beam attenuation coefficient of the medium, it can be computed using the single scattering approximation. These observations are applicable to all but the most reflective of natural waters.

In addition, two other papers were published (Gordon and Castaño 1988, Gordon and Castaño 1989) which, although they had no bearing on the specific problems under consideration here, were completed while Diego Castaño was supported as a Graduate Assistant on the Contract and thus acknowledgement of ONR support for these papers is appropriate. The first paper shows that the atmospheric correction algorithm for the Coastal Zone Color Scanner (CZCS) should be largely unaffected by the eruption of the volcano El Chichón in late March – early April 1982, while the second provides a novel method for examining oceanic aerosols using CZCS imagery. For completeness, these are reproduced in Appendices 5 and 6 respectively.

References

Gordon, H. R. 1987. A Bio-Optical Model Describing the Distribution of Irradiance at the Sea Surface Resulting from a Point Source Imbedded in the Ocean. Applied Optics 26: 4133–4148.

——— 1988. Influence of Vertical Stratification on the Distribution of Irradiance at the Sea Surface from a Point Source in the Ocean. Applied Optics 27: 2643–2645.

——— 1989a. Can the Lambert-Beer Law Be Applied To the Diffuse Attenuation Coefficient of Ocean Water?. Limnology and Oceanography (Submitted).

——— 1989b. Dependence of the Diffuse Reflectance of Natural Waters on the Sun Angle. Limnology and Oceanography (Submitted).

Gordon, H. R. and D. J. Castaño 1988. The Coastal Zone Color Scanner Atmospheric Correction Algorithm: Influence of El Chichón. Applied Optics 27: 3319–3321.

——— 1989. Aerosol Anslysis with the Coastal Zone Color Scanner: A Simple Method for Including Multiple Scattering Effects. Applied Optics 28: 1320–1326.

Publications and Papers

Supported wholly or in part by

ONR Contract no. **N00014-84-K-0451**

Refereed Publications

H.R. Gordon, A Bio-Optical Model Describing the Distribution of Irradiance at the Sea Surface Resulting from a Point Source Embedded in the Ocean, *Applied Optics*, **26**, 4133–4148 (1987).

H.R. Gordon, Influence of Vertical Stratification on the Distribution of Irradiance at the Sea Surface from a Point Source in the Ocean, *Applied Optics*, **27**, 2643–2645 (1988).

H.R. Gordon and D.J. Castaño, The Coastal Zone Color Scanner Atmospheric Correction Algorithm: Influence of El Chichón, *Applied Optics*, **27**, 3319–3321 (1988).

H.R. Gordon and D.J. Castaño, Aerosol Analysis with the Coastal Zone Color Scanner: A Simple Method for Including Multiple Scattering Effects, *Applied Optics* **28** 1320–1326 (1989).

H.R. Gordon, Can the Lambert-Beer Law Be Applied to the Diffuse Attenuation Coefficient of Ocean Water?, *Limnology and Oceanography* (Submitted).

H.R. Gordon, Dependence of the Diffuse Reflectance of Natural Waters on the Sun Angle, *Limnology and Oceanography* (Submitted).

Other Papers and Publications

H.R. Gordon, Distribution of Irradiance on the Sea Surface Resulting from a Point Source Imbedded in the Ocean, *Ocean Optics VIII*, Proceedings of SPIE, **637**, 66–71, 1986.

H.R. Gordon, Radiant Energy in the Upper Layers of the Ocean, American Geophysical Union / American Society of Limnology and Oceanography Ocean Sciences Meeting, New Orleans, LA, 13–17 Jan. 1986.

H.R. Gordon, Ocean Color Remote Sensing: Influence of the Particle Scattering Phase Function and the Solar Zenith Angle. American Geophysical Union / American Society of Limnology and Oceanography Ocean Sciences Meeting, San Francisco, CA, Dec. 8–12, 1986.

H.R. Gordon, Ocean Color Algorithms, Contributed Paper at American Geophysical Union / American Society of Limnology and Oceanography, Ocean Sciences Meeting, New Orleans, Jan 18–22, 1988.

SOME PROBLEMS IN OCEANIC RADIATIVE TRANSFER

Submitted by

Howard R. Gordon

Principal Investigator

FINAL REPORT

for

OFFICE OF NAVAL RESEARCH

Contract No. N00014-84-K-0451

University of Miami
Department of Physics
Coral Gables, FL 33124

May 1989

Foreward

This report describes work performed under ONR Contract N00014-84-K-0451. The author wishes to thank Dr. Eric O. Hartwig and Dr. Richard W. Spinrad of ONR for their encouragement during the coarse of the investigation, and ONR for financial support.

Introduction

The research described in this report constitutes a part of the long-term scientific goal of the Principal Investigator, i.e., to better understand the distribution of phytoplankton in the world's oceans through their influence on the optical properties of the water. Optically, phytoplankton reveal their presence through the absorption of light by their photosynthetic (chlorophyll a) and accessory pigments. However, this absorption is seldom directly observed outside a laboratory setting. Instead, it is usually indirectly inferred by virtue of its effect on the apparent optical properties: the diffuse reflectance of the water, e.g., the color of the water, or the downwelling irradiance attenuation coefficient. Thus, an understanding of the relationship between the inherent and apparent optical properties is fundamental to the interpretation of field observations. Although ultimately our understanding of such relationships must be based on field experiments, the approach taken here — the construction of mathematical models which simulate as closely as possible the physical processes — can make a very valuable contribution because the various parameters, many of which may be either difficult to measure or highly variable in space and time, are known and carefully controlled in the models.

There were two specific interrelated goals for the present research: (1) to understand the influence of the optical properties of the ocean as determined by the concentration of constituents in Case 1 waters, e.g., phytoplankton, detrital particles, dissolved organic material, etc., on the transport of light from a point source in the ocean to the sea surface, for possible application to the remote (surface) detection of bioluminescence; and (2) to understand the dependence of the classical apparent optical properties (the irradiance attenuation coefficient and the diffuse reflectance) on the inherent optical properties (absorption and scattering coefficient and the volume scattering function). The interrelationship between these goals is threefold: first, the propagation of the radiant energy in both cases is governed by the radiative transfer equation; next, the same inherent optical properties (and their dependence on the constituent concentrations) are required in

both problems; and finally, a useful approximate solution to (1) requires results from the solution to (2).

Summary of Research Performed

The main problem of concern in this research was the transport of radiant energy from a point source in the ocean, e.g., a flash of light emitted by a bioluminescent organism, to the surface. The goal was to determine a way of predicting the horizontal distribution of irradiance on the surface from the spatial distribution and power of extended sources in the ocean and from the optical properties of the medium. To this end it was necessary to model the inherent optical properties of the water in terms of easily measured quantities such as the phytoplankton pigment concentration, [a] as well as to solve the radiative transfer equation in the given geometry.

Briefly (Gordon 1987), a model of the optical properties of the ocean was developed providing the absorption and scattering coefficients of the medium as nonlinear functions of the concentration of pigments associated with phytoplankton and their immediate detrital material. Monte Carlo computations of the attenuation coefficient of downwelling irradiance, K_d, for an ocean-atmosphere system illuminated by the sun at zenith, were found to agree well with experimental data, and thus demonstrated the validity of the bio-optical model for studying the influence of phytoplankton biomass on the propagation to the surface of light generated through bioluminescence. The radiative transfer equation for the irradiance at the sea surface resulting from illumination by a point source imbedded in a *homogeneous* ocean was then solved by Monte Carlo techniques. The solution technique

[a] By the term pigment concentration (C) we mean the concentration (mg/m^3) of chlorophyll a and all chlorophyll-like pigments, which absorb in the same spectral bands as chlorophyll a, such as phaeophytin a, and which are contained in phytoplankton or in their detrital materials. The sum of the concentrations of chlorophyll a and phaeophytin a is frequently used as an indicator of plankton biomass.

Appendix 1

H.R. Gordon, A Bio-Optical Model Describing the Distribution of Irradiance at the Sea Surface Resulting from a Point Source Embedded in the Ocean, *Applied Optics*, **26**, 4133–4148 (1987).

Bio-optical model describing the distribution of irradiance at the sea surface resulting from a point source embedded in the ocean

Howard R. Gordon

A model of the optical properties of the ocean, providing the absorption and scattering coefficients of the medium as nonlinear functions of the concentration of pigments associated with phytoplankton and their immediate detrital material, is presented. Monte Carlo computations of the attenuation coefficient of downwelling irradiance K_d for an ocean–atmosphere system illuminated by the sun at zenith, agree well with experimental data and demonstrate the validity of such a model for studying the influence of phytoplankton biomass on the propagation to the surface of light generated through bioluminescence. The radiative transfer equation for the irradiance at the sea surface resulting from illumination by a point source embedded in the water is solved by Monte Carlo techniques. The solution technique is validated through comparison with an asymptotic analytic solution for isotropic scattering. The computations show that the irradiance distribution just beneath the surface as a function of R, the distance measured along the surface from a point vertically above the source, is described by two regimes: (1) a regime in which the irradiance is governed mostly by absorption and geometry with scattering playing a negligible role—the near field; (2) a regime in which the light field at the surface is very diffuse and the irradiance decays approximately exponentially in R and is a very weak function of the source depth—the diffusion regime. The near field is of primary interest because it contains most of the power reaching the sea surface. An analytical model of the irradiance distribution just beneath the surface as a function of R, the source depth, and the pigment concentration for the near field is presented. This model is based on the observation that at most scattering events the change in the photon's direction is slight, and therefore, scattering is rather ineffective in attenuating the irradiance. An analytic solution for the irradiance from the point source, then, is first carried out ignoring scattering altogether; however, recognizing that backscattering will attenuate the irradiance, the absorption coefficient is replaced by an effective attenuation coefficient k. This effective attenuation coefficient is determined by fitting the total power just beneath the surface determined from the Monte Carlo computations to the analytical model. The resulting k is closely related to K_d, and the Monte Carlo irradiance as a function of R and source depth in the near-field regime can be approximated with high accuracy using the model. These results indicate K_d can be estimated at night by releasing a point source in the water, measuring the irradiance at the surface as it sinks, and fitting the measurements to the relationships developed here to determine k. The analytic model also enables estimation of the source depth and power from the irradiance distribution just beneath the surface.

I. Introduction

In an effort to examine the extent to which marine bioluminescent emissions can be studied from ships and/or aircraft it is necessary to understand the surface manifestation of the bioluminescent signal in terms of the optical properties of the water and the strength of the emission. Thus the problem examined here consists of determining the distribution of irradiance at the sea surface due to an isotropically emitting point source embedded in the ocean and the dependence of this irradiance on the optical properties of the water, i.e., given a distribution of isotropically emitting point sources embedded in the ocean, the variation of the associated light field at the sea surface with the optical properties of the water is determined. Since the duration of bioluminescent flashes tends to be long compared to the mean lifetime of a photon in the water (absorption mean free path/speed of light) of at most $\sim 1\ \mu s$, the light field can be described by steady-state radiative transfer theory. The steady-state radiative transfer equation (RTE), which describes the transport of the radiance $[L(\mathbf{r},\hat{\xi})]$ at $\mathbf{r}$ in a direction specified by the unit vector $\hat{\xi}$, is given by

The author is with University of Miami, Physics Department, Coral Gables, Florida 33124.

Received 26 January 1987.
0003-6935/87/194133-16$02.00/0.

$$(\hat{\xi}\cdot\nabla)L(\mathbf{r},\hat{\xi}) + c(\mathbf{r})L(\mathbf{r},\hat{\xi}) = \int_{4\pi}\beta(\mathbf{r},\hat{\xi}'\to\hat{\xi})L(\mathbf{r},\hat{\xi}')d\Omega(\hat{\xi}') + Q(\mathbf{r},\hat{\xi}), \quad (1)$$

where $\beta(\mathbf{r},\hat{\xi}'\to\hat{\xi})$ is the volume scattering function at $\mathbf{r}$ for scattering from the direction $\hat{\xi}'$ into the direction $\hat{\xi}$, $c(\mathbf{r})$ is the beam attenuation coefficient at $\mathbf{r}$, and $Q(\mathbf{r},\hat{\xi})$ is the intensity (power per unit solid angle) per unit volume of sources at $\mathbf{r}$ in the direction $\hat{\xi}$. $c(\mathbf{r})$ can be related to the absorption coefficient $a(\mathbf{r})$ and the scattering coefficient $b(\mathbf{r})$ by

$$c(\mathbf{r}) = a(\mathbf{r}) + b(\mathbf{r}), \quad (2)$$

where

$$b(\mathbf{r}) = \int_{4\pi}\beta(\mathbf{r},\hat{\xi}'\to\hat{\xi})d\Omega(\hat{\xi}'). \quad (3)$$

It can be shown[1] that for a closed volume V with $\omega_0(\mathbf{r}) \equiv b(\mathbf{r})/c(\mathbf{r}) < 1$, surrounded by a surface S, the RTE possesses unique solutions given the sources $Q(\mathbf{r},\hat{\xi})$ within V and the radiance into V from the outside, i.e., $[L(\mathbf{r}_s,\hat{\xi})]$ for $\hat{\xi}\cdot\hat{n} < 1$ (defined to be $[L^{(\mathrm{inc})}(\mathbf{r}_s,\hat{\xi})]$), where $\mathbf{r}_s$ is on the bounding surface S, and $\hat{n}$ is the outward unit normal to S. In the problem of interest here, the energy source is isotropically emitting radiation of unit intensity at a point $\mathbf{r}_0$ in the water, and there is no energy incident from the sea surface, i.e.,

$$Q(\mathbf{r},\hat{\xi}) = \delta(\mathbf{r}-\mathbf{r}_0),$$

$$L^{(\mathrm{inc})}(\mathbf{r}_s,\hat{\xi}) = 0.$$

Thus the quantities $a(\mathbf{r})$ and $\beta(\mathbf{r},\hat{\xi}'\to\hat{\xi})$ are all that are required to predict the transport of the radiant energy to the sea surface. Traditionally, the volume scattering function $\beta(\mathbf{r},\hat{\xi}'\to\hat{\xi})$ is normalized to the local scattering coefficient, replacing it by the scattering phase function $P(\mathbf{r},\hat{\xi}'\to\hat{\xi})$, defined according to

$$P(\mathbf{r},\hat{\xi}'\to\hat{\xi}) = \beta(\mathbf{r},\hat{\xi}'\to\hat{\xi})/b(\mathbf{r}).$$

Assuming that the optical properties of the medium are independent of position and introducing these definitions into the RTE, we have

$$(\hat{\xi}\cdot\nabla)L(\mathbf{r},\hat{\xi}) + cL(\mathbf{r},\hat{\xi}) = b\int_{4\pi}P(\hat{\xi}'\to\hat{\xi})L(\mathbf{r},\hat{\xi}')d\Omega(\hat{\xi}') + \delta(\mathbf{r}-\mathbf{r}_0). \quad (4)$$

Dividing by c and recalling that $\delta(ax) = a^{-1}\delta(x)$ yields

$$(\hat{\xi}\cdot\nabla')L(c\mathbf{r},\hat{\xi}) + L(c\mathbf{r},\hat{\xi}) = \omega_0\int_{4\pi}P(\hat{\xi}'\to\hat{\xi})L(c\mathbf{r},\hat{\xi}')d\Omega(\hat{\xi}') + \delta(c\mathbf{r}-c\mathbf{r}_0), \quad (5)$$

where the prime on the gradient operator indicates that the derivatives are now with respect to the optical variables cx, cy, and cz. Using the optical variables we see that the radiance in the medium is governed completely by ω_0 and $P(\hat{\xi}'\to\hat{\xi})$.

It is important to note that the scattering and absorption properties of the medium can be conveniently separated into those due to the water itself and those due to materials dissolved or suspended in water, i.e.,

$$a = a_w + \sum_i a_i,$$

$$\beta = \beta_w + \sum_i \beta_i,$$

and so

$$b = b_w + \sum_i b_i$$

$$bP = bP_w + \sum_i bP_i,$$

where the subscript w refers to the water itself, and the subscript i refers to the ith constituent of the medium. It is necessary then to determine ω_0 and P, given a_w, a_i, β_w, and β_i.

We will consider only a two-component system consisting of water and phytoplankton (and their immediate derivatives), i.e.,

$$a = a_w + a_p$$

$$\beta = \beta_w + \beta_p \quad \text{or} \quad bP = b_wP_w + b_pP_p,$$

where the subscript p refers to phytoplankton. Given the above quantities, ω_0 and P can be determined from

$$\omega_w \equiv \frac{b_w}{c_w}, \quad \omega_p \equiv \frac{b_p}{c_p}, \quad \text{and} \frac{c_p}{c_w},$$

i.e.,

$$\omega_0 = \frac{\omega_p(c_p/c_w) + \omega_w}{c_p/c_w + 1}, \quad (6)$$

$$\omega_0 P = \frac{\omega_p P_p(c_p/c_w) + \omega_w P_w}{c_p/c_w + 1}. \quad (7)$$

The choice of these parameters and the particle scattering phase function is discussed in the next section.

II. Optical Model of Water and Its Constituents

To provide a realistic computation of the transport of radiant energy from a point source in the ocean, a model for the optical properties of the medium is needed. Such a model must provide the scattering phase and absorption coefficients of the water and its constituents. In waters labeled Case 1 by Morel and Prieur[2] (and comprising much of the open ocean) the optical properties are controlled by phytoplankton and their associated detrital material. Thus the model should provide the optical properties of the phytoplankton and their associated detrital material as a function of some convenient measure of the biological activity in the water. The usual indicator of the biological activity is the concentration of chlorophyll *a*.[3] This is taken to be a measure (although imprecise) of the phytoplankton biomass. In Case 1 waters it is to be expected, that to the extent the phytoplankton concentration can be parametrized by the chlorophyll *a* concentration, the optical properties of the biological material can also be specified by the chlorophyll *a* concentration. This has been found to be the case,

although this specification can only be made in a statistical sense due to the natural variability of the relative concentrations of the absorbing pigments associated with phytoplankton.

A. Optical Properties of Pure Seawater

The absorption coefficient of pure seawater has been inferred from measurements of downwelling and upwelling irradiance in oligotrophic waters such as the Sargasso Sea.[2,4] The scattering coefficient has been measured directly for pure water and for saline solutions of pure water corresponding to salinities between 35 and 39 ppt by Morel.[5] The results of these measurements are presented in Table I. The scattering phase function for pure water is given by the familiar Rayleigh scattering formula:

$$P_w(\Theta) = \frac{3}{8\pi}\left[\frac{1-\delta}{2+\delta}\right]\left[1 + \frac{1-\delta}{1+\delta}\cos^2\Theta\right]. \quad (8)$$

Morel's measurements suggest a depolarization factor δ of ~0.09; thus

$$P_w(\Theta) = P_u(90°)(1 + 0.835\cos^2\Theta). \quad (9)$$

B. Optical Properties of the Particles

The scattering coefficient of particles in the ocean has been studied as a function of the pigment concentration by Morel[6] (also see Ref. 7.) The result of measurements in Case 1 waters from several locations indicates that the scattering coefficient at 550 nm, $b_C(550)$, is nonlinearly related to the pigment concentration C through

$$b_C = B_C C^{0.62}, \quad (10)$$

where $b_C(550)$ is in m^{-1} and C is in mg/m^3. The constant B_C, the scattering coefficient at a pigment concentration of 1 mg/m^3, varies from 0.12 to 0.45 with an average value of 0.30. This variation in B_C is due to the natural variability of scattering over the various species of phytoplankton as well as a variability in scattering by the detrital particles associated with the phytoplankton.

The absorption of phytoplankton and their associated detrital material (excluding yellow substances) has been deduced from irradiance measurements by Prieur and Sathyendranath.[8] Their study indicated a nonlinear relationship between absorption and pigment concentration similar to that described by Smith and Baker.[9,10] The source of the nonlinearity in the absorption–pigment concentration relationship (and also the scattering–pigment concentration relationship) is believed to be a systematic variation in the ratio of the concentration of phytoplankton to that of detrital material as a function of the concentration of phytoplankton. Hobson *et al.*[11] observed that as the concentration of phytoplankton increases (and thus the pigment concentration also) the ratio of phytoplankton carbon to detrital carbon also increases. Thus, in the two-component absorption system of phytoplankton and their detrital material, the relative amounts of the components vary with the pigment concentration forcing the total absorption to be a nonlinear function of the pigment concentration. This nonlinearity can be molded in many ways. Smith and Baker[9,10] used a linear relationship between absorption (diffuse attentuation coefficient K_d) and pigment concentration but with different slopes (dK_d/dC) above and below 1 mg/m^3. Prieur and Sathyendranath[8] found that a similar relationship could be used to explain their absorption data but also discovered that for $C < 10$ mg/m^3 a single equation

$$a_C(\lambda) = 0.06A_C(\lambda)C^{0.602}, \quad (11)$$

where $a_C(\lambda)$ is in m^{-1} and C is in mg/m^3, fit the experimental data as well as the segmented linear relationship. In this equation $A_C(\lambda)$ is the absorption coefficient of phytoplankton normalized to 440 nm, i.e.,

$$A_C(\lambda) = \frac{a_C(\lambda)}{a_C(440)}.$$

The relative absorption of phytoplankton $A_C(\lambda)$ deduced by Prieur and Sathyendranath agrees well with absorption measurements made on phytoplankton cultures by Sathyendranath.[12] Note that $a_C(\lambda)$ is the absorption coefficient of "phytoplankton and their immediate derivatives or by-products having similar optical effects."[8] We assume here that there are no other sources of particles in the water, such as resuspended particles from the bottom in coastal areas; i.e., we limit the discussion to Case 1 waters, and as such $a_C(\lambda)$ represents the absorption coefficient of all the particles in the water. A similar meaning is also attached to $b_C(\lambda)$.

It is interesting to note that $b_C(\lambda)$ and $a_C(\lambda)$ vary with pigment concentration in nearly the same manner, i.e., approximately as $C^{0.6}$. This suggests that $b_C(\lambda)/a_C(\lambda)$ is nearly independent of the pigment concentration, and in fact

$$\frac{b_C(\lambda)}{a_C(\lambda)} \approx 16.6\frac{B_C(\lambda)}{A_C(\lambda)}. \quad (12)$$

This provides an estimation of $\omega_p(\lambda)$ and shows that this quantity is in the first approximation independent of the pigment concentration. Table II gives $\omega_p(\lambda)$ at 440 and 550 nm for the three different values of $B_C(550)$: the minimum, mean, and maximum observed in Case 1 waters. To estimate $\omega_p(440)$ it is

Table I. Absorption and Scattering Coefficients of Pure Seawater

λ (nm)	b_w (m^{-1})	a_w (m^{-1})	ω_w
420	0.0061	0.0153	0.285
440	0.0049	0.0145	0.253
460	0.0041	0.0156	0.208
480	0.0034	0.0176	0.162
500	0.0029	0.0257	0.101
520	0.0024	0.0477	0.048
540	0.0021	0.0558	0.036
550	0.0019	0.0638	0.029
560	0.0018	0.0708	0.025
580	0.0016	0.108	0.015
600	0.0014	0.244	0.006
620	0.0012	0.309	0.004

Table II. $\omega_p(\lambda)$ for Seawater Particles Assuming $B_C(\lambda) = B_C(550) \times (550/\lambda)^n$

$B_C(550)$	$\omega_p(440)$			$\omega_p(550)$
	$n = -1$	$n = 0$	$n = 1$	
0.12	0.606	0.660	0.713	0.848
0.30	0.800	0.833	0.862	0.933
0.45	0.857	0.882	0.903	0.954

Table III. $\omega_p(\lambda)$ for Four Species of Phytoplankton (after Bricaud *et al.*[13])

Species	$\omega_p(440)$	$\omega_p(550)$
Hymenomonas elongata	0.65	0.89
Platymonas Sp	0.76	0.90
Tetraselmis maculata	0.76	0.91
Coccolithus huxleyi	0.88	0.97

necessary to assume a wavelength dependence for $B_C(\lambda)$. The computations presented in Table II of $\omega_p(440)$ have been made assuming $B_C(\lambda) \sim \lambda^{-n}$ with $n = -1$, 0, and 1. Since the scattering by absorbing particles tends to be depressed in the absorption bands,[13] values of $n = -1$ to 0 will be favored for phytoplankton in the 440–550-nm spectral region.[14] Table III provides values of $\omega_p(\lambda)$ for four species of cultured phytoplankton studied by Bricaud *et al.*[13] Clearly, values of $B_C(550)$ can be found which will bring $\omega_p(\lambda)$ into conformity with the culture measurements. One must remember, however, that $b_C(\lambda)$ and $a_C(\lambda)$ include the contribution of any detritus which covaries with C. The apparent lack of any dependence of ω_p on C suggests that the plankton and their immediate detritus must have very similar absorption and scattering properties at least in a statistical sense.

To model the transport of bioluminescent emission in the water, the optical properties of the medium near the wavelength of maximum emission are required. This is centered near 480 nm. The data in Table II for the mean value of $B_C(550)$ indicate that ω_p is likely to fall in the 0.80–0.94 range. The actual choice ω_p requires a choice for n; however, the value of ω_p is very insensitive to n, ranging from 0.845 to 0.891 as n varies from -1 to 2. Since, for the most part, we are interested in pigment concentrations smaller than 1 mg/m^3, for which a significant portion of the scattering will be due to the detrital material, we choose $n = 1$, yielding a nominal value of 0.88 for $\omega_p(480)$. Also, we have chosen 0.16, the value at 480 nm, for ω_w.

The remaining parameters needed to specify the optical properties of the medium are c_p/c_w and the particle phase function. From Table I it is seen that $c_w = 0.021$ m^{-1} at 480 nm. Noting that $A_C(480) = 0.798$ and using the mean value of $B_C(550)$ with a λ^{-1} spectral variation, we have

$$c_p \simeq (0.34 + 0.048)C^{0.6},$$

or

$$\frac{c_p}{c_w} = 18.5C^{0.6}, \tag{13}$$

at 480 nm. This provides the connection between c_p/c_w and the pigment concentration.

The particle phase function is the most difficult quantity to parametrize, because it requires the individual phase functions of the plankton and the detrital material and their respective scattering coefficients. This presents a serious problem, since neither phase function has ever been measured. Thus we are forced to rely on measurements of the total particle function

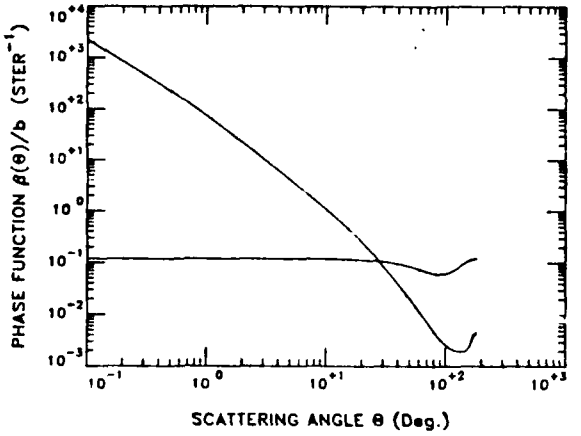

Fig. 1. Particle scattering phase function used in this study. The water phase function (lower curve at small scattering angles) is also shown for comparison.

(plankton plus detrital material). Petzold[15] has measured volume scattering functions at 530 nm for waters in several locations with very different turbidities (total scattering coefficients). After the scattering by pure water is subtracted, the resulting particle phase functions have a standard deviation which is within ~30% of the mean. This is remarkable considering that the particle scattering coefficient varied over a factor of ~50. The mean particle phase function and its standard deviation are shown in Fig. 1 along with the phase function for scattering by the water itself [$P_w(\Theta)$]. This mean particle phase function derived from Petzold's measurements is adopted for this study. It should be pointed out, however, that this phase function will be adequate only for simulations such as those under investigation in this study, which are expected to be insensitive to the particle backscattering probability $(\tilde{b}_b)_p$ defined according to

$$(\tilde{b}_b)_p \equiv (b_b)_p/b_p, \tag{14a}$$

where

$$b_b \equiv 2\pi \int_{\pi/2}^{\pi} \beta(\Theta) \sin\Theta d\Theta. \tag{14b}$$

This restriction arises because $(\tilde{b}_b)_p$ measured for oligotrophic waters, where the concentration of detrital material is relatively high compared with phytoplankton, is significantly higher than $(\tilde{b}_b)_p$ measured in euthrophic waters, where the detrital concentration is low, and in plankton cultures where the detritus is essentially absent. Thus a single phase function, independent of the viable-phytoplankton-to-detrital-particle ratio, cannot be expected to be useful for compu-

tations of the diffuse reflectance of the ocean, which is proportional to b_b/a.[7]

C. Range of Validity of the Optical Model

To provide a measure of the extent to which this optical model, relating the inherent optical properties of the ocean to the pigment concentration, can reproduce the apparent optical properties of the ocean, the RTE has been solved for sunlight at 480 nm incident on the top of the atmosphere from the zenith to obtain the downwelling irradiance attenuation coefficient $K_d(z)$ defined by

$$K_d(z) = -\frac{d[\ln E_d(z)]}{dz}, \tag{15}$$

where $E_d(z)$ is the downwelling irradiance at a depth z. Rayleigh and aerosol scattering are both accounted for in the simulation; however, the sky is assumed to be cloud free. The computations were carried out using Monte Carlo techniques for pigment concentrations varying from 0 to about 4.5 mg/m^3. The computations at $C = 0$ yield the diffuse attenuation coefficient for pure seawater K_w at 480 nm, which was determined to be 0.0206 m^{-1}, in reasonably good agreement with the 0.0194 m^{-1} estimated by Baker and Smith.[4] After the coefficient for pure water was subtracted, an excellent fit to the data for the mean $K_d - K_w$ over a depth interval of about half of the euphotic depth ($z = 0$ to $z \approx 2.3/K_d$) to

$$K_d - K_w = 0.070C^{0.615} \tag{16a}$$

was obtained. This should be compared with Morel's (see Ref. 7) fit of the same quantity to actual experimental data, which yielded

$$K_d - K_w = 0.074C^{0.703} \tag{16b}$$

For the range in pigment concentration between 0.05 and 2 mg/m^3 these two results agree within 20%, allowing the determination of K_d to better than 5% for $0 \le C \le 1$ mg/m^3 and better than 10% for $0 \le C \le 2$ mg/m^3. The comparison between the measurements and the model is much poorer for larger C, reaching ~30% for C near 10 mg/m^3. This agreement between the present model and the Morel measurements should not be surprising, considering that part of the model itself is based on an empirical relationship between a and C which was derived from the Morel data set.[8] The agreement however, does attest to the correctness of the empirical $b - C$ relationship and the reasonableness of the scattering phase function used in the computations.

The standard approximation $K_d \simeq a + b_b$, yielded

$$K_d - K_w \simeq 0.052C^{0.6}, \tag{16c}$$

while the Monte Carlo computations yielded

$$K_D - K_w = 0.057C^{0.617}, \tag{16d}$$

when the irradiance attenuation coefficients were evaluated just beneath the surface. The agreement between the approximation and the exact computations near the surface attests to the accuracy of the approximation. It must be noted, however, that K_d is a function of depth, while the standard approximation results in a constant K_d. The basic difference between the surface value of K_d and that measured over a depth range $z = 0$ to $z \approx 2.3/K_d$ is an increase of the value of $K_d - K_w$ at $C = 1$ mg/m^3; the functional dependence on C is essentially unchanged.

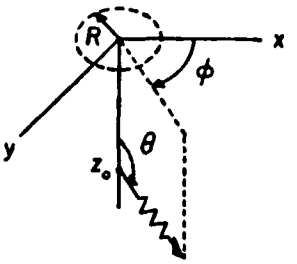

Fig. 2. Physical setting for defining R, z_0, θ, and ϕ. The sea surface is in the x-y plane. Note that the light field in the medium is independent of ϕ for an isotropic point source at z_0.

The ability of the model to reproduce the $K_d - C$ relationship derived from Morel's data[7] suggests that the model of the inherent optical properties as a function of the pigment concentration will be useful in studying the propagation of light emitted from a point source in the ocean.

III. Solution of the RTE for a Point Source in the Ocean

Most standard techniques for solving the RTE require that the spatial dependence of the light field be described by a single coordinate, i.e., in the case of the ocean illuminated by solar radiation, the radiance is assumed to be a function of depth only, not the horizontal coordinates. Clearly, in the case of point-source illumination, the radiance depends on both depth and horizontal position [Eq. (4)], and the standard solution techniques will no longer be applicable. Thus in this study the RTE is solved using Monte Carlo techniques, which are applicable to all geometries and which can easily be modified to include both vertical and horizontal variations of the optical properties of the water if desired.

A. Monte Carlo Technique

Given an isotropically emitting point source in the ocean, we wish to calculate the spatial and angular distribution of the irradiance transmitted to the sea surface as a function of the pigment concentration in the water. Since all the inherent optical properties of the medium have been given above as a function of C, it is only necessary to solve the RTE to determine the desired distributions. The solution is effected by Monte Carlo techniques. Photons are emitted isotropically from a point at depth z_0 beneath the surface (see Fig. 2). This emission can be accomplished by choosing the polar angle θ (the angle between the photon's direction and the nadir) from $\cos\theta = 1 - \rho_1$, where ρ_1 is a random number distributed uniformly on [0,1], and choosing the azimuth angle ϕ according to $\phi = 2\pi\rho_2$, where ρ_2 is a second random number with the same distribution as ρ_1. However, in the ocean, scattering is mostly in the near-forward direction so pho-

tons emitted downward from the source, i.e., away from the interface, have little chance of reaching the surface to contribute to the irradiance. Following these photons is, for all practical purposes, a waste of computational time. Therefore, in the present code we have chosen to sample θ from a distribution which yields an increased number of photons starting toward the surface. The normalized probability density for this distribution is

$$p_f(\theta) = \frac{\sqrt{1-\epsilon^2}}{\pi(1+\epsilon\cos\theta)}, \tag{17}$$

where $0 \le \epsilon < 1$, and the subscript f indicates false in that the true probability density from which θ should be chosen is $p_t(\theta) = \frac{1}{2}\sin\theta$. Sampling θ from the incorrect probability distribution introduces a bias which can be removed by providing each photon with an initial statistical weight W given by

$$W = \frac{p_t(\theta)}{p_f(\theta)}.$$

Using $p_f(\theta)$ above, given a random number ρ_1, the angle θ is chosen from

$$\cos\theta = \frac{1-y^2}{1+y^2}, \tag{18}$$

where

$$y = \frac{1+\epsilon}{\sqrt{1-\epsilon^2}}\tan\left(\frac{\pi\rho_1}{2}\right), \tag{19}$$

and the weight of the associated photon is initialized to

$$W = \pi\frac{1+\epsilon\cos\theta}{2\sqrt{1-\epsilon^2}}\sin\theta. \tag{20}$$

The photon's path is then followed using standard Monte Carlo techniques. At each collision its weight is multiplied ω_0. On encountering the surface its horizontal position R is determined, and the associated upwelling irradiance $E_u(R,z_0)$ (its weight) is recorded. If the scalar irradiance, in general defined according to

$$E_0(\mathbf{r}) = \int_\Omega L(\mathbf{r},\hat{\xi})d\Omega(\hat{\xi}), \tag{21}$$

where the integration is taken over 4π Sr, is desired at the surface, i.e., $E_0(R,z_0)$, the photon's weight divided by the cosine of the angle its path makes with the vertical is recorded on impact with the surface. If the photon penetrates the surface, it also makes a contribution to the associated irradiance above the surface.

B. Validation Tests of the Monte Carlo Code

The reciprocity principle[1] can be used to provide some information concerning the validity of the resulting Monte Carlo code. For example, let $E_u^e(R,z_0)$ be the upward irradiance exiting the sea surface due to a point source at z_0 emitting one photon per second (Fig. 2), and $E_0(z_0)$ be the scalar irradiance at z_0 resulting from an incident uniform radiance distribution of unit irradiance. Then using the reciprocity principle it can be shown that (see Ref. 16 for the derivation of a similar relationship)

$$E_0(z_0) = 8\pi m^2\int_0^\infty E_u^e(R,z_0)dR. \tag{22}$$

This relationship was tested by evaluating the integral using the present code and $E_0(z_0)$ using an existing and well-tested Monte Carlo code with diffuse illumination. The phase functions used were similar to those measured in the ocean, and the computations agree to within ½%.

Unfortunately, reciprocity cannot guarantee the correct functional dependence of the point source light field on R at the surface. This requires comparison of the code's output with the results of exact computations. For the case of pure absorption, i.e., $b = 0$, the exact computation is trivial to perform, and the Monte Carlo code agrees well with it. When scattering is included, the only point source case for which an exact[17] solution is available is that of an isolated source in an infinite medium, which scatters isotropically, i.e., $P(\hat{\xi}' \to \hat{\xi}) = 1/4\pi$. Unfortunately, the medium for which the present code is applicable is semi-infinite with the detector at the surface. To our knowledge the RTE has never been solved exactly for such a geometry. Elliott,[19] however, has obtained an asymptotic solution for the scalar irradiance to the problem of a point in an isotropically scattering half-space of unit refractive index. Elliott's result for the scalar irradiance at the surface due to a point source emitting unit power isotropically at depth z_0 is

$$[E_0(\tau_R,\tau_z)]_N = \frac{\Psi_0(\tau_z)}{2\pi\sqrt{3}\tau_R^3}(1+k_0\tau_R)\exp(-k_0\tau_R), \tag{23}$$

where $\tau_z = cz_0$, $\tau_R = cR$, and k_0 and $\Psi_0(\tau_z)$ are constants $[k_0 = k_0(\omega_0)]$ which have been tabulated by various authors.[20,21] The asymptotic solution is valid for $z_0/R \ll 1$. The error is of the order of z_0^3/R^5. The notation $[E_0(\tau_R,\tau_z)]_N$ means the scalar irradiance in nondimensional or *scaled* optical units. The actual scalar irradiance, and, in general, the radiance, at the surface of the half-space depends on c as well as z_0 and R, i.e., unlike a homogeneous ocean illuminated by sunlight, for which the radiometric quantities depend on c and depth only through their product, the point source illumination produces a light field that depends on these quantities individually. The actual scalar irradiance is derived from the scaled scalar irradiance through

$$E_0(R,z_0,c) = c^2[E_0(\tau_R,\tau_z)]_N, \tag{24}$$

where R and z_0 are in meters, and c is in m^{-1}. The source power is 1 W/nm, and, since the actual scalar irradiance $E_0(R,z_0c)$ has units of W/m^2nm, the scaled scalar irradiance $[E_0(\tau_R,\tau_z]_N$ has the same units as the power (W/nm). Equation (24) is exact and a manifestation of the inverse square decrease in the irradiance with distance from the source. It applies to other radiometric quantities, such as the irradiance and radiance as well.

The Monte Carlo computations for an isotropically scattering half-space (with $\omega_0 = 0.9$) illuminated by an embedded point source are compared with Elliott's asymptotic theory in Fig. 3. The individual panels in

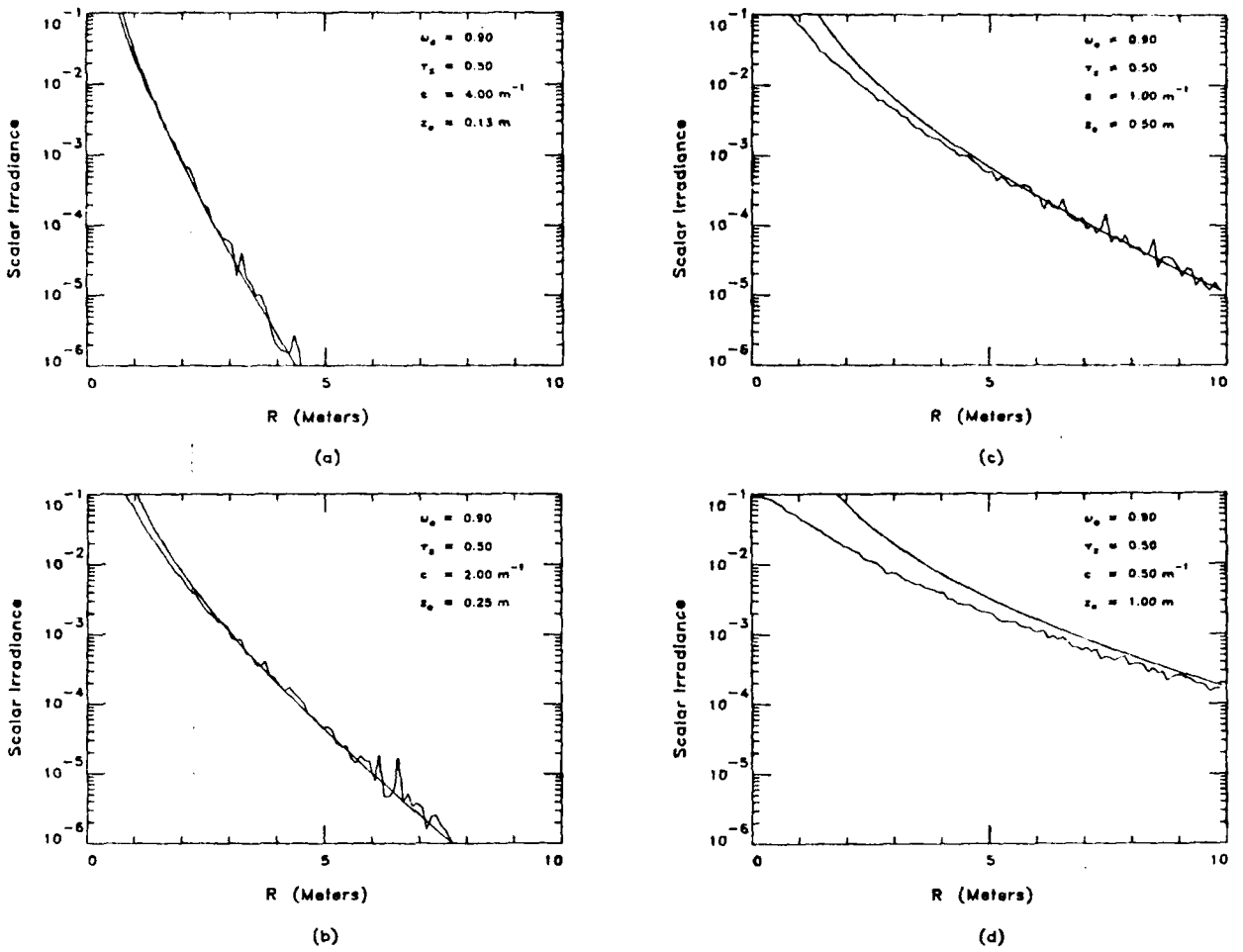

Fig. 3. Comparison between the Monte Carlo determined scalar irradiance at the surface $[E_0(\tau_R,\tau_z)]_N$ in W/nm, (noisy curves) and Elliott's asymptomatic solution for isotropic scattering (smooth curves), which is valid for $R \gg z_0$. For all the cases τ_z is 0.5, while the physical depth of the source is varied from 0.125 m (a) to 1 m (d).

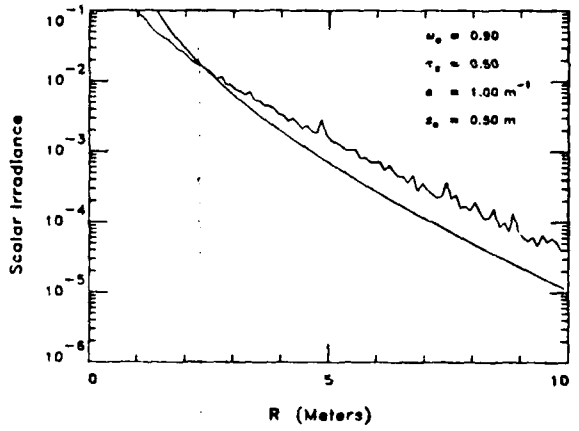

Fig. 4. Effect of changing the refractive index of the medium m from 1.000 [Fig. 3(c)] to 1.333 for isotropic scattering. The noisy line is the Monte Carlo result for the scalar irradiance just beneath the surface with $m = 1.333$, and the smooth curve is Elliott's asymptomatic theory for $m = 1.000$.

this figure all refer to a source at an optical depth τ_z of one-half but physical depths z_0 of 1, 0.5, 0.25, and 0.125 m. The agreement is excellent for $R \gg z_0$ and provides a quantitative measure of the range of parameters over which Elliott's theory is valid, i.e., $R/z_0 \gtrsim 10$ or $\tau_R/\tau_z \gtrsim 10$. Statistical fluctuations in the Monte Carlo estimates are clearly evident for small values of $[E_0(\tau_R,\tau_z)]_N$. Figure 4 shows the effect of changing the refractive index of the scattering medium from 1.00 to 1.33 for $z_0 = 0.5$ m [compare with Fig. 3(c)]. For this particular case the scalar irradiance at the surface is increased at all depths, and for $R \simeq 10$ m this increase reaches a factor of 4. This increase is easy to understand: isotropic scattering with large values of ω_0 produces a very diffuse light field, for which about half of the flux incident on the interface is reflected back into the medium and then can be scattered back to the interface.

The above tests of the present code suggest it is correct and can be used to compute the irradiance

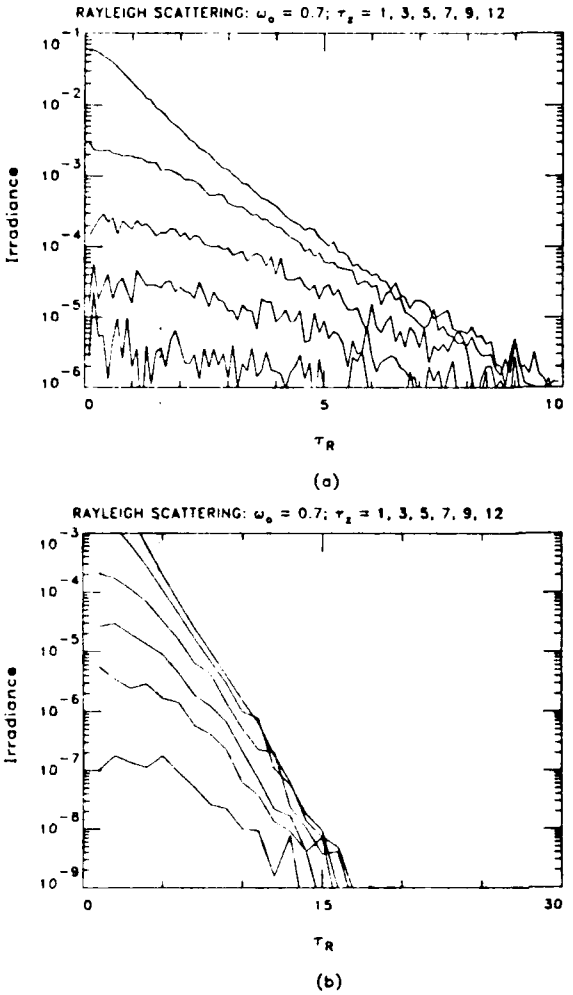

Fig. 5. Upwelling irradiance just beneath the surface $[E_u(\tau_R,\tau_z)]_N$ in W/nm for source optical depths 1, 3, 5, 7, 9, and 12, ω_0 of 0.7, and the Rayleigh scattering phase function: (a) $0 \le \tau_R \le 10$; (b) $0 \le \tau_R \le 30$.

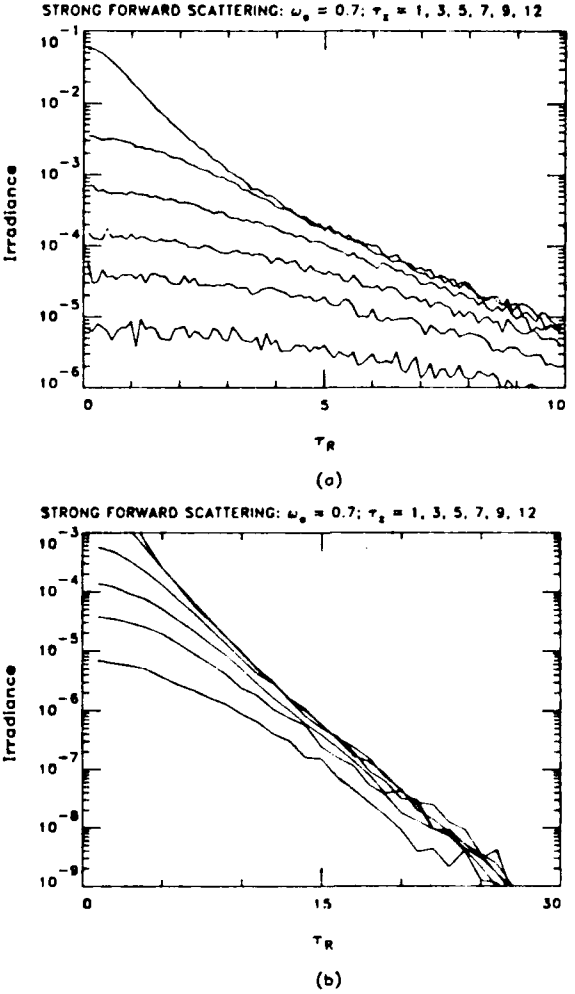

Fig. 6. Upwelling irradiance just beneath the surface $[E_u(\tau_R,\tau_z)]_N$ in W/nm for source optical depths 1, 3, 5, 7, 9, and 12, ω_0 of 0.7, and a strongly forward scattering phase function (a combination of Rayleigh scattering and Petzold's particle phase function with $c_p/c_w \approx 7$): (a) $0 \le \tau_R \le 10$; (b) $0 \le \tau_R \le 30$.

distribution from a point source embedded in the water.

C. Examples of the Computations

Computations of the distribution of upwelling irradiance, $[E_u(\tau_R,\tau_z)]_N$ or $E_u(R,z_0,c)$ (not the scalar irradiance used for comparisons with Elliott's computations), at the sea surface (just beneath the surface) has been carried out for a range of values of the parameters involved. Figures 5 and 6 contrast the scaled irradiance distributions $[E_u(\tau_R,\tau_z)]_N$, i.e., $E_u(R,z,c)/c^2$ in W/nm, obtained in an ocean exhibiting, respectively, pure Rayleigh scattering and scattering according to Petzold's mean particle phase function. A point source emitting a power of 1 W/nm is placed at optical depths of 1, 3, 5, 7, 9, and 12, and ω_0 for the medium is 0.7. Again, the noisy nature of the results is due to statistical fluctuations in the Monte Carlo estimates. The contrast between Rayleigh scattering (Fig. 5) and strong forward scattering (Fig. 6) is seen to be very large, except for small source depths and small values of τ_R i.e., when the source is close to the observation point. In this regime the variation in the irradiance with τ_R is governed largely by geometry rather than by the optical properties of the water. Most photons propagate directly from the source to the detector with no interaction with the medium. Scattering plays a very small role in determining the irradiance. The irradiance is proportional to z_0/X^3, where $X^2 = R^2 + z_0^2$ (see below).

For larger values of τ_R (but still small source depths) the disparity between the irradiances for these two cases becomes apparent with the strong forward scattering irradiance becoming an order of magnitude higher than the Rayleigh irradiance by $\tau_R = 10$ for $\tau_z = 1$ or 3. The rate of decay of the irradiance with τ_R appears to be independent of the source depth for sufficiently large τ_R. This is particularly evident in Fig. 6, in which the curves for various τ_R values tend to become parallel for large τ_R. Elliott's asymptotic theory for isotropic scattering predicts that this should be

true for the scalar irradiance, since the dependence of E_0 on τ_z is completely contained in the multiplicative $\Psi_0(\tau_z)$ term. Figure 6 confirms that this result is valid for a strongly forward scattering phase function as well. This is the diffusion regime; the light field is completely dominated by multiple scattering. Photons scatter many times before encountering the surface. In the diffusion approximation the irradiance would be expected to vary with R according to

$$\frac{E_u(R,z_0,c)}{c^2} \sim \frac{1}{\tau_X^2} \exp(-k_d \tau_X/c), \tag{25}$$

where

$$\tau_X^2 = \tau_z^2 + \tau_R^2,$$

and k_d is explicitly provided in terms of ω_0 and the phase function asymmetry parameter (or average cosine) g through[21]

$$\frac{k_d}{c} = \sqrt{3(1-\omega_0)(1-\omega_0 g)}. \tag{26}$$

In this approximation, k_d is the downwelling (and upwelling) irradiance attenuation coefficient (K_d) of the light field when illuminated by solar radiation. The diffusion approximation is valid only at very large values of τ_R and τ_z and values of ω_0 near 1, i.e., $k_d/c \ll 1$. The irradiance reaching the surface is significantly larger with strong forward scattering than with Rayleigh scattering, and this phase function effect, expressed through the parameter g in Eq. (26), becomes increasingly stronger as τ_R and τ_z increase. For large τ_R the exponential dominates the algebraic function, and the result is essentially exponential decay. It is natural to expect the exponential decay constant κ associated with this exponential decay to be related to the attenuation coefficient of irradiance K_∞ in the asymptotic light regime.[22] The asymptotic decay coefficients K_∞ have been computed for the two cases examined, along with κ, which was determined by fitting the computation for large τ_R ($\tau_R > 10$) to Eq. (25) with k_d replaced by κ. These are compared in Table IV, which gives the results for Rayleigh and forward scattering with $\omega_0 = 0.7$ (first two rows) and for forward scattering with $\omega_0 = 0.9$ (last row). Figure 5 shows that the Rayleigh irradiance is very noisy for large τ_z and large τ_R, and hence the κ/c determined from the computations is likely to be inaccurate. The strong forward scattering irradiance, on the other hand, (Fig. 6), is much better behaved at large τ_R, and we can expect a more accurate κ/c. The values of κ/c for $\omega_0 = 0.7$ (first two rows in Table IV) usually agree with K_∞ within the accuracy of the κ/c determination, with the exception of the Rayleigh scattering case with $\tau_z = 1$ and 3. The case of strong forward scattering with $\omega_0 = 0.9$ (last row in Table IV) was included for two reasons: the irradiance decays much more slowly with τ_R, enabling larger values of τ_R to be reached in the computations (the fits for κ/c include only results for $\tau_R > 15$ rather than the $\tau_R > 10$ in the other cases); and the diffusion approximation becomes more appropriate for larger values of ω_0. The agreement between κ/c and K_∞ is seen to be better and more stable with source depth for $\omega_0 = 0.9$ compared with the other case. In the two forward scattering cases, which provide a realistic approximation to the real ocean, equality between κ/c and K_∞ is obtained within 10% for all source depths.

Table IV. Derived Values of κ/c for Comparison with K_∞/c

$P(\Theta)$	ω_0	cz_0						K_∞/c
		1	3	5	7	9	12	
Rayleigh	0.7	0.929	1.050	0.864	0.939	1.013	1.010	0.821
Forward	0.7	0.470	0.423	0.449	0.465	0.480	0.414	0.467
Forward	0.9	0.245	0.226	0.232	0.238	0.242	0.240	0.253

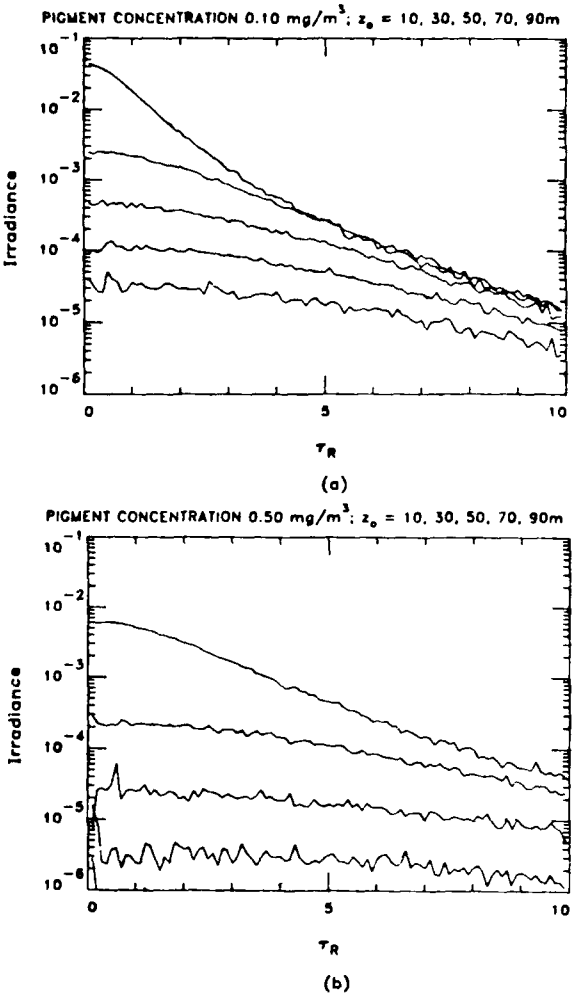

Fig. 7. Upwelling irradiance just beneath the surface $[E_u(\tau_R,\tau_z)]_N$ in W/nm and source physical depths 10, 30, 50, 70, and 90 m for pigment concentrations of 0.1 (a) and 0.5 (b) mg/m³. Note: to compute the actual irradiance (W/m²nm) the scaled irradiance given here must be multiplied by c^2.

Figure 7 shows the results of computations of $[E_u(\tau_R,\tau_z)]_N$ carried out for source depths of 10, 30, 50, 70, and 90 m in an ocean exhibiting optical properties at 480 nm consistent with the bio-optical model described above for pigment concentrations of 0.1 and 0.5 mg/m³. Such concentrations are typical of central ocean gyres at times of medium to high productivity.

These results are very similar to the forward scattering cases described above. As expected, the higher pigment concentration results in a lower level of irradiance at the surface for all source depths. For a detailed comparison of these two cases, one must work with actual (as opposed to scaled) irradiances. As described above, the actual irradiance is derived from the scaled irradiance by multiplication by c^2. For C of 0.1 and 0.5 mg/m^3, c is 0.12 and 0.28 m^{-1}, respectively. Thus to compare the two cases at, say R = 30 m, we must compute $\tau_R = cR$ and multiply the nondimensional irradiance by c^2. This gives at z_0 = 10 m irradiances of $\sim 1.15 \times 10^{-5}$ and 6.3×10^{-6} W/m^2 μm for C of 0.1 and 0.5 mg/m^3, respectively, if the source power is 1 W/μm. It may seem surprising at first that the surface irradiance in the clearer water is only 1.8 times greater than that in the more turbid water. However, one must remember that the plankton scatter much more strongly than they absorb (ω_0 = 0.88) and that most of the scattering is in the near forward direction (Fig. 1). Hence, in the first approximation, the irradiance decay is governed by the absorption and geometry. At 480 nm the absorption coefficients for the plankton and detritus are 0.012 and 0.032 m^{-1}, respectively, for the low and high pigment concentrations. From the geometry of the problem the irradiance must travel at least 31.6 m before reaching the surface; thus considering only the differential absorption loss, the ratio of the two irradiances should be $\exp[-31.6(0.012 - 0.032)] = 1.88$, in good agreement with the result derived from Fig. 7.

D. Analytic Approximations to the Monte Carlo Results

It would be useful to be able to describe the irradiance distribution on the surface with simple analytic formulas. The diffusion approximation above, and Elliott's result, are examples for which this is possible, their value is limited since they basically apply in a regime ($\tau_R \gg 1$) where the irradiance is very small or negligible. What is really needed is to be able to describe $[E_u(\tau_R,\tau_z)]_N$ for the more important region $0 \le \tau_R \le 10$, where most of the irradiance is found. The success of the simple computation above in explaining the Monte Carlo result for small z_0 suggests a simple model to explain quantitatively the results in this interval. Consider the irradiance on the surface due to photons emitted from a point source of unit power at a depth z_0 in the absence of scattering. This is

$$E_u(R,z_0,c) = \frac{1}{4\pi z_0^2} \cos^3\theta \exp(-az_0/\cos\theta), \tag{27}$$

where $\tan\theta = R/z_0$. Rewriting,

$$\frac{E_u(R,z_0,c)}{c^2} = [E_u(\tau_R,\tau_z)]_N = \frac{1}{4\pi} \frac{\tau_z^3}{\tau_X^3} \exp(-a\tau_X/c), \tag{28}$$

where $a = c(\tau_X$ was defined earlier). Now in the case of a strongly forward scattering medium, most photons are scattered with very little change in direction, so we expect this to still be approximately correct, but with a replaced by an effective attenuation coefficient k, which is expected to be related to K_d in some manner. Note, however, the K_d is not a uniquely defined constant; in general, it is a function of depth.

There are probably many ways to determine a suitable value of k, for example, one could fit the Monte Carlo results to

$$\frac{E_u(R,z_0,c)}{c^2} = [E_u(\tau_R,\tau_z)]_N = \frac{A}{4\pi} \frac{\tau_z^3}{\tau_X^3} \exp(-k\tau_X/c) \tag{28'}$$

and determine A and k. Although this technique provides excellent fits to the Monte Carlo results in the nondiffusion regime, it is not easy to interpret A and k in terms of physically measurable quantities, e.g., c, K_d. The approach taken here is based on trying to fit the total power reaching the surface to Eq. (28) with a replaced by k. The total power reaching the surface is found by multiplying Eq. (28) by $2\pi c^2 R dR$ and integrating from 0 to ∞, i.e.,

$$P_{\text{total}} = \int_0^\infty 2\pi E_u(R,z_0,c) R dR. \tag{29}$$

This integral can be evaluated in terms of an exponential integral yielding the remarkably simple formula

$$P_{\text{total}} = \frac{1}{2} E_2\left(\frac{k}{c}\tau_z\right) = \frac{1}{2} E_2(kz_0), \tag{30}$$

where

$$E_n(\alpha) = \int_1^\infty \frac{\exp(-\alpha t)}{t^n} dt,$$

which is tabulated in Abramowitz and Stegun.[23] The total power reaching the surface thus depends only on k and the depth of the source z_0.

The determination of k/c was made by trial and error with the restriction that only computations for which $P_{\text{total}} > 10^{-5}$ would be included for a point source of unit power. This restriction was placed on the analysis because (1) it encompasses the most interesting region and (2) it was believed that smaller values of P_{total} would place the problem in the diffusion regime for which even the form of Eq. (28) is incorrect. Briefly, in the first attempt, the traditional value of K_d at the surface, i.e., $a + b_b$, was tried for k. This value worked well for larger values of P_{total}, i.e., smaller values of τ_z, but overestimated P_{total} for larger values of τ_z. Realizing that K_d varies with depth, the next try was to estimate k by the asymptotic value of K_d, which was computed for each simulation. This time good agreement between the Monte Carlo results and Eq. (30) was found at large values and at very small values of P_{total}, but for intermediate values, $P_{\text{total}} \approx 10^{-3}$, it was underestimated. A linear combination of these two k values did not yield better results. Finally, it was decided to try a linear combination weighted by a function of τ_z so that for small values of τ_z the value of K_d at the surface, K_{surf}, would be used, while for very large values of τ_z the asymptotic K_d value K_∞ would be used. This scheme worked fairly well for $10^{-5} \le P_{\text{total}} \le 1$; however, it was felt to be unsatisfactory because, although K_{surf} could be easily measured in the ocean, measurement of K_∞ is difficult. This blemish is easy to remove, because K_{surf} and K_∞ are found to be closely

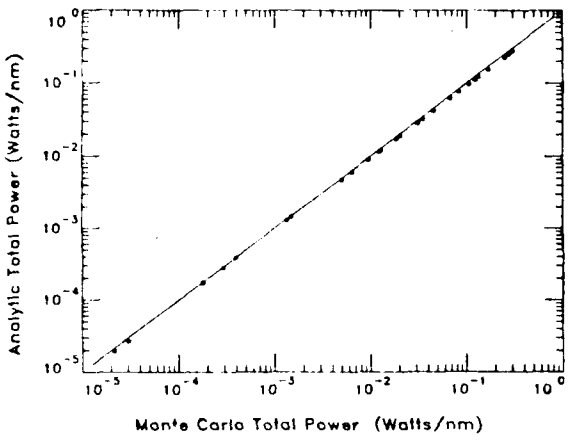

Fig. 8. Comparison between the total power just beneath the sea surface (from a source of unit power) computed via Monte Carlo techniques with that computed using the analytic model with k determined from Eqs. (31)–(33).

related in the present model for the pigment range $0.01 \le C \le 4.4$ mg/m^3:

$$0.0836 \le \frac{K_\infty}{c} - \frac{K_{surf}}{c} \le 0.114.$$

Similar relationships have been suggested by other investigators.[24,25] By trial and error, the final relationship for K_∞ was taken to be

$$K_\infty = K_{surf} + 0.09c, \tag{31}$$

and the best value of k to be used in Eq. (30) is

$$k = \gamma(\tau_z)K_{surf} + [1 - \gamma(\tau_z)]K_\infty, \tag{32}$$

where the weighting function $\gamma(\tau_z)$ is given by

$$\gamma(\tau_z) = \exp\left(-0.08\frac{K_{surf}}{c}\tau_z\right) = \exp(-0.08K_{surf}z_0). \tag{33}$$

Figure 8 compares the Monte Carlo computations of the total power with that computed from Eq. (30) (Analytic Total Power) with k determined from Eqs. (31)–(33) for pigment concentrations ranging from 0.01 to 4.4 mg/m^3 and source depths from 10 to 90 m. K_{surf} is taken from Eq. (16c). Equation (30) clearly provides an excellent approximation to the total power reaching the surface from a point source of unit power for $10^{-5} \le P_{total} \le 1$. K_∞ and K_{surf} can be directly related to C using Eqs. (13) and (16), i.e., $K_{surf} = 0.020 + 0.052C^{0.6}$, and $K_\infty = 0.022 + 0.087C^{0.6}$. These provide k as a function of C and z_0 directly through Eqs. (32) and (33).

Having determined the value of k that reproduces the total power, this value can be substituted into Eq. (28) (replacing a) to estimate the distribution of irradiance on the sea surface $[E_u(\tau_R,\tau_z)]_N$. These distributions for $\tau_R \le 10$ are shown in Fig. 9 with pigment concentrations of 0.01, 0.5, 0.1, and 0.5 mg/m^3. Clearly, the simple model reproduces the Monte Carlo computations in this nondiffusion regime very well. It is interesting to note that these results imply that an estimate of K_d can be made at night by releasing a point source of light in the water, measuring the irradiance at the surface as it sinks, i.e., as a function of the depth of the source, and fitting the results to the equations developed here to determine k.

This simple model can be used to estimate the surface manifestation of bioluminescent emissions, given the optical properties of the medium, or as seen in the present model, the pigment concentration. For example, one can determine the fraction of the total power reaching the surface in a circle of radius R, i.e., the effective size of the spot on the sea surface. The power reaching the surface enclosed in a circle of radius R is given by

$$P(R) = \int_0^R 2\pi E_u(R',z_0)R'dR'. \tag{34}$$

This is easily evaluated in terms of exponential integrals, and the result is

$$P(R) = \tfrac{1}{2}[E_2(kz_0) - \frac{1}{\eta}E_2(kz_0\eta)], \tag{35}$$

where $\eta = \sqrt{1 + R^2/z_0^2}$. The fraction f of the total power contained within R is $f = P(R_f)/P_{total}$, where R_f is the value of R corresponding to f. Thus the radius of the circle containing the fraction f of the total power reaching the surface is found by solving the equation.

$$E_2(kz_0\eta) = \eta(1 - f)E_2(kz_0) \tag{36}$$

for η. The resulting values of R_f for $f = 0.5$ and 0.9 are presented in Fig. 10. Choosing $f = 0.9$ gives the effective size of the spot on the sea surface. The accuracy of this determination can be estimated from Fig. 11 in which τ_{R_f} ($= cR_f$) determined from the individual Monte Carlo simulations is compared with the same quantity determined analytically using Eqs. (31)–(36). The excellent agreement for $f = 0.5$ is seen to be degraded only slightly for $f = 0.9$. The possibility of inverting Eq. (36) for z_0 given R and some measure of k is discussed in the Appendix.

Since our computations of $E_u(R,z,c)$ are for a point source, the results represent the Green's function for the time-independent transport equation and, therefore, Eq. (28), with a replaced by k, represents an approximation to the Green's function. Thus, for an extended distribution of sources of power $P(\mathbf{r}_0)$ distributed throughout the medium, the upwelling irradiance just beneath the surface will be given by

$$E_u(\mathbf{r}_s,z_0,c) = \frac{1}{4\pi}\int_V P(\mathbf{r}_0)\frac{z_0}{|\mathbf{r}_0 - \mathbf{r}_s|^3} \times \exp[-k|\mathbf{r}_0 - \mathbf{r}_s|]d\mathbf{r}_0, \tag{37}$$

where $\mathbf{r}_s$ is the point on the surface at which the irradiance is required, and $d\mathbf{r}_0$ is an abbreviation for $dx_0dy_0dz_0$.

Finally, the irradiance just above the sea surface, i.e., the component of $[E_u(\tau_R,\tau_z)]_N$ that is transmitted through the air–sea interface remains to be discussed. This quantity is easy to derive by combining the radiance just beneath the sea surface with the Fresnel equations for specular reflection and is carried out in the Monte Carlo code; however, these computations

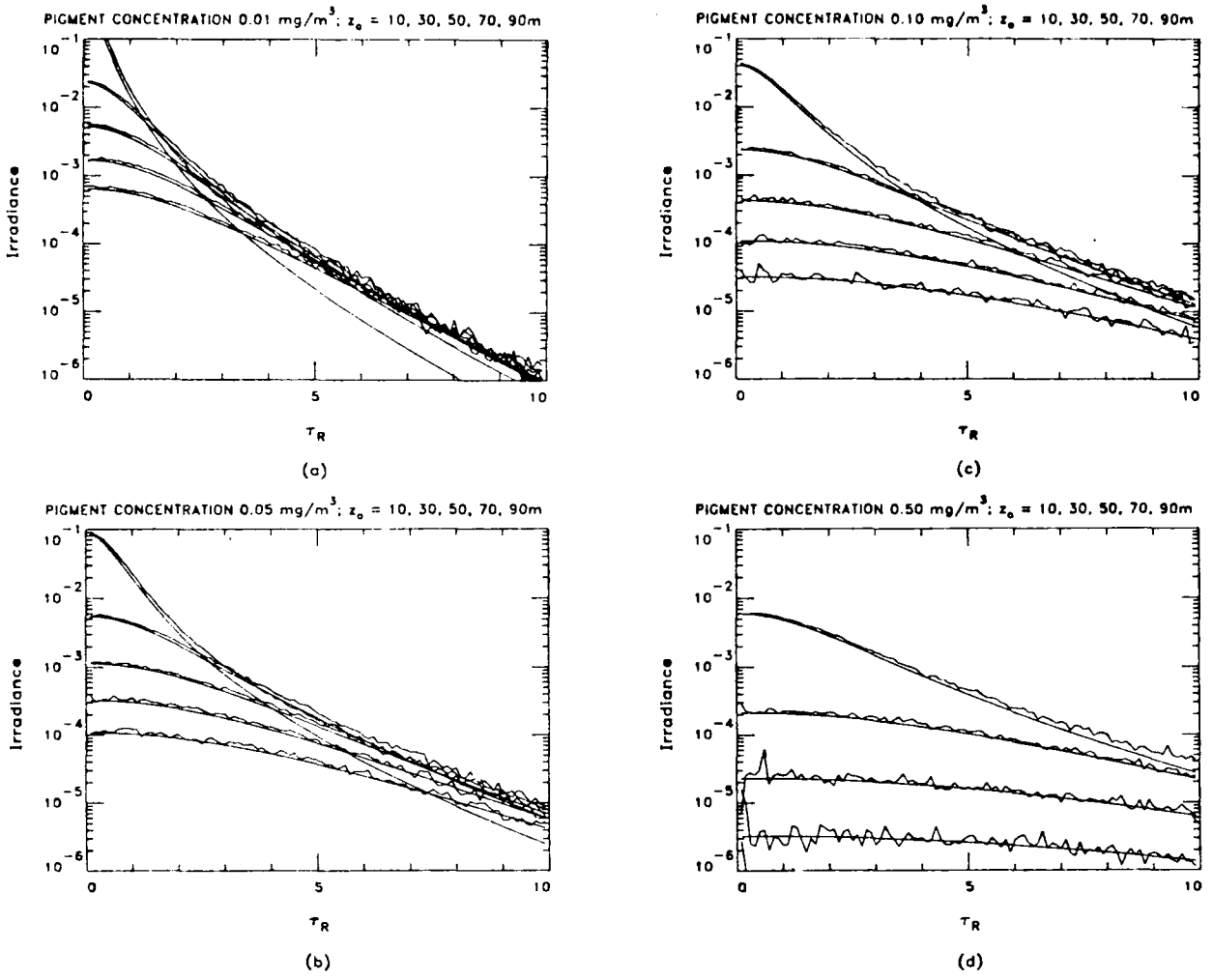

Fig. 9. Upwelling irradiance just beneath the surface, $[E_u(\tau_R,\tau_z)]_N$ in W/nm, and source physical depths 10, 30, 50, 70, and 90 m for pigment concentrations of 0.01 (a), 0.05 (b), 0.10 (c), and 0.50 (d) mg/m^3. The noisy curves are the Monte Carlo results, and the smooth curves are computed from the analytical model.

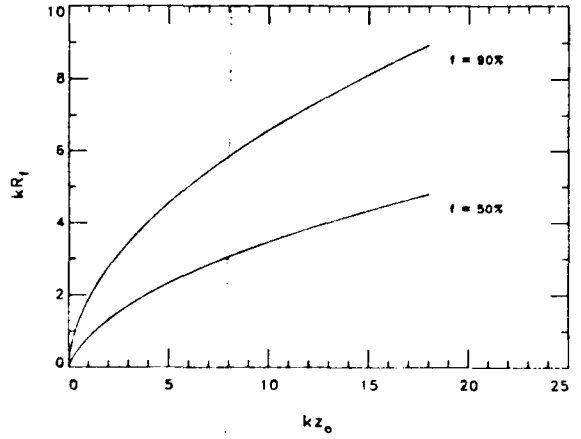

Fig. 10. Analytic approximation to the radius of the circle at the sea surface R_f containing a fraction f of the total power plotted as a function of the source depth z_0.

are less important than those for $[E_u(\tau_R,\tau_z)]_N$, since the actual irradiance leaving the surface will depend significantly on the roughness of the surface, which here has been assumed to be perfectly flat. The results are similar to $[E_u(\tau_R,\tau_z)]_N$; however, when τ_z is small the irradiance shows a rapid decrease with τ_R, beyond $\tau_R \approx \tau_z$, because unscattered photons, and photons scattered through very small angles, strike the sea surface at incident angles greater than the critical angle for total internal reflection. It is of interest to see how well the analytical model above represents the irradiance above the surface. This is shown in Fig. 12 [compare with Fig. 9 for $[E_u(\tau_R,\tau_z)_N]$, in which the scaled irradiance is plotted as a function of τ_R and z_0 for pigment concentrations ranging from 0.01 to 0.5 mg/m^3 along with the predictions of the analytical model derived by multiplying Eq. (28), with a replaced by k, by the Fresnel transmittance evaluated for an incident

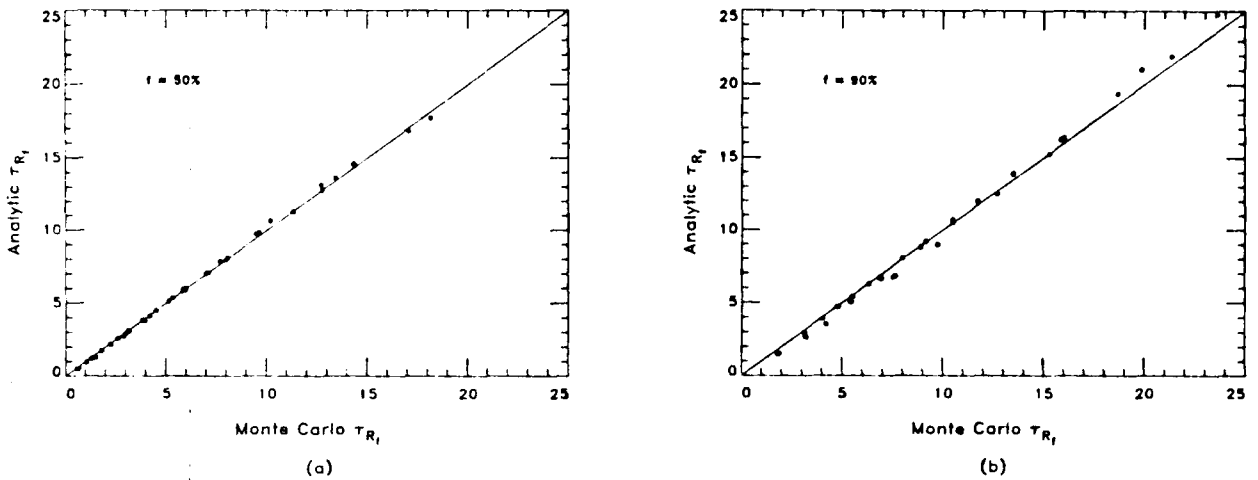

Fig. 11. Comparison between the analytic approximation to the radius of the circle at the sea surface, $\tau_{R_f} \equiv cR_f$, containing a fraction f of the total power, plotted as a function of the source optical depth $\tau_z \equiv cz_0$: (a) $f = 50\%$; (b) $f = 90\%$.

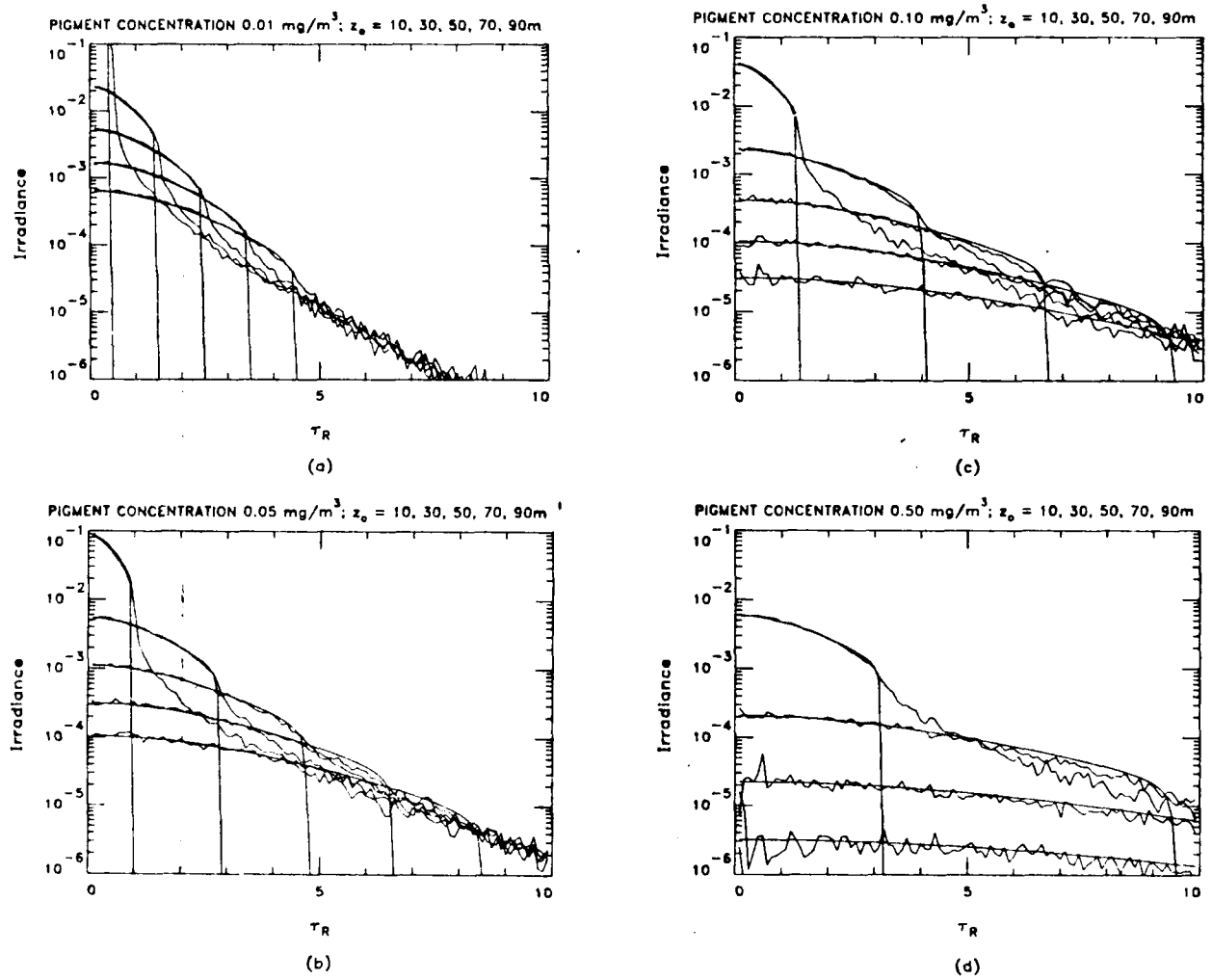

Fig. 12. Scaled upwelling irradiance W/nm just above the surface for source physical depths 10, 30, 50, 70, and 90 m and pigment concentrations of 0.01 (a), 0.05 (b), 0.10 (c), and 0.50 (d) mg/m^3. The noisy curves are the Monte Carlo results, and the smooth curves are computed from the analytical model accounting for refraction and reflection at the sea-air interface.

angle θ, where $\tan\theta = \tau_R/\tau_z$. The rapid reduction of the irradiance with τ_R, after $\tau_R \approx \tau_z$, is clearly evident for the smaller values of z_0. The analytical model, of course, predicts that the irradiance above the surface is identically zero for incident angles greater than $\theta \approx 48.6°$, i.e., the vertical lines in Fig. 12. Clearly the analytical model fits the Monte Carlo data well for values of τ_R and τ_z such that $\theta < 48.6°$, and for small values of z_0, this regime contains most of the total power exiting the surface. For large values of z_0 the light field at the surface becomes very diffuse and the effect of the critical angle is hardly observed. In this regime, a significant fraction of the total power exiting the water is outside the range of applicability of the analytic model. Figure 13 shows the comparison between the total power computed using the analytical model and the Monte Carlo computations. Clearly the analytical model provides excellent results for cases where the total power exiting the surface is greater than $\sim 10^{-2}$ of the source power, but for the 10^{-5}–10^{-3} range it underestimates the total power by as much as a factor of 2.

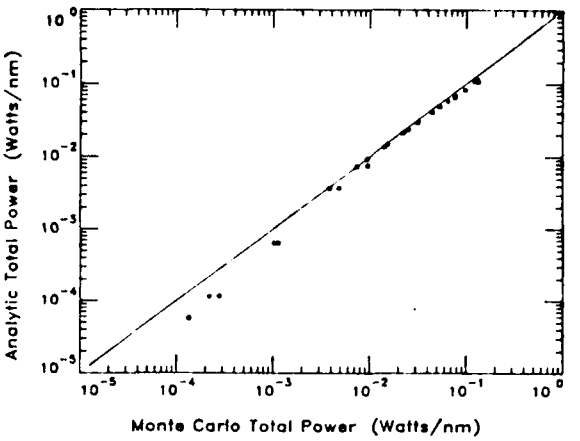

Fig. 13. Comparison between the total power just above the sea surface (from a source of unit power) computed via Monte Carlo techniques with that computed using the analytic model with k determined from Eqs. (31)–(33).

IV. Summary and Conclusions

A model of the optical properties of the ocean, providing the absorption and scattering coefficients of the medium as nonlinear functions of the concentration of pigments associated with phytoplankton and their immediate detrital material, is presented. Monte Carlo computations of the attenuation coefficient of downwelling irradiance K_d for an ocean–atmosphere system illuminated by the sun at zenith agree well with experimental data and demonstrate the validity of such a model for studying the influence of biomass on the propagation to the surface of light generated through bioluminescence. The radiative transfer equation for the irradiance at the sea surface resulting from illumination by a point source embedded in the water is solved by Monte Carlo techniques. The solution technique is validated through comparison with an asymptotic analytic solution for isotropic scattering. The computations show that the irradiance distribution just beneath the surface as a function of R, the distance measured along the surface from a point on the surface vertically above the source, is described by two regimes: (1) a regime in which the irradiance is governed mostly by absorption and geometry, with scattering playing a negligible role, the near field; and (2) a regime in which the light field at the surface is very diffuse and the irradiance decays approximately exponentially in R, with a decay coefficient K_∞, and is a very weak function of the source depth, the diffusion regime. The near field is of primary interest because it contains most of the power reaching the sea surface.

An analytical model of the irradiance distribution just beneath the surface as a function of R, the source depth, and the pigment concentration for the near field is presented. This model is based on the observation that at most scattering events the change in the photon's direction is slight and, therefore, ineffective in attenuating the irradiance. A solution for the irradiance from the point source, then, is first carried out ignoring scattering altogether; however, recognizing that backscattering will attenuate the irradiance, the absorption coefficient is replaced by an effective attenuation coefficient k. This effective attenuation coefficient is determined by fitting the total power just beneath the surface determined from the Monte Carlo computations to the analytical model. The resulting k is closely related to K_d, with $k \approx a + b_b$ for small source depths, and $k \to K_\infty$ as the source depth becomes very large. A relationship is developed giving k as a function of the source depth and the pigment concentration, which reproduces the total power incident on the surface with remarkable precision. Using k determined in this manner, the Monte Carlo irradiance as a function of R and source depth in the near-field regime can be approximated with high accuracy. These results indicate that K_d can be estimated at night by releasing a point source in the water, measuring the irradiance at the surface as it sinks, and fitting the measurements to the relationships developed here to determine k. The analytic model also enables estimation of the source depth and power from the irradiance distribution just beneath the surface.

The irradiance exiting the water was also determined in the Monte Carlo simulations, but in this case the usefulness of the analytical model is limited because it predicts that the exiting irradiance is zero for values of R greater than $R_c \equiv z_0 \tan\theta_c$, where θ_c is the critical angle for total internal reflection. When the depth of the source is small, only an insignificant amount of power falls outside a circle of radius R_c, but when it is large this is not always the case and the analytic model can lead to significant errors in the estimation of the total power exiting the ocean. However, for $R < R_c$ the analytical model fits the Monte Carlo computed irradiance above the surface with excellent accuracy.

This work received support from the Office of Naval Research under contract N00014-84-K-0451 as part of the Biowatt Program.

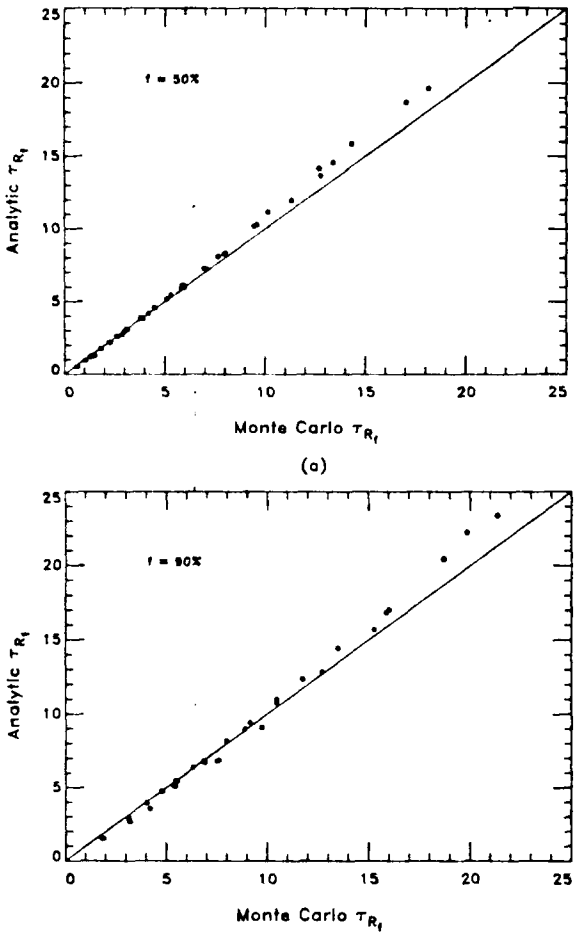

Fig. 14. Comparison between the analytic approximation to the radius of the circle at the sea surface, $\tau_{R_f} \equiv cR_f$, containing a fraction f of the total power, plotted as a function of the source optical depth $\tau_z \equiv cz_0$. In this case k has been approximated by K_{surf}: (a) $f = 50\%$; (b) $f = 90\%$.

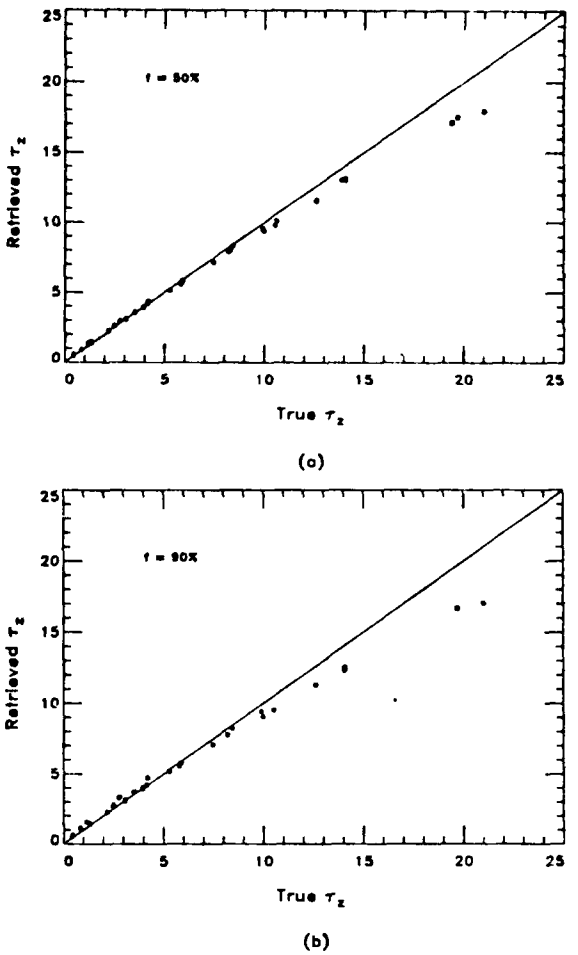

Fig. 15. Comparison between the source optical depth, $\tau_z \equiv cz_0$, retrieved by inverting Eq. (36) for various pigment concentrations and source physical depths: (a) $f = 50\%$; (b) $f = 90\%$.

Appendix: Surface Estimation of the Source Depth and Power

Figure 10 suggests the possibility of remote estimation of the emission depth given $P(R)/P_{total}$, i.e., if k were known, z_0, the emission depth, could be determined remotely from observations of the spot size R_f. The difficulty, however, is in the determination of k, since this requires knowing z_0, i.e., Eq. (33). Thus it is of interest to know how well the analytic formulation predicts τ_{R_f} without using z_0 to compute k. A reasonable approximation to k is K_{surf}, which, although it does not produce as good a fit to the total power as that determined using Eqs. (31)–(33) (Fig. 8), yields a $[E_u(\tau_R,\tau_z)]_N$ as a function of τ_R and τ_z having the correct shape. Figure 14 compares the Monte Carlo and analytic determinations of τ_{R_f} using Eq. (36) with $k = K_{surf}$. The results show only a slight degradation from those in Fig. 11 obtained using the optimum value of k. In both cases ($f = 50$ and 90%) most of the degradation occurs for larger values of τ_{R_f}, for which the approximate formulation ($k = K_{surf}$) overestimates the value of τ_{R_f} given τ_z. Figure 15 shows the τ_z retrievals from the Monte Carlo determined τ_{R_f} derived by inverting Eq. (36) with $k = K_{surf}$. Clearly, such an inversion appears possible for moderate values of τ_z, i.e., $\tau_z \leq 10$, even in the presence of the noise inherent in the Monte Carlo simulations. This inversion in the presence of Monte Carlo noise suggests that it may be feasible in the real ocean.

Another possibility for inverting the irradiance distribution is to use the pigment concentration to determine K_{surf} using Eq. (16d). This would approximate the K_d value, which would actually be measured (during the day with the sun near the zenith) near the surface. Figure 16 shows the result of using this K_{surf} to retrieve z_0. The retrievals become progressively poorer at all source depths as the pigment concentration increases, i.e., the retrieval becomes poorer as τ_z increases. Nevertheless, the retrievals are remarkably accurate with $-0.15 \leq \delta z_0/z_0 \leq 0.08$ for $f = 50\%$ and $0.05 \leq C \leq 1$ mg/m^3. This is particularly impressive for the case where $z_0 = 120$ m and $C = 1$ mg/m^3 for which $c = 0.46$ m^{-1}, $\tau_z = 55.2$, and the probability that a photon will reach the surface without interacting with the medium is $<10^{-24}$! Note that the value of the

eam attenuation coefficient c is not used anywhere in ıese retrievals.

Once z_0 is determined, the power emitted by the ɔurce (W/nm) can be estimated by adapting Eq. (30) ɔ a source of power P_0, i.e.,

$$P_{\text{total}} = \frac{P_0}{2} E_2(K_{\text{surf}} z_0).$$

It is unlikely that this inversion can be extended to ıeasurements of the upwelling irradiance above the urface, because the analytic model does not provide a ood approximation to the irradiance at large R, and he distribution above the sea surface will be a function f the surface roughness.

lote added in proof: The angle θ shown in Fig. 2 is incorrect. θ is ıe angle between nadir and the photon direction, i.e., the correct ngle θ is the supplement of the angle shown in the figure.

leferences

1. K. M. Case, "Transfer Problems and the Reciprocity Principle," Rev. Mod. Phys. **29**, 651 (1957).
2. A. Morel and L. Prieur, "Analysis of Variations in Ocean Color," Limnol. Oceanogr. **22**, 709 (1977).
3. By the term chlorophyll *a* we mean the concentration (mg/m^3) of chlorophyll *a* and all chlorophyll-like pigments which absorb in the same spectral bands as chlorophyll *a*, such as phaeophytin *a*, and are contained in phytoplankton or in their detrital materials. The sum of the concentrations of chlorophyll *a* and phaeophytin *a* is frequently used as an indicator of plankton biomass. It is usually referred to as the pigment concentration.
4. K. S. Baker and R. C. Smith, "Bio-optical Classification and Model of Natural Waters. 2," Limnol. Oceanogr. **27**, 500 (1982).
5. A. Morel, "Optical Properties of Pure Water and Pure Sea Water," in *Optical Aspects of Oceanography*, N. G. Jerlov and E. Steemann Nielsen, Eds. (Academic, New York, 1974).
6. A. Morel, "In-water and Remote Measurement of Ocean Color," Boundary-Layer Meteorol. **18**, 177 (1980).
7. H. R. Gordon and A. Y. Morel, *Remote Assessment of Ocean Color for Interpretation of Visible Satellite Imagery: A Review* (Springer-Verlag, New York, 1983).
8. L. Prieur and S. Sathyendranath, "An Optical Classification of Coastal and Oceanic Waters Based on the Specific Absorption of Phytoplankton Pigments, Dissolved Organic Matter, and Other Particulate Materials," Limnol. Oceanogr. **26**, 671 (1981).
9. R. C. Smith and K. S. Baker, "The Bio-optical State of Ocean Waters and Remote Sensing," Limnol. Oceanogr. **23**, 247 (1978).
0. R. C. Smith and K. S. Baker, "Optical Classification of Natural Waters," Limnol. Oceanogr. **23**, 260 (1978).
1. L. A. Hobson, D. W. Menzel, and R. T. Barber, "Primary Productivity and the Sizes of Pools of Organic Carbon in the Mixed Layer of the Ocean," Mar. Biol. **19**, 298 (1973).
2. S. Sathyendranath, "Influence des Substances en Solution et en Suspension dans les Eaux de Mer sur L'absorption er La Reflectance. Modelisation et Applications a'la Teledetection," Ph.D. Thesis, 3rd cycle, U. Pierre et Marie Curie, Paris (1981), 123 pp.
3. A. Bricaud, A. Morel, and L. Prieur, "Optical Efficiency Factors of Some Phytoplankters," Limnol. Oceanogr. **28**, 816 (1983).
4. In general phytoplankton scattering will not satisfy the law $B_C(\lambda) \sim \lambda^{-n}$ for a constant value of n over the entire visible spectrum. This law is used here only to provide an analytical representation of the possible spectral behavior over this very limited portion of the spectrum.
5. T. J. Petzold, *Volume Scattering Functions for Selected Natural Waters*, Scripps Institute of Oceanography, Visibility Laboratory, San Diego, CA 92152, SIO Ref. 72-78 (1972).

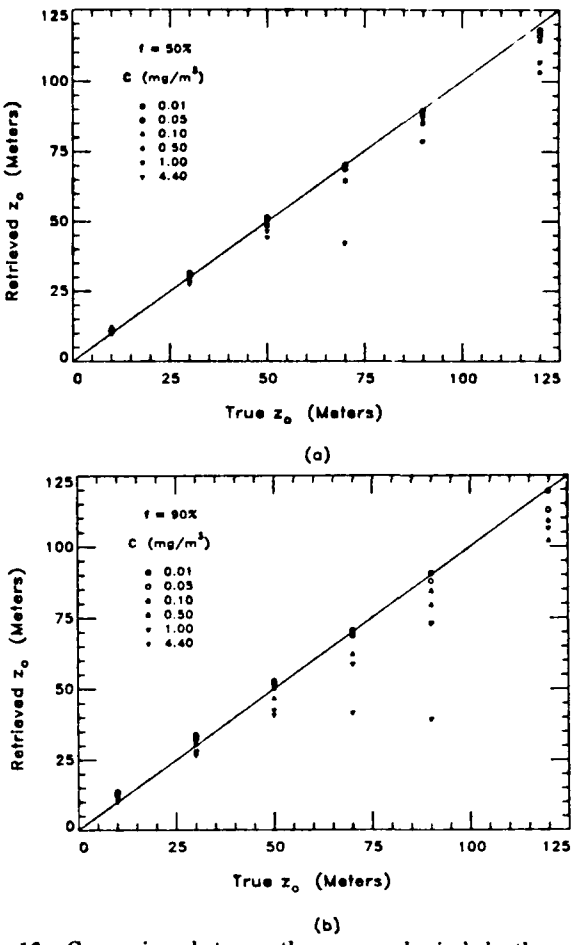

Fig. 16. Comparison between the source physical depth z_0 retrieved by inverting Eq. (36) for various pigment concentrations: (a) $f = 50\%$; (b) $f = 90\%$.

16. H. R. Gordon, "Ship Perturbation of Irradiance Measurements at Sea. 1: Monte Carlo Simulations," Appl. Opt. **24**, 4172 (1985).
17. By the term exact, we mean in the sense that the solutions are given in terms of functions which can be evaluated numerically, e.g., Chandrasekhar's[18] H function.
18. S. Chandrasekhar, *Radiative Transfer* (Dover, New York, 1960).
19. J. P. Elliott, "Milne's Problems with a Point Source," Proc. R. Soc. London Ser. A **228**, 424 (1955).
20. C. Mark, "Neutron Density Near a Plane Surface," Phys. Rev. **72**, 558 (1947).
21. R. W. Preisendorfer, *Hydrological Optics. Vol. III: Solutions.*, PB-259795/3ST (National Technical Information Service, U.S. Department of Commerce, 5285 Port Royal Rd., Springfield, VA 22161 (1976).
22. R. W. Preisendorfer, "On the Existence of Characteristic Diffuse Light in Natural Waters," J. Mar. Res. **18**, 1 (1959).
23. M. Abramowitz and I. A. Stegun, *Handbook of Mathematical Functions* (Dover, New York, 1965).
24. G. Beardsley and J. R. V. Zaneveld, "Theoretical Dependence of the Near-Asymptotic Apparent Optical Properties on the Inherent Optical Properties of Sea Water," J. Opt. Soc. Am. **59**, 373 (1969).
25. L. Prieur, "Transfert radiatif dans les eaux de mer. Application a la determination de parametres optiques caracterisant leur teneur en substances dissoutes et leur contenu en particules," D.Sci. Thesis, U. Pierre et Marie Curie (1976), 243 pp.

Appendix 2

H.R. Gordon, Influence of Vertical Stratification on the Distribution of Irradiance at the Sea Surface from a Point Source in the Ocean, *Applied Optics*, **27**, 2643–2645 (1988).

Influence of vertical stratification on the distribution of irradiance at the sea surface from a point source in the ocean

Howard R. Gordon

University of Miami, Physics Department, Coral Gables, Florida 33124.

Received 25 November 1987.
0003-6935/88/132643-03$02.00/0.

In this Letter, a bio-optical[1] model describing the distribution of irradiance at the sea surface resulting from a point source embedded in a homogeneous ocean is extended to a stratified ocean. In particular, the phytoplankton pigment concentration[2] C is allowed to vary with depth. Briefly, following Ref. 1, the absorption $a_C(z,\lambda)$ and scattering $b_C(z,\lambda)$ coefficients of the phytoplankton and their immediate detrital material at a wavelength λ are given by

$$b_C(z,\lambda) = B_C(\lambda)C(z)^{0.62},$$
$$a_C(z,\lambda) = 0.06A_C(\lambda)C(z)^{0.602}, \quad (1)$$

where z is depth, $A_C(\lambda)$ is the absorption coefficient of plankton pigments normalized to that at 440 nm, and $B_C(\lambda) = 0.3(550/\lambda)$. b_C and a_C have units of m^{-1} when λ is in nanometers and C is in mg/m^3. The beam attenuation coefficient $c(z,\lambda)$ is then

$$c(z,\lambda) = a_w(\lambda) + b_w(\lambda) + a_C(\lambda,z) + b_C(\lambda,z), \quad (2)$$

where $a_w(\lambda)$ and $b_w(\lambda)$ are, respectively, the scattering coefficients for pure seawater. The scattering phase function for the particles is taken from Ref. 1 and is independent of depth and pigment concentration. However, the total scattering phase function (water plus particles) does depend on z because the relative importance of scattering by particles and water depends on $C(z)$. The radiative transfer equation is solved by Monte Carlo techniques to describe the distribution of irradiance at the surface produced by a point source of unit power (1 W/nm) at a depth z_0. Specifically, the irradiance distribution just beneath the surface $E_u(R,z_0)$ is determined as a function of R, the distance measured along the surface from a point vertically above the source. Figure 1 shows the results of four Monte Carlo simulations at 480 nm [$A_C(480) = 0.798$] in which the source was at $z_0 = 30$ m, and the pigment concentration was (a) 0.5 mg/m^3 from 0 to 10 m and 0.1 mg/m^3 elsewhere, (b) 0.5 mg/m^3 from 10 to 20 m and 0.1 mg/m^3 elsewhere, (c) 0.5 mg/m^3 from 20 to 30 m and 0.1 mg/m^3 elsewhere, and (d) a uniform distribution of pigments with a concentration equal to the mean concentration in (a), (b), and (c) above the source (0.2333 mg/m^3). The computations presented in Fig. 1 clearly show that the vertical distribution of pigments is unimportant in determining the irradiance distribution at the surface; only the mean pigment concentration and the source depth appear to be relevant.

In Ref. 1 a simple analytical model was presented for computing the irradiance distribution from a point source of unit power embedded in a homogeneous ocean. It consisted of computing the distribution in the absence of scattering and replacing the absorption coefficient by an effective attenuation coefficient k, i.e.,

$$E_u(R,z_0) = \frac{1}{4\pi}\frac{z_0}{X^3}\exp(-kX), \quad (3)$$

where $X^2 = R^2 + z_0^2$ and

$$k = \gamma(z_0)K_{surf} + [1 - \gamma(z_0)]K_\infty, \quad (4)$$

with K_{surf} and K_∞ being the downwelling irradiance attenuation coefficients, respectively, just beneath the surface and in the asymptotic regime. $\gamma(z_0)$ is given by

$$\gamma(z_0) = \exp(-0.08\,K_{surf}z_0), \quad (5)$$

$$K_{surf} = a_w + a_C + 0.5b_w + (b_b)_C b_C, \quad (6)$$

where $(b_b)_C$ is the backscattering probability associated with the particle scattering phase function. K_∞ was approximated by

$$K_\infty = K_{surf} + 0.09c. \quad (7)$$

The model reproduced both the distribution $E_u(R,z_0)$ in the nondiffusion regime and the total power reaching the surface,

$$P_{total} = \int_0^\infty 2\pi E_u(R,z_0)RdR = \frac{1}{2}E_2(kz_0),$$

where E_2 is the exponential integral, with high accuracy. Since Fig. 1 shows that $E_u(R,z_0)$ is apparently independent of the stratification in C, one expects that the analytical model should apply equally well in the presence of the stratification if a suitable value of k can be found. Indeed, the following provides a straightforward procedure for the determination of k by considering an equivalent homogeneous ocean.

First, an effective pigment concentration $\langle C\rangle$ is defined to be the (constant) value of C, which, for a homogeneous ocean and given source depth z_0, would yield the same value for the source optical depth τ as the stratified ocean, i.e.,

$$\tau(\lambda) = \int_0^{z_0} c(z,\lambda)dz \equiv \langle c(\lambda)\rangle z_0, \quad (8)$$

where $c(z,\lambda)$ is found by inserting the pigment profile $C(z)$ into Eqs. (1) and (2), and $\langle c(\lambda)\rangle$ is the beam attenuation coefficient for the equivalent homogeneous ocean. Next $c(z,\lambda)$ and $C(z)$ in Eqs. (1) and (2) are replaced by $\langle c(\lambda)\rangle$ and $\langle C\rangle$, respectively, and solved for $\langle C\rangle$. Finally, this value of $\langle C\rangle$ is used in Eqs. (3)–(7) [which also employ Eqs. (1) and (2) with $C(z)$ replaced by $\langle C\rangle$] to estimate k.[3] An example of the performance of the analytical model using this procedure with a realistic pigment profile[4] is presented in Figs. 2 and 3. The source is assumed to be located just below the pigment maximum at $z_0 = 64$ m and is marked with a dot in Fig. 2. The results of a Monte Carlo simulation (noisy curve) and the analytical model (smooth curve) for $E_u(R,z_0)$ are shown in Fig. 3, and the excellent agreement suggests that the analytical model can provide a good approximation to the time-independent Green's function for an internal source even in the case of a stratified ocean.

In sum, the vertical distribution of pigments is unimportant in determining the horizontal distribution of irradiance (and P_{total}) from a point source in the water. Also, the simple model for computing the irradiance distribution presented in Ref. 1 provides excellent agreement with the exact results computed using Monte Carlo techniques when the pigment concentration is replaced by (a constant) $\langle C\rangle$.

This work received support from the Office of Naval Research under contract N00014-84-K-0451 as part of the Biowatt Program.

References

1. H. R. Gordon, "Bio-optical Model Describing the Distribution of Irradiance at the Sea Surface Resulting from a Point Source Embedded in the Ocean," Appl. Opt. 26, 4133 (1987).

2. By the term pigment concentration we mean the concentration (mg/m^3) of chlorophyll a and all chlorophyll-like pigments, which absorb in the same spectral bands as chlorophyll *a*, such as phaeophytin *a*, and which are contained in phytoplankton or in their detrital materials. The sum of the concentrations of chlorophyll *a* and phaeophytin *a* is frequently used as an indicator of phytoplankton biomass.
3. Note that

$$\langle C \rangle \neq \bar{C} \equiv z_0^{-1} \int_0^{z_0} C(z)dz,$$

the mean pigment concentration, because the dependence of $b_C(z,\lambda)$ and $a_C(z,\lambda)$ on C in Eq. (1) is nonlinear.
4. E. Swift, U. Rhode Island; personal communication.

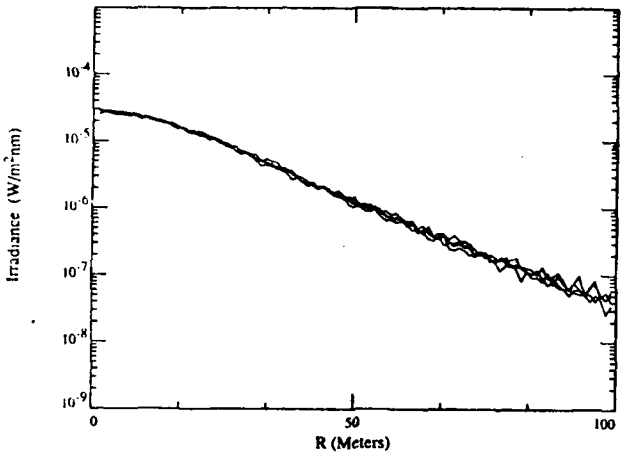

Fig. 1. Irradiance distribution at the surface for four different pigment profiles having the same total amount of pigment above the source (see text for details).

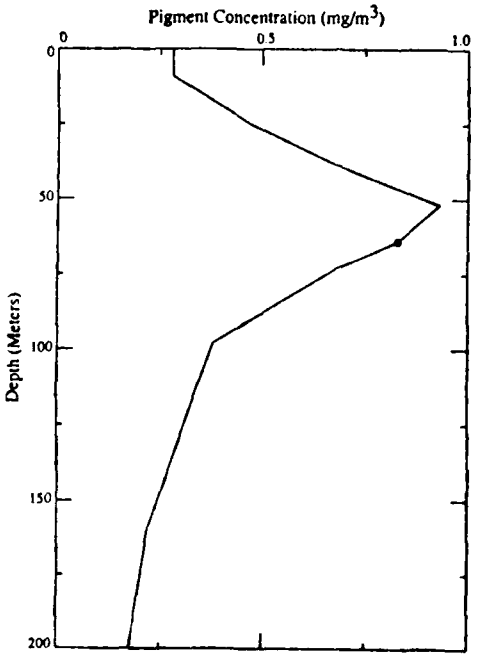

Fig. 2. Pigment concentration as a function of depth for the irradiance distribution in Fig. 3. The dot at 64 m represents the position of the source.

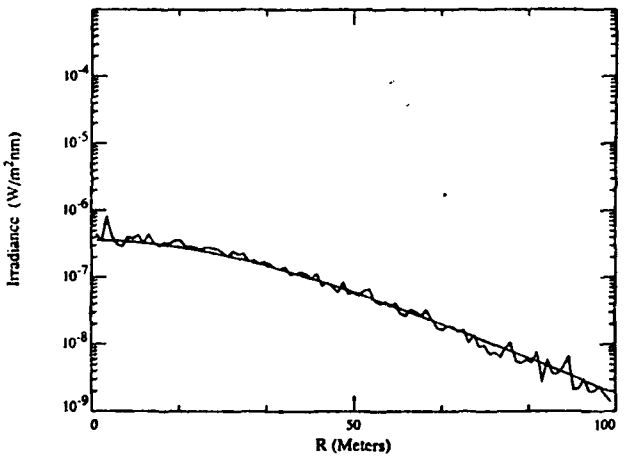

Fig. 3. Irradiance distribution at the surface for the pigment profile in Fig. 2. The noisy curve represents the results of a Monte Carlo simulation, and the smooth curve is the result of the analytical model [Eqs. (3)–(7)].

Appendix 3

H.R. Gordon, Can the Lambert-Beer Law Be Applied to the Diffuse Attenuation Coefficient of Ocean Water?, *Limnology and Oceanography* (Submitted).

Running head: Lambert-Beer law applied to K

Can the Lambert-Beer law be applied to the diffuse attenuation coefficient of ocean water?

by

Howard R. Gordon
Department of Physics
University of Miami
Coral Gables, FL 33124

(Submitted to *Limnology and Oceanography*)

Acknowledgement

This work received support from the Office of Naval Research under Contract N00014-84-K-0451 as part of the Biowatt Program and from the National Aeronautics and Space Administration under grant NAGW-273.

List of Symbols

Symbol	Name	Units
a	total absorption coefficient	m^{-1}
a_p	particle absorption coefficient	m^{-1}
a_w	water absorption coefficient	m^{-1}
b	total scattering coefficient	m^{-1}
b_b	total backscattering coefficient	m^{-1}
$\tilde{b_b}$	total backscattering probability	
b_p	particle scattering coefficient	m^{-1}
b_w	water scattering coefficient	m^{-1}
$\beta(\Theta)$	total volume scattering function	$m^{-1}Ster^{-1}$
$\beta_p(\Theta)$	particle volume scattering function	$m^{-1}Ster^{-1}$
$\beta_w(\Theta)$	water volume scattering function	$m^{-1}Ster^{-1}$
c	total attenuation coefficient $(a+b)$	m^{-1}
c_p	particle attenuation coefficient (a_p+b_p)	m^{-1}
c_w	water attenuation coefficient (a_w+b_w)	m^{-1}
c_i	attenuation coefficient of component i	m^{-1}
c_i^*	specific attenuation coefficient c_i/C_i	m^2mg^{-1}
C	pigment concentration	$mg\ m^{-3}$
C_i	concentration of i^{th} constituent	$mg\ m^{-3}$
D_0	downwelling distribution function $(\omega_0 = 0)$	
f	direct sun fraction of $E_d(0)$	
F	total forward scattering probability $(1-\tilde{b_b})$	
F_p	particle forward scattering probability	
F_w	water forward scattering probability	
F_0	extraterrestrial solar irradiance	$mW\ cm^{-2}\mu m^{-1}$
$E_d(z)$	downwelling irradiance at z	$mW\ cm^{-2}\mu m^{-1}$
$K_d(z)$	attenuation coefficient for $E_d(z)$	m^{-1}
K	$K_d(0)$	m^{-1}

Symbol	Name	Units
K_w	pure water component of $K_d(0)$ and $K_d(z)$	m^{-1}
K_p	water component of K	m^{-1}
K_C	pigment component of $K_d(z)$	m^{-1}
K_x	nonpigment-nonwater component of $K_d(z)$	m^{-1}
$\langle K \rangle$	mean $K_d(z)$ from surface to z_{10}	m^{-1}
$\langle K \rangle_w$	water component of $\langle K \rangle$	m^{-1}
$\langle K \rangle_p$	particle component of $\langle K \rangle$	m^{-1}
$\langle K \rangle_B$	Lambert-Beer value of $\langle K \rangle$ ($\langle K \rangle_w + \langle K \rangle_p$)	m^{-1}
$\langle K \rangle_T$	true value of $\langle K \rangle$	m^{-1}
λ	wavelength	nm
$P(\Theta)$	scattering phase function (β/b)	$Ster^{-1}$
$P_p(\Theta)$	particle scattering phase function (β_p/b_p)	$Ster^{-1}$
$P_w(\Theta)$	water scattering phase function (β_w/b_w)	$Ster^{-1}$
σ^2	surface slope variance	
t	Fresnel transmittance of sea surface	
τ	optical depth ($\tau = cz$)	
τ_{10}	optical depth at 10% surface irradiance (cz_{10})	
τ_A	aerosol optical thickness of atmosphere	
τ_{Oz}	ozone optical thickness of atmosphere	
τ_R	Rayleigh optical thickness of atmosphere	
Θ	scattering angle	
ϑ_0	solar zenith angle	
ϑ_{0w}	solar zenith angle below surface	
ω_0	total scattering albedo (b/c)	
ω_p	particle scattering albedo (b_p/c_p)	
ω_w	water scattering albedo (b_w/c_w)	
z	depth	m
z_{10}	depth at 10% surface irradiance	m
z_x, z_y	surface slope components	

Abstract

The transport of radiation in a realistic ocean-atmosphere system is simulated, and the results are treated as experimental data, to show that the downwelling irradiance attenuation coefficient just beneath the surface K and the mean irradiance attenuation coefficient from the surface to the depth where the irradiance falls to 10% of its value at the surface $\langle K \rangle$ can be corrected for the geometric structure of the in-water light field to yield quantities that are, to a high degree of accuracy, inherent optical properties. These geometry-corrected quantities are shown to satisfy the Lambert-Beer law to a reasonable degree of accuracy, with the largest error ($\approx 15\%$) in the case of $\langle K \rangle$ arising from mixing nonabsorbing particles, e.g., white sand, with strongly absorbing water (wavelengths > 600 nm). This near-validity of the Lambert-Beer law, when there are compelling reasons to believe that it should fail, is shown to result from three *independent* facts: (1) the dependence of the diffuse attenuation coefficients on the geometric structure of the light field can be removed; (2) pure sea water is a much better absorber than scatterer at optical frequencies; and (3) the phase functions for particles suspended in the ocean differs significantly from that of pure sea water. Finally, it is shown that extrapolation of the corrected diffuse attenuation coefficients to the limit $c \to c_w$ yields quantities which are within 2% the corresponding quantities that would be measured for an ocean consisting of pure sea water with the sun at the zenith and the atmosphere removed.

Introduction

In a series of papers, Smith and Baker (Baker and Smith 1982, and references therein) have developed a "bio-optical" model for relating the optical properties of near-surface ocean water to the content of biological material. Specifically, the attenuation coefficient K_d of downwelling irradiance E_d defined by $K_d = -(1/E_d)dE_d/dz$, where z is depth, is related to the phytoplankton pigment concentration C through

$$K_d = K_w + K_C(C) + K_x. \tag{1}$$

C is the concentration (mg/m^3) of chlorophyll a and all chlorophyll-like pigments, which absorb in the same spectral bands as chlorophyll a, such as phaeophytin a, and which are contained in phytoplankton or in their detrital materials. In Equation 1, the Lambert-Beer law applied to K_d, K_w is the contribution to K_d from the water itself, K_x is the contribution from material suspended or dissolved in the water and not covarying with C, and $K_C(C)$ represents the contribution to K_d from phytoplankton and their immediate detrital material. This decomposition of K_d is very attractive for the optical analysis of ocean water because of the relative ease in measuring E_d, the absence of the requirement for absolute radiometry to determine K_d, and the possibility of measuring K_d remotely (Austin and Petzold 1981, Gordon 1982) and even at night (Gordon 1987). To utilize it, measurements of K_d for a given wavelength and from a variety of oceanic waters are plotted as a function of C and the minimum envelope of the resulting curve $[(K_d)_{\min}]$ is assumed to correspond to $K_x = 0$. Taking the limit of $(K_d)_{\min}$ as $C \to 0$ yields K_w. Then, $K_C(C)$ is given by $(K_d)_{\min} - K_w$. [For examples of this procedure see Figure 1 in Baker and Smith (1982) or Figure 7 in Gordon and Morel (1983).] Assuming that $K_C(C)$ is a valid for all waters, Equation 1 can then be applied to specific cases to estimate K_x from K_d and C, or to estimate C from K_d in waters for which K_x is known to be negligible. These latter waters are usually referred to as "Case 1 waters," and are defined to be waters for which the optical properties are controlled by phytoplankton and their immediate detrital material (Gordon and Morel 1983, Morel and Prieur 1977).

Equation 1 has been criticized by Morel and Bricaud (1981) and Stavn (1988) on the basis that, unlike the absorption coefficient and the volume scattering function, K_d is not an inherent optical property of the medium Preisendorfer (1961). This is because it depends on the depth and on the geometric structure of the in-water light field, as well as on the inherent optical properties

of the medium. Since a given K_d is unique only to the particular situation in which it is measured, and there is no reason to expect that the three components of K_d will vary in the same manner with depth and with the structure of the light field, it is correctly asserted that Eq. 1 is only an approximation. However, Gordon, Brown and Jacobs (1975) have shown with Monte Carlo simulations of the in-water light field, that for simple modes of illumination, i.e., a sky of uniform radiance or a parallel beam of irradiance incident at an angle ϑ_0 with the vertical, the dependence of K_d on the structure of the light field can be removed without any knowledge of the optical properties of the medium. Because of this, they called the light field-corrected K_d a *quasi-inherent* optical property of the medium. Later, Gordon (1976) showed that the correction factor required to remove the light field dependence from K_d could be reasonably accurately computed by knowing only the relative amounts of skylight and direct sunlight incident on the sea surface in the spectral band in question. Later, Baker and Smith (1979) directly verified that for turbid water under clear skies with the sun near the zenith, K_d was nearly independent of ϑ_0. Finally, Gordon (1980) demonstrated that for a stratified ocean with sun at the zenith, the value of K_d at a given depth z depended mostly on the inherent optical properties of the medium at that depth, i.e., K_d is a *local* property of the medium. These observations concerning the quasi-inherent nature of K_d suggest that if K_d-values corrected for variations in the illumination, e.g., corrected so that the resulting K_d is that value which would be measured in the same ocean illuminated by the sun at the zenith in the absence of the atmosphere (no sky light), are used in Eq. 1 the error resulting from the fact that K_d is not a true inherent optical property would be considerably reduced. However, a residual error would still remain in Eq. 1 because K_d depends on depth.

In this paper the earlier computations (Gordon, Brown and Jacobs 1975) of K_d are extended to cases of more realistic illumination of the surface and a more realistic model of the inherent optical properties of the water itself. The results confirm that when K_d for the water is measured either just beneath the surface, or an average value is determined between the surface and the depth where the surface irradiance is reduced to 10% of its value at the surface, the resulting K_d's can be corrected to yield a quantity that can be directly expressed in terms of the *inherent* optical properties of the medium. Furthermore, this quantity is shown to depend nearly linearly on the inherent optical properties of the medium, which are linearly additive over the constituents, and so it satisfies the Lambert-Beer law with reasonable accuracy. Finally, the results show that the value of K_ω determined by extrapolation of K_d to $C = 0$ in Case 1 waters is in fact very nearly equal to the value of K_d that would be measured in an ocean consisting of only pure sea water.

Optical Model of the Ocean-Atmosphere System

Our study of the efficacy of Equation 1 is based on simulating the transfer of radiation in the ocean-atmosphere system by Monte Carlo techniques. Such simulations provide the distribution of radiation in the entire system. The radiation field is treated as experimental data, albeit data collected under carefully controlled conditions, a cloud free sky and a homogeneous ocean of precisely known inherent optical properties, from which the irradiances, K_d, etc., can be derived as a function of the inherent optical properties of the ocean and ultimately as a function of the constituent concentrations. To accomplish this, optical models of the ocean and the atmosphere that are as realistic as possible are required. Such models are described below..

A. The Ocean

Water and its constituents influence K_d through their effect on the inherent optical properties of the medium: a the absorption coefficient; and $\beta(\Theta)$ the volume scattering function. For simplicity, we limit the modeling of these properties to Case 1 waters. Moreover, we also limit the model to those waters for which optically active dissolved organic materials — yellow substances — are absent. The rational for this is that the effect of yellow substance absorption on the results would be identical to that of increasing the absorption coefficient of pure sea water by an appropriate amount. Therefore, the medium is described by an absorption coefficient given by

$$a = a_w + a_p, \tag{2}$$

where the subscripts w and p here, and hereafter, refer to the contribution from water and suspended particles, respectively, and a volume scattering function given by

$$\beta(\Theta) = \beta_w(\Theta) + \beta_p(\Theta), \tag{3}$$

where Θ is the scattering angle. The total scattering coefficient b is defined by

$$b = 2\pi \int_0^\pi \beta(\Theta) \sin\Theta \, d\Theta, \tag{4}$$

and $b = b_w + b_p$. The total attenuation coefficient is defined to be

$$c = c_w + c_p = a + b. \tag{5}$$

It is convenient to define two other auxiliary parameters, the single scattering albedo $\omega_0 = b/c$ and the scattering phase function $P(\Theta) = \beta(\Theta)/b$. The value of ω_0 is the probability that at each interaction within the medium the photon will be scattered rather than absorbed, while

$$2\pi \int_{\Theta_1}^{\Theta_2} P(\Theta) \sin\Theta \, d\Theta$$

is the probability that, when a photon is scattered, the scattering angle will be between Θ_1 and Θ_2. A quantity which is needed later, the backscattering probability $\tilde{b}_b$, is defined by

$$\tilde{b}_b = 2\pi \int_{\pi/2}^{\pi} P(\Theta) \sin\Theta \, d\Theta, \tag{6}$$

and is, therefore, seen to be the probability that a photon is scattered through an angle larger than $90°$. The backscattering coefficient, b_b, is then given by $b_b = b\tilde{b}_b$.

It is easy to verify from the radiative transfer equation that for a homogeneous ocean the internal radiation field is completely specified by providing c, ω_0, $P(\Theta)$, and the distribution of radiation incident on the sea surface, and also that the field depends on depth only through the product cz. $P(\Theta)$ and ω_0 can be related to the similar water and particle quantities $P_w(\Theta)$, $P_p(\Theta)$, ω_w, and ω_p, through

$$\omega_0 = \frac{\omega_p(c_p/c_w) + \omega_w}{c_p/c_w + 1}, \tag{7}$$

and

$$\omega_0 P = \frac{\omega_p P_p(c_p/c_w) + \omega_w P_w}{c_p/c_w + 1}. \tag{8}$$

Thus, in this simple model, given c_w, c_p, ω_w, ω_p, $P_w(\Theta)$, and $P_p(\Theta)$, representing the inherent optical properties of the water and the particles, ω_0 and $P(\Theta)$ are specified by the ratio c_p/c_w. This ratio is proportional to the particle concentration.

Experimental measurements must be used to provide a realistic parameterization of the optical properties ω_w, ω_p, $P_w(\Theta)$, and $P_p(\Theta)$. The model used here is identical to that developed by the author (Gordon 1987) to study the propagation of irradiance from a point source embedded in the ocean. Briefly, the absorption coefficient a_w has been inferred from measurements of downwelling and upwelling irradiance in oligotrophic waters such as the Sargasso Sea (Baker and Smith 1982, Morel and Prieur 1977, Prieur and Sathyendranath 1981), and the scattering coefficient b_w and the volume scattering function $\beta_w(\theta)$ have been measured directly for pure water and for saline solutions of pure water corresponding to salinities between 35 and 39 ppt by Morel (1974). The

resulting a_w, b_w and ω_w are given in Table 1 for the wavelengths used in the present computations. Note that these values of ω_w represent the *upper limit* of the scattering albedo for water plus any *dissolved* material such as yellow substances, since the small concentrations of dissolved material typically found in sea water can contribute to the absorption coefficient but not to the scattering coefficient. The scattering phase function for pure sea water is taken from Morel (1974).

The optical properties of the suspended particles for Case 1 waters, can be related to the pigment concentration. The scattering coefficient of particles at 550 nm, $b_p(550)$, is nonlinearly related to the pigment concentration C through (Morel 1980)

$$b_p = B_C C^{0.62}, \tag{9}$$

where $b_p(550)$ is in m^{-1} and C is in mg/m^3, (See, also, Gordon and Morel (1983)). The constant B_C, the scattering coefficient at a pigment concentration of 1 mg/m^3, ranges from 0.12 to 0.45 and has an average value of 0.30. The variation in B_C is due to the natural variability of scattering over the various species of phytoplankton, as well as a variability in scattering by the detrital particles associated with the phytoplankton. Similarly the absorption coefficient of the particles has been studied as a function of C by Prieur and Sathyendranath (1981) yielding for $C < 10$ mg/m^3:

$$a_p(\lambda) = 0.06 A_C(\lambda) C^{0.602}, \tag{10}$$

where $a_p(\lambda)$ is in m^{-1} and C is in mg/m^3. In this equation $A_C(\lambda)$ is the absorption coefficient of phytoplankton normalized to 440 nm, *i.e.*,

$$A_C(\lambda) = \frac{a_p(\lambda)}{a_p(440)}. \tag{11}$$

These nonlinear relationships between b_p and C and a_p and C are believed to be due to a systematic variation in the ratio of the concentration of phytoplankton to that of detrital material as a function of the concentration of phytoplankton (Hobson, Menzel and Barber 1973, Smith and Baker 1978a). The relative absorption of phytoplankton $A_C(\lambda)$ deduced by Prieur and Sathyendranath (1981) agrees well with absorption measurements made on phytoplankton cultures by Sathyendranath (1981). Note that $a_p(\lambda)$ includes both phytoplankton and their detrital material and thus represents the absorption of all components other than the water itself.

Since $b_p(\lambda)$ and $a_p(\lambda)$ vary with pigment concentration in nearly the same manner, $b_p(\lambda)/a_p(\lambda)$ is nearly independent of the pigment concentration, i.e.,

$$\frac{b_p(\lambda)}{a_p(\lambda)} \approx 16.6 \frac{B_C(\lambda)}{A_C(\lambda)}. \tag{12}$$

This provides an estimate of $\omega_p(\lambda)$, and shows that this quantity is, in the first approximation, *independent* of the pigment concentration. At 550 nm, where B_C is known, this yields $\omega_p(550) = 0.933$ in good agreement with the range for those measured by Bricaud, Morel and Preiur (1983) for four species of cultured phytoplankton: $0.89 \leq \omega_p(550) \leq 0.97$. In order to fix reasonable values of $\omega_p(\lambda)$ at the other wavelengths of interest, the variation of B_C with λ is required. Following Gordon (1987) we assume $B_C(\lambda)$ obeys a power law with wavelength, i.e., $B_C(\lambda) \propto \lambda^{-n}$, and take $n = +1$. This yields $B_C(480) \approx 0.34$ and $B_C(440) \approx 0.38$. The resulting values of $\omega_p(\lambda)$ and $\omega_w(\lambda)$ used in the computations are provided in Table 2. It should be noted that the assumption $B_C(\lambda) \propto \lambda^{-1}$ often overestimates the dependence of b_c on λ since the scattering by absorbing particles, e.g., phytoplankton, tends to be *depressed* in the pigment absorption bands (Bricaud, Morel and Preiur 1983). This depression of scattering would make $\omega_p(440)$ and $\omega_p(480)$ in smaller than given in Table 2; however, the effect is not large, e.g., changing n from $+1$ to -1 only reduces $\omega_p(440)$ from 0.86 to 0.80. To insure that wide departures of ω_p from those used in Table 2 do not influence the results of this work, simulations also have been carried out for $\omega_p(480) = 0.5$, 0.7, and 0.99.

The particle phase function is the most difficult quantity to parameterize because it requires the individual phase functions of the plankton and the detrital material, neither of which have ever been measured in the field. Thus, we must rely on measurements of the total particle phase function (plankton plus detrital material). Measurements of the volume scattering function at 530 nm have been made for waters in several locations with very different turbidities (total scattering coefficients) by Petzold (1972). When the scattering by pure sea water is subtracted, the resulting particle phase functions are very similar, having a standard deviation which is within about 30% of the mean, over waters for which the particle scattering coefficient varied over a factor of 50. This mean particle phase function derived from Petzold's measurements is adopted for this study and designated by the symbol "M." Also, two other particle phase functions are used to represent the extremes of the phase functions given by Petzold's measurements. These are (1) the mean of three phase functions measured in the turbid waters of San Diego Harbor and designated by "T," and (2) a phase function measured in the clear waters of the Tongue of the Ocean, Bahamas, and

designated by "C." The three particle phase functions are shown in Figure 1 along with the phase function for scattering by the water itself $(P_w(\Theta))$. It is seen that these model phase functions differ principally in their scattering at angles greater than 25°. The backscattering probabilities, $\widetilde{(b_b)_p}$, associated with them are 0.0120, 0.0144, and 0.0181, respectively for C, M, and T.

This completes the specification of the quantities needed for the simulation: ω_w, ω_p, $P_w(\Theta)$, and $P_p(\Theta)$. Varying the parameter c_p/c_w from 0 to ∞ results in models which range from a particle free ocean to an ocean in which the optical properties of the particles are completely dominant. This parameter can be related to the pigment concentration through the bio-optical model by noting that $c_p = a_p + b_p$ and using Equations 9 and 10. The result is

$$\frac{c_p(\lambda)}{c_w(\lambda)} \simeq \gamma(\lambda)\, C^{0.6}, \tag{13}$$

where $\gamma(\lambda) = 22.4$, 18.5, and 4.9 at 440, 480, and 550 nm, respectively.

B. The Atmosphere

The atmosphere influences K_d by distributing a portion of the near-parallel solar beam over the entire upward hemisphere, i.e., in producing sky light from direct sunlight. In order to simulate the angular distribution of radiation entering the ocean, an atmospheric model is required. This model atmosphere consisted of fifty layers and included the effects of aerosols, ozone, and Rayleigh scattering, vertically distributed according to data taken from the work of Elterman (1968). The aerosol phase functions were computed by Fraser (R. Fraser, NASA/GSFC, Personal Communication) from Mie theory using the Deirmendjian (1969) Haze C size distribution. This model simulates optical properties of the cloud-free atmosphere only.

Computations and Properties of K_d

The model presented above is used to specify hypothetical ocean-atmosphere systems for which the radiative transfer equation is solved by Monte Carlo techniques to provide the internal radiation field. The radiation field is then treated as experimental data and used to derive the quantities of interest. In most of the simulations the ocean is flat. The various model oceans are specified

by allowing the pigment concentration C to vary from 0 to about 4.5 mg/m^3 which in turn causes c_p/c_w to vary according to Eq. 13. This variation in c_p/c_w then induces variations in ω_0 and $P(\Theta)$ determined by Equations 7 and 8. Figure 2 shows, for example, the change in the shape of the total phase function at 480 nm as c_p/c_w is varied from 0 to 100. Note how the phase function deviates strongly from that of pure water (Rayleigh scattering) even when $c_p/c_w = 1$, i.e., even when the total attenuation is shared equally between water and particles.

From the Monte Carlo solution of the transfer equation the irradiance as a function of depth can be estimated. Actually, $E_d(\tau)$, where τ is called the *optical depth* ($\tau = cz$), is computed in the simulations. The irradiance attenuation coefficient K_d can then be determined from

$$\frac{K_d}{c} = -\frac{d\left[\ell n(E_d(\tau))\right]}{d\tau} \tag{14}$$

by numerical differentiation. Individual values of K_d computed at the midpoint of the euphotic zone using particle phase function "T" and c_p/c_w very large, but in the absence of the atmosphere, agree well with the values computed by Kirk (1984). Figure 3 provides some samples of the resulting profiles of the irradiance attenuation coefficient. In these examples K_d/c is computed for $c_p/c_w = 0$, 1.4, and 5.6 for particle phase function "M" at 440 nm with the sun at the zenith. The deepest computed point for each profile corresponds to $\bar{\tau} = 9$. These particular profiles represent a reasonably clear ocean, i.e., $C \leq 0.1$ mg/m^3. The immediate conclusion to be drawn from these simulations is, as mentioned in the introduction, that K_d is dependent on the depth even for a homogeneous ocean. Also, K_d increases more rapidly with z at larger values of c_p/c_w. In fact, from the surface to $z = 100$ m, K_d increases by 2.5%, 10% and 20% for $c_p/c_w = 0$, 1.4, and 5.6, respectively. It is also seen that the rate of increase in K_d is more rapid near the surface. Analysis of K_d just beneath the surface shows that the rate of change of K_d with depth, i.e., $\frac{d(K_d/c)}{dz}$, is approximately $(0.02 \pm 0.005) \times c$.

These computations confirm the argument that K_d cannot be considered an inherent optical property because it depends on depth, and also the suspicion that the manner of the dependence of K_d on depth is a function of the particle concentration. [An exception to this of course is the asymptotic light field ($z \rightarrow \infty$) for which it has been shown (Preisendorfer 1959) that K_d becomes independent of depth.] Thus, if one attempts to use K_d as an inherent optical property, it is

necessary to specify in some manner the depth at which the measured value applies. In the present work, we focus on the irradiance attenuation coefficient (K) just beneath the surface, i.e.,

$$K = \lim_{\tau \to 0} K_d(\tau), \tag{15}$$

and on the average diffuse attenuation coefficient ($\langle K \rangle$) over the upper half of the euphotic zone,

$$\frac{\langle K \rangle}{c} = \frac{\ell n(E_d(\tau_{10})/E_d(0))}{\tau_{10}}, \tag{16}$$

where τ_{10} is the optical depth for which E_d falls to 10% of its value just beneath the surface $[E_d(\tau_{10})/E_d(0) = 0.1]$.

In order to simulate all cloud free situations, the computations have been carried out for solar zenith angles ϑ_0 of 0, 20°, 25°, 30°, 40°, 60° and 80°. Also, to simulate a totally overcast sky, each ocean model has been studied with the atmosphere removed and a totally diffuse light field incident on the sea surface. Thus, only situations with broken clouds are not considered in this work. A sky with broken clouds is particularly difficult to examine because the radiation field is no longer independent of the observer's horizontal position in the medium.

Figures 4 and 5 provide the computations of K/c and $\langle K \rangle/c$, respectively, as a function of ω_0 for 334 simulations comprising a variety of ϑ_0's and C's for each particle phase function and wavelength. Note that $1 - \omega_0 = a/c$, so these figures relate K and $\langle K \rangle$ to the absorption coefficient a. Based on the number of photons contributing to K and $\langle K \rangle$, the statistical uncertainty $\delta K/c$ in K/c is $\approx \pm 0.017$, while the *relative* error $\delta\langle K \rangle$ in $\langle K \rangle$ is approximately ± 0.006, i.e., $\delta\langle K \rangle / \langle K \rangle \approx \pm 0.006$. Although a strong trend of increasing K/c and $\langle K \rangle/c$ with an increasing absorption component in the total attenuation is observed, it is clear, as expected, that the variation in K and $\langle K \rangle$ cannot be explained solely on the basis of the total absorption and scattering coefficients of the medium alone.

In order to proceed further it is useful to review the results of earlier investigations. Gordon, Brown and Jacobs (1975) found that the dependence of $K_d(\tau)$ on the scattering phase function could be approximately removed by expressing $K_d(\tau)$ as a function of $\omega_0 F$, where F is the forward scattering probability ($F = 1 - \tilde{b}_b$), rather than ω_0 alone. Also, they found that the effect of the nature of the illumination of the ocean on $K_d(\tau)$ could be understood by examining $K_d(\tau)/D_0(\tau)$,

where $D_0(\tau)$ was the downwelling distribution function (Preisendorfer 1961) for a *totally absorbing ocean* with the same surface illumination, i.e.,

$$D_0(\tau) = \frac{E_{0d}(\tau)}{E_d(\tau)} \tag{17}$$

with $\omega_0 = 0$, where E_{0d} is the downwelling *scalar* irradiance. In the revised suggested notation (Morel and Smith 1982) for optical oceanography $D_0(\tau) = 1/\overline{\mu}_d$ for $\omega_0 = 0$, where $\overline{\mu}_d$ is the "average cosine" of the downwelling light field evaluated just beneath the surface. In the study in Gordon, Brown and Jacobs (1975) there was no atmosphere over the ocean, and in that case $D_0(\tau) = 1/\cos\vartheta_{0w}$, where ϑ_{0w} is the solar zenith angle measured *beneath* the sea surface. In the present simulations D_0 depends on wavelength because the amount of skylight produced by scattering in the atmosphere is a function of wavelength. Also, the relative amounts of skylight and direct sunlight depends on ϑ_0. Therefore, D_0 has been computed at each wavelength and for each solar zenith angle by directly solving the transfer equation for the given λ and ϑ_0 with $\omega_0 = 0$. The results of this computation for D_0 just beneath the surface ($\tau = 0$) are provided in Table 3. Note that, as expected, D_0 usually increases with increasing ϑ_0; however, for 440 nm the contribution from the increasing amount of skylight compared to direct sunlight from $\vartheta_0 = 60°$ to $\vartheta_0 = 80°$ actually causes a small decrease in D_0. Also, for $\vartheta_0 \leq 60°$ the difference between $D_0(0)$ and $1/\cos\vartheta_{0w}$ is usually less than about 3%. $D_0(\tau)$ also depends on τ; however, this dependence is of little interest here.

Applying the observations from previous studies to the computations in Figures 4 and 5, Figures 6 and 7 provide K/cD_0 and $\langle K\rangle/cD_0$, respectively, as a function of $1 - \omega_0 F$, where D_0 is the value of $D_0(0)$ taken from Table 3. It is seen that when the computations are presented in this manner, K/cD_0 and $\langle K\rangle/cD_0$ fall on what appear to be *universal* curves. The curves on the figures are least-squares fits of the points to

$$\frac{K}{cD_0} = \sum_{n=1}^{2} k_n (1 - \omega_0 F)^n, \tag{18}$$

and

$$\frac{\langle K\rangle}{cD_0} = \sum_{n=1}^{3} \langle k\rangle_n (1 - \omega_0 F)^n, \tag{19}$$

with $k_1 = 1.0617$, $k_2 = -0.0370$, $\langle k\rangle_1 = 1.3197$ $\langle k\rangle_2 = -0.7559$, and $\langle k\rangle_3 = 0.4655$. The average error in the least-squares fit to Equations 18 and 19, is 1.8% and 2.2%, respectively. (Replacing

$D_0(0)$ by $D_0(\tau_{10})$ in Equation 19 provides no significant increase in the quality of the expansion.) Also, a linear fit of K/cD_0 to $(1-\omega_0 F)$ is almost as good as Eq. 18, i.e.,

$$\frac{K}{cD_0} = 1.0395(1-\omega_0 F), \tag{20}$$

which implies that

$$\frac{K}{D_0} = 1.0395(a+b_b), \tag{21}$$

with an average error of 2.5%. It is seen that the points on Figures 6 and 7 with $1-\omega_0 F > 0.85$ do not fit Equations 18 and 19 quite as well as the rest. This stems from the fact that these points correspond to pure sea water, the phase function of which differs considerably from an ocean containing particles (see Figure 2). The $K/cD_0 - (1-\omega_0 F)$ relationship computed for an ocean free of particles is presented in Figure 8 (for $\vartheta_0 = 0$) and is seen to differ considerably from that in Figures 6 and 7. Since the minimum value of $(1-\omega_w F_w)$ is 0.85 (near 400 nm), and over the range $0.85 \leq (1-\omega_w F_w) \leq 1$ the $K/cD_0 - (1-\omega_0 F)$ relationship for water and for the strongly forward scattering particles are very similar, the computations for the model ocean all fall very near the universal curves even though there is a large variation in the shape of the scattering phase function.

The above analysis shows that K/D_0 and $\langle K\rangle/D_0$ can be written as *explicit* algebraic functions of the inherent optical properties c, ω_0 and F (independently of the geometrical nature of the light field) with an accuracy that is likely better than the accuracy with which K or $\langle K\rangle$ can be measured. Therefore we are justified in regarding the quantities K/D_0 and $\langle K\rangle/D_0$ as *inherent optical properties*. Physically, K/D_0 and $\langle K\rangle/D_0$ are the values of K and $\langle K\rangle$ that would be measured for a given ocean if the atmosphere were removed, the sun placed at the zenith, and the sea surface rendered absolutely flat. In such a well-defined setting, it should not be surprising that K and $\langle K\rangle$ can be considered to be inherent optical properties. What is surprising, however, is that the results of measurements in real situations can be transformed to this ideal setting through the simple division by D_0.

To consider applying this result to a real ocean, the effect of surface roughness on this simple observation must be examined. In order to include surface waves in the radiative transfer code a statistical model of the waves is required. For simplicity, we assume that the surface roughness has no preferred direction, i.e., the structure of the surface is independent of the wind *direction*. Then using the measurements of Cox and Munk (1954) the probability density that the sea surface

at a given point has slope components z_x and z_y, respectively, in the x and y directions is given approximately by

$$p(z_x, z_y) = \frac{1}{\pi\sigma^2} \exp\left(-\frac{z_x^2 + z_y^2}{\sigma^2}\right),$$

where σ^2, the slope variance, is related to the wind speed V (in m/s) through

$$\sigma^2 = 0.003 + 0.00512\,V.$$

The rough surface described by $p(z_x, z_y)$ is incorporated into the Monte Carlo radiative transfer code used in this work in the manner similar to that described by Plass, Kattawar and Guinn (1975). A complete examination of the effect of surface roughness on K and $\langle K \rangle$ requires a significant computational effort; however, only a few computations are required to show that the basic result above — division by D_0 renders K and $\langle K \rangle$ inherent optical properties — is still valid for an ocean with waves. A sample of the computations carried out is presented in Table 4 which provides computations of D_0, K and $\langle K \rangle$ as a function of the surface roughness at 480 nm for $\vartheta_0 = 60°$ and $c_p/c_w = 12.3$ ($C \approx 0.5$ mg/m^3). Note the slow increase in D_0 with σ indicating an increasingly diffuse incident light field beneath the surface as the roughness increases. This increases K with increasing roughness; however, division of K by D_0 provides a quantity that is nearly independent of the surface roughness. Interestingly, the effect of surface roughness on both $\langle K \rangle / c$ and $\langle K \rangle / cD_0$ is small ($< 3\%$) up to wind speeds of 17 m/s. These computations suggest that K/D_0 and $\langle K \rangle / D_0$ remain inherent optical properties even in the presence of surface waves; however, the value of D_0 used to form these ratios must be that which is valid in the *presence* of the rough surface.

Determination of D_0 from field measurements requires the radiance distribution incident on the sea surface. This can be quantitatively determined using a camera equipped with a fisheye lens (Smith 1974, Smith, Austin and Tyler 1970); however, analysis of the resulting sky photographs is not simple. Earlier, (Gordon 1976) I proposed a simple scheme for estimating D_0. Briefly, if $E_d(i)$ is the irradiance incident on the sea surface from source i; e.g., direct sunlight, skylight, clouds, etc., then it is easy to show that

$$D_0 = \frac{\sum_i D_0(i)\, t(i)\, E_d(i)}{\sum_i t(i)\, E_d(i)}, \tag{22}$$

where $t(i)$ is the irradiance transmittance for light from source i and $D_0(i)$ is the value of D_0 that would result from source i acting alone. For a cloud free atmosphere the only sources are the sun and the sky and Equation 22 reduces to

$$D_0 = f\,D_0(\text{Sun}) + (1-f)\,D_0(\text{Sky}), \tag{23}$$

where f is the fraction of direct sunlight in the incident irradiance transmitted through the interface, i.e.,

$$f = \frac{t(\text{Sun})\,E_d(\text{Sun})}{t(\text{Sun})\,E_d(\text{Sun}) + t(\text{Sky})\,E_d(\text{Sky})}.$$

If skylight is assumed to have a uniform radiance distribution, i.e., radiance (brightness) independent of direction of viewing, then Equation 23 simplifies to

$$D_0 = \frac{f}{\cos\vartheta_{0w}} + 1.1969(1-f). \tag{24}$$

Given ϑ_0 the only unknown in Equation 24 is f. This can be estimated by placing an irradiance meter above the surface, measuring the total incident irradiance $E_d(\text{Sun}) + E_d(\text{Sky})$, and then measuring the sky irradiance, $E_d(\text{Sky})$, by casting a shadow over the opal diffuser of the instrument.

To test the efficacy of Equation 24 with the Monte Carlo simulations, $E_d(\text{Sun})$ is computed from

$$E_d(\text{Sun}) = \cos\vartheta_0\,F_0\,\exp\left[-(\tau_A + \tau_R + \tau_{Oz})/\cos\vartheta_0\right], \tag{25}$$

where F_0 is the extraterrestrial solar irradiance, and τ_A, τ_R, and τ_{Oz} are, respectively, the contributions to the optical thickness of the atmosphere from aerosol scattering, molecular (Rayleigh) scattering, and Ozone absorption. $E_d(\text{Sky})$ is then determined by subtraction from the total irradiance falling on the sea surface. Even though Equation 25 is exact, for our purposes it underestimates $E_d(\text{Sun})$ because all photons scattered by the aerosol are assumed to be uniformly distributed over the sky, whereas in reality a significant fraction of the aerosol scattering is through small angles and these scattered photons are still traveling in nearly the same direction as the unscattered photons. To compensate for this effect, we can obtain an upper limit on $E_d(\text{Sun})$ by ignoring the aerosol scattering entirely, i.e., by computing $E_d(\text{Sun})$ according to

$$E_d(\text{Sun}) = \cos\vartheta_0\,F_0\,\exp\left[-(\tau_R + \tau_{Oz})/\cos\vartheta_0\right], \tag{26}$$

which clearly overestimates $E_d(\text{Sun})$ since aerosol scattering does contribute something to $E_d(\text{Sky})$. Thus, for our purposes Equations 25 and 26, respectively, provide lower- and upper-bound estimates

of E_d(Sun) and therefore of f. Comparison between D_0 computed from Equation 24 using Equation 25 for E_d(Sun) and the "exact" values (Table 3) show that for $0 \leq \vartheta_0 \leq 60°$ the error is less than $\pm 3\%$, and for $\vartheta_0 = 80°$ Equation 24 yields a value for D_0 which is 5–8% too low. The corresponding computations with Equation 24 using Equation 26 for E_d(Sun) show that for $0 \leq \vartheta_0 \leq 60°$ the error is less than $\mp 2\%$, and for $\vartheta_0 = 80°$ the computed value is 0.5–4% too high.

We can apply this computation to the "shadow" method suggested above for estimating f. Assume that the object used to cast the shadow of the sun is a circular disk of diameter somewhat larger than the collecting face of the irradiance meter. Then, if the disk is relatively close to the irradiance meter, a portion of the sky in the vicinity of the sun is also obscured. This would approximately correspond to estimating f using Equation 26, i.e., photons scattered at small angles from the sun would be included in E_d(Sun). Conversely, if the disk were at a great distance from the instrument only the solar disk itself would be obscured, and photons scattered at small angles from the sun become part of E_d(Sky), approximately corresponding to using Equation 25 to estimate f. Thus we conclude that the shadow method of determining f should yield values of D_0 between the estimated obtained using Equations 25 and 26.

In the presence of surface waves, computation of the correct value of D_0 is facilitated by the empirical observation that D_0 increases approximately in proportion to σ^2 for wind speeds up to $\approx$ 20 m/s. This is demonstrated in Figure 9 for an overcast sky and for solar illumination (no atmosphere) with $\vartheta_0 = 60°$, $70°$, and $80°$. The dots on Figure 9 are the computed values of D_0 and the lines are least-squares fits to $D_0 = c_1 + c_2\sigma^2$, where c_1 and c_2 are constants. The least-squares lines allow the estimation of D_0 with and error of $\lesssim 2\%$. For $\vartheta_0 \leq 50°$ the variation in D_0 for $0 \leq \sigma \leq 0.3$ is less than about 2%. Thus, for $\vartheta_0 \leq 50°$ D_0 can be computed by assuming that the sea surface is flat, while for larger values of ϑ (or for an overcast sky) the flat-surface values of D_0(Sun) and D_0(Sky) for use in Equation 23 must be increased in accordance with Figure 9.

Finally, in the atmospheric model used here τ_A at 550 nm was taken to be 0.25. This is very conservative, since it would correspond to a coastal atmosphere (it is typical of a continental aerosol) and is a factor of 2–3 higher than would be expected for a "clear" marine atmosphere. Therefore an estimate of f based on Equation 26 alone, i.e., without any measurements above the surface, will provide excellent estimates of D_0 in clear marine atmospheres.

The Lambert-Beer Law Applied to K_d

Having established that K and $\langle K \rangle$ can be transformed into inherent optical properties in a variety of realistic situations, we now turn to the main question of this paper: the extent to which K_d satisfies the Lambert-Beer law. Consider an ocean consisting of m components one of which is pure sea water. Let c_i^* be the specific attenuation coefficient of constituent i. Then, $c_i = c_i^* C_i$, and the total attenuation coefficient can be written

$$c = \sum_{i=1}^{m} c_i = \sum_{i=1}^{m} c_i^* C_i, \tag{27}$$

where C_i is the *concentration* of the i^{th} constituent. These relationships comprise the Lambert-Beer law, i.e., the individual attenuation coefficients are proportional to the individual concentrations and the total attenuation coefficient is a linear sum of the individual or partial attenuation coefficient. [On the surface, Equations 9 and 10 appear to suggest that c_p is not proportional to the concentration of phytoplankton, but rather on the concentration to the 0.6 power. However, this is an artifact because c_p in the present bio-optical model includes not only the contribution of phytoplankton but also the contribution from detrital material, the relative concentration of which varies with the concentration of phytoplankton (Hobson, Menzel and Barber 1973). In reality the attenuation coefficient of *particles* in Case 1 waters should be written $c_p = c_{ph}^* C_{ph} + c_d^* C_d$, where the subscripts "*ph*" and "*d*" refer to phytoplankton and detritus, respectively.] Since K/D_0 and $\langle K \rangle / D_0$ are inherent optical properties, the relevant question concerns the validity of the expressions

$$\frac{K}{D_0} = \sum_{i=1}^{m} \frac{K_i}{D_0} \tag{28}$$

and

$$\frac{\langle K \rangle}{D_0} = \sum_{i=1}^{m} \frac{\langle K \rangle_i}{D_0}. \tag{29}$$

For a given observation, the D_0's cancel from Equations 28 and 29; however, we will keep D_0 on both sides of these equations because Equations 18–21 express K/D_0 and $\langle K \rangle / D_0$ as functions of the inherent optical properties, and also because later we will consider combining measurements made under differing environmental conditions, i.e., measurements with different values of D_0 as would be carried out in the field.

Clearly, if Equation 21 is used for K/D_0, its linear dependence on the inherent optical properties means that the error in Equation 28 is no more than the error in Equation 21, i.e.,

$$\frac{K}{D_0} = 1.0395(a + b_b) = 1.0395\Big(\sum_{i=1}^{m} a_i + \sum_{i=1}^{m} (b_b)_i\Big) = \sum_{i=1}^{m} 1.0395(a_i + (b_b)_i) = \sum_{i=1}^{m} \frac{K_i}{D_0}.$$

Thus, any errors in Equations 28 and 29 over and above the error in K_i/D_0 and $\langle K\rangle_i/D_0$ will result from *nonlinearities* in the dependence of these quantities on the inherent optical properties. To understand the magnitude of these additional errors we consider a hypothetical model. Assume that Equation 19, the more nonlinear of the two relationships, is exact and that the ocean consists only of water and plankton. With ω_w and ω_p given in Table 2 and $F_w = 0.50$ and $F_p = 0.985$, the relative concentration of particles, as measured by c_p/c, is varied from 0 to 1. The true value of $\langle K\rangle/D_0$, $\langle K\rangle_T/D_0$, is then computed from Equation 19 using the value of $\omega_0 F$ for the mixture, i.e., using

$$\omega_0 F = \frac{\omega_p F_p c_p + \omega_w F_w c_w}{c_p + c_w}.$$

The Lambert-Beer law value, $\langle K\rangle_B/D_0$, is computed from

$$\frac{\langle K\rangle_B}{D_0} = \frac{\langle K\rangle_w}{D_0} + \frac{\langle K\rangle_p}{D_0}$$

with $\langle K\rangle_w/D_0$ and $\langle K\rangle_p/D_0$ individually determined by Equation 19 using $\omega_w F_w$ and $\omega_p F_p$, respectively. Graphically, in Figure 7 $\langle K\rangle_B/cD_0$ would fall on a ***straight line*** between the points on the least-squares curve at $\omega_0 F = \omega_w F_w$ and $\omega_0 F = \omega_p F_p$, while $\langle K\rangle_T/cD_0$ would be on the curve. The relative error in $\langle K\rangle_B/D_0$ is then computed by means of

$$\frac{\langle K\rangle_B - \langle K\rangle_T}{\langle K\rangle_T}.$$

This error is shown in Figure 10 as a function of the fraction of particles (c_p/c). It is seen that the maximum error at 440 nm is $\approx$ 3%, while the maximum error at 550 nm is $\approx$ 6%. Had $\omega_p(440) = 0.80$ been used in this example the error at 440 *nm* would have been $< 2\%$. Since $\omega_p(440) = 0.86$ is near the upper limit for phytoplankton, e.g , Bricaud, Morel and Preiur (1983) measured $\omega_p(440) = 0.88$ for the coccolithophore *Emiliana huxleyi* which is known to be a very strong scatterer, it is believed that the error at 440 nm will usually be less than 2%. The dotted curve on Figure 10 corresponds to a mixture of water and nonabsorbing particles (such as white sand) at wavelengths $\gtrsim$ 600 nm for which $\omega_w \approx 0$. This curve provides the *maximum* error incurred in $\langle K\rangle_B$.

Using Equation 13, c_p/c can be related to the pigment concentration for this two-component example. At 440 nm, $C > 0.05$ mg/m^3 yields $c_p/c \gtrsim 0.75$, while at 550 nm $C > 0.5$ mg/m^3 yields $c_p/c \gtrsim 0.75$. Thus, for pigment concentrations in the range $0.5 \leq C \leq 10$ mg/m^3, Figure 10 and the discussion above suggest that $\langle K \rangle_B / D_0$ is about $1 - 2\%$ too low at 440 nm and about 6% too low at 550 nm. Furthermore, considering the small errors in Equations 18 and 19, these computations suggest that the Lambert-Beer law for K_d as expressed in Equations 28 and 29 is unlikely to be in error by more than 5% at 440 nm or 10% at 550 nm.

It should be noted that the example above of the error in the Lambert-Beer law applied to $\langle K \rangle / D_0$ concerns adding strong scatterers (plankton) to a strongly absorbing medium (sea water). If weak scatters ($\omega_p \approx 0$) are added to sea water, the Lambert-Beer law will be much better satisfied. For example, if pure absorbers are added to pure water, the maximum error in the Lambert-Beer applied to $\langle K \rangle / D_0$ will be $< 0.25\%$. The extension of these computations to media with $m > 2$ is straightforward.

It is important to understand that the near-validity of the Lambert-Beer law rests squarely on the near-linearity of the relationships shown in Figures 6 and 7, i.e., that the quantities involved must be inherent optical properties is a necessary but not sufficient condition for the validity of the law. For example, if all particles in the ocean were sufficiently small to scatter light with the same phase function as pure sea water, the dependence of K/cD_0 and $\langle K \rangle / cD_0$ on $1 - \omega_0 F$ would be given by Figure 8. In such a case, if nonabsorbing particles were mixed with strongly absorbing water, according to the Lambert-Beer law the K's for the resulting mixture would fall along a straight line from $1 - \omega_0 F = 0.5$ to $1 - \omega_0 F = 1$ ($F = 0.5$), while the actual K's would fall along the curve. Clearly, large departures from Lambert-Beer law would be seen for all values of c_p/c in such an ocean. Thus, the near-validity of the Lambert-Beer law in the case of a realistic ocean is seen to result from the interplay of three *independent* facts: (1) the dependence of the diffuse attenuation coefficients on the geometric structure of the light field can be removed (division by D_0); (2) pure sea water is a much better absorber than scatterer at optical frequencies ($1 - F_w \omega_w \gtrsim 0.85$); and (3) the phase functions for particles suspended in the ocean differs significantly from that of pure sea water (Figure 1).

Finally it is of interest to determine the accuracy with which one can estimate the diffuse attenuation coefficient of an ocean consisting of pure sea water alone through extrapolation of K_d-values measured in a real ocean to the limit of zero particle concentration. As mentioned in the

introduction, this is the scheme that Smith and Baker and others use to estimate K_d for pure water (Baker and Smith 1982, Smith and Baker 1978a, Smith and Baker 1978b, Smith and Baker 1981). For this purpose we have computed $\langle K \rangle$ as a function of c at 480 nm by letting C in Equation 13 range from 0 to 4.5 mg/m^3. Figure 11 shows the results for $\vartheta = 0°$, $60°$, and for overcast skies. The lines on the graph correspond to linear least-squares fits to the computed points with $C > 0$ ($c_p > 0$ or $c > c_w$), i.e., the point on each line corresponding to pure water was left out of the fit. The least-squares line was then extrapolated to $c_p = 0$ to determine $\langle K \rangle$ in the absence of particles. This corresponds to extrapolating C to zero pigment concentration. As seen from the figure, the extrapolated line falls very close to the computed values of $\langle K \rangle$ for pure sea water. In fact, the difference between the computed and extrapolated values of $\langle K \rangle_w$ are, respectively, 3.8, 1.9, and 1.5%. $\vartheta_0 = 0°$, $60°$, and an overcast sky.

In this example, the incident illumination is the same for each value of c along the least-squares line. In practice this would be impossible to arrange experimentally. In the field, each data point would likely correspond to a different incident light field. However, we have seen that division $\langle K \rangle$ by D_0 removes the effects of the geometric structure of the light field. To assess the efficacy of determining $\langle K \rangle_w$ from extrapolation to $c_p = 0$ in more realistic situations, for each wavelength the above extrapolation procedure was applied to $\langle K \rangle / D_0$ obtained from *all* of the simulations, i.e., all illumination conditions were treated equally and included in the analysis. Figure 12 shows the results of the extrapolation at 480 nm, and Table 5 compares the extrapolated value of $\langle K \rangle_w / D_0$ with the true value of $\langle K \rangle_w$ — the value of $\langle K \rangle$ for an ocean composed of pure sea water computed with the atmosphere removed and with the sun at the zenith. Table 5 suggests that the extrapolation procedure can yield the true value of $\langle K \rangle_w$ to within about 2%. However, Figure 12 shows that large errors in $\langle K \rangle_w$ are possible if it is determined from a small amount of data for which $c_p \gg c_w$. For example, if the highest value of $\langle K \rangle / D_0$ at $c \approx 0.27$ m^{-1} and the lowest value at $c \approx 0.42$ m^{-1} the extrapolated value of $\langle K \rangle_w / D_0$ would be ≈ 0.038 m^{-1}, an error of nearly a factor of 2. Thus, experimental determination of $\langle K \rangle_w$ must be carried out by excluding turbid waters from the analysis.

Concluding Remarks

By simulating the transport of radiation in a realistic ocean-atmosphere system and treating the results as experimental data obtained under carefully controlled conditions, it has been shown that K and $\langle K \rangle$ when modified through division by D_0 are, to a high degree of accuracy, inherent optical properties. A simple scheme for estimating D_0 for individual experimental situations is provided. Furthermore it is shown that K/D_0 and $\langle K \rangle / D_0$ satisfy the Lambert-Beer law to a reasonable degree of accuracy, with the largest error ($\approx 15\%$ using $\langle K \rangle / D_0$) arising from mixing nonabsorbing particles, e.g., white sand, with strongly absorbing water ($\lambda > 600$ nm); however, leaving D_0 out of Equations 1,28, and 29 will result in extra variance in K_d, K, and $\langle K \rangle$, which Table 3 suggests will be as much as $\pm 8\%$ even for measurements restricted to $0 \leq \vartheta_0 \leq 40°$. In the case of a two component system composed of pure sea water and plankton, the error in the application of the Lambert-Beer law to $\langle K \rangle / D_0$ is $\approx 5\%$ at 440 nm and 10% at 550 nm. This accounts for the success of Equation 1 for *in-situ* observation and analysis of phytoplankton absorption. The near-validity of the Lambert-Beer law in this situation, where there are compelling reasons to believe that it should fail, is traced to three *independent* facts: (1) the dependence of the diffuse attenuation coefficients on the geometric structure of the light field can be removed; (2) pure sea water is a much better absorber than scatterer at optical frequencies; and (3) the phase functions for particles suspended in the ocean differs significantly from that of pure sea water. If any of these facts were false the Lambert-Beer law would fail. Finally, it is shown that extrapolation of K/D_0 and $\langle K \rangle / D_0$ to the limit $c \to c_w$ yields quantities which are within 2% of K_w and $\langle K \rangle_w$, i.e., the value of K and $\langle K \rangle$ that would be measured for an ocean consisting of pure sea water with the sun at the zenith and the atmosphere removed.

The analysis of oceanic properties using K_d is attractive because of the relative simplicity of the instrumentation required for its measurement. The near-validity of the Lambert-Beer law, for all but the most strongly scattering of natural waters, allows the partial diffuse attenuation coefficients (in the sense of Equations 1, 28, and 29) to be determined. Since the partial, as well as the total, K_d functions (K and $\langle K \rangle$) are in the first approximation proportional to $a + b_b$, for those species for which $a \gg b_b$, e.g., phytoplankton and dissolved organic material, measurement of K or $\langle K \rangle$ provides a direct estimate of a from K_i/D_0 or $\langle K \rangle_i / D_0$. Thus, until the development of an *in-situ* spectral absorption meter, measurement of K_d would appear to be the only available *in-situ* means of estimating $a(\lambda)$. Note, however, that in general the medium will contain more

than two components, e.g., water, plankton, and detritus, and the separation of the components can only be carried out in a statistical sense.

Application of these results to field experiments present several difficulties. The first, stems from the fact that K, which satisfies the Lambert-Beer law better than $\langle K \rangle$, is very difficult to measure in practice due to the strongly fluctuating irradiance at the surface resulting from the presence of surface capillary waves, and the difficulty of accurately determining the depth of the instrument near the surface due to the presence of surface gravity waves. Thus, measurement of $\langle K \rangle$, which is significantly less influenced by the surface effects, is preferred from an experimental point of view; however, in the case of oceanic water, the mixed layer must be sufficiently deep so that $z_{10} = \tau_{10}/c$ is within the mixed layer and the water may be treated as homogeneous. For the limiting case of an ocean free of particles, this would require a mixed layer of $\approx$ 125, 115, and 35 m, respectively at 440, 480, and 550 nm. A second difficulty concerns the determination of D_0 in the presence of broken clouds. In this case Equation 24 will not apply and the only viable method of is to photograph with a fisheye camera. Finally, the presence of whitecaps on the sea surface will further modify the internal geometry of the light filed and influence D_0. Their effect cannot be discussed further without knowledge of their optical properties.

Unfortunately, the results of this paper are not directly applicable to measurements of K_d made with moored instruments in a fixed configuration since K_d is a function of depth and is dependence on depth depends on c. [The dependence of K_d on depth was not relevant to the present work because measurements were considered to be made at the unique depth, $z = 0$, or at a given fraction of surface irradiance.] The question of interpretation of measurements from moorings will require further study.

References

Austin, R. W. and T. J. Petzold 1981. Remote Sensing of the Diffuse Attenuation Coefficient of Sea Water using the Coastal Zone Color Scanner, pp. 239–256. *In* J. R. F. Gower [ed.] Oceanography from Space. Plenum Press.

Baker, K. S. and R. C. Smith 1979. Quasi-inherent Characteristics of the Diffuse Attenuation Coefficient for Irradiance. Society of Photo-Optical Instrumentation Engineers, Ocean Optics VI 208: 60–63.

_____ 1982. Bio-optical Classification and Model of Natural Waters. 2. Limnology and Oceanography 27: 500–509.

Bricaud, A., A. Morel and L. Preiur 1983. Optical Efficiency Factors of Some Phytoplankters. Limnology and Oceanography 28: 816–832.

Cox, C. and W. Munk 1954. Measurements of the Roughness of the Sea Surface from Photographs of the Sun's Glitter. Jour. Opt. Soc. of Am. 44: 838–850.

Deirmendjian, D. 1969. Electromagnetic Scattering on Spherical Polydispersions, Elsevier, New York, NY. 290 pp.

Elterman, L. April 1968. UV, Visible, and IR Attenuation for Altitudes to 50 km, 1968, AFCRL, Bedford, MA, Report AFCRL-68-0153.

Gordon, H. R. 1976. Radiative Transfer in the Ocean: A Method for Determination of Absorption and Scattering Properties. Applied Optics 15: 2611–2613.

_____ 1980. Irradiance Attenuation Coefficient in a Stratified Ocean: A Local Property of the Medium. Applied Optics 19: 2092–2094.

_____ 1982. Interpretation of Airborne Oceanic Lidar: Effects of Multiple Scattering. Applied Optics 21: 2996–3001.

_____ 1987. A Bio-Optical Model Describing the Distribution of Irradiance at the Sea Surface Resulting from a Point Source Imbedded in the Ocean. Applied Optics 26: 4133–4148.

Gordon, H. R., O. B. Brown and M. M. Jacobs 1975. Computed Relationships Between the Inherent and Apparent Optical Properties of a Flat Homogeneous Ocean. Applied Optics 14: 417–427.

Gordon, H. R. and A. Y. Morel 1983. Remote Assessment of Ocean Color for Interpretation of Satellite Visible Imagery: A Review, Springer-Verlag. 114 pp.

Hobson, L. A., D. W. Menzel and R. T. Barber 1973. Primary Productivity and the Sizes of Pools of Organic Carbon in the Mixed Layer of the Ocean. Marine Biology 19: 298–306.

Kirk, J. T. O. 1984. Dependence of relationship between inherent and apparent optical properties of water on solar altitude. Limnology and Oceanography 29: 350–356.

Morel, A. 1974. Optical Properties of Pure Water and Pure Sea Water, pp. 1–24. *In* N. G. Jerlov and E. S. Nielsen [eds.] Optical Aspects of Oceanography. Academic Press.

_____ 1980. In-water and Remote Measurement of Ocean Color. Boundary-Layer Meteorology 18: 177–201.

Morel, A. and A. Bricaud 1981. Theoretical Results Concerning Light Absorption in a Discrete Medium, and Application to Specific Absorption of Phytoplankton. Deep-Sea Research 28A: 1375–1393.

Morel, A. and L. Prieur 1977. Analysis of Variations in Ocean Color. Limnology and Oceanography 22: 709–722.

Morel, A. and R. C. Smith 1982. Terminology and Units in Optical Oceanography. Marine Geodesy 5: 335–349..

Petzold, T. J. 1972. Volume Scattering Functions for Selected Natural Waters, Scripps Institution of Oceanography, Visibility Laboratory, San Diego, CA. 92152, SIO Ref. 72–78.

Plass, G. N., G. W. Kattawar and J. A. Guinn 1975. Radiative transfer in the earth's atmosphere: influence of ocean waves. Applied Optics 14: 1924–1936.

Preisendorfer, R. W. 1959. On the Existence of Characteristic Diffuse Light in Natural Waters Sea. Jour. Mar. Res. 18: 1–9.

———— 1961. Application of Radiative Transfer Theory to Light Measurements in the Sea. Union Géodésique et Géophysique Internationale 10: 11–30.

Prieur, L. and S. Sathyendranath 1981. An Optical Classification of Coastal and Oceanic Waters Based on the Specific Absorption Curves of Phytoplankton Pigments, Dissolved Organic Matter, and Other Particulate Materials. Limnology and Oceanography 26: 671–689.

Sathyendranath, S. 1981. Influence des Substances en Solution et en Suspension dans les Eaux de Mer sur L'absorption er La Reflectance. Modelisation et Applications a'la Teledetection, Ph.D. thesis, 3rd cycle, Univ. Pierre et Marie Curie, Paris. 123 pp.

Smith, R. C. 1974. Structure of Solar Radiation in the Upper Layers of the Sea, pp. 95–119. *In* N. G. Jerlov and E. S. Nielsen [eds.] Optical Aspects of Oceanography. Academic Press.

Smith, R. C., R. W. Austin and J. E. Tyler 1970. An Oceanographic Radiance Distribution Camera System. Applied Optics 9: 2015–2022.

Smith, R. C. and K. S. Baker 1978a. The Bio-optical State of Ocean Waters and Remote Sensing. Limnology and Oceanography 23: 247–259 .

———— 1978b. Optical Classification of Natural Waters. Limnology and Oceanography 23: 260–267.

———— 1981. Optical Properties of the Clearest Natural Waters (200-800 nm). Applied Optics 20: 177–184.

Stavn, R. H. 1988. Lambert-Beer Law in Ocean Waters: Optical Properties of Water and of Dissolved/Suspended Material, Optical Energy Budgets. Applied Optics 27: 222–231.

Figure Captions

Figure 1. Phase functions for particles and water. To facilitate plotting, phase functions "M" and "C" have been multiplied by 2 and 4, respectively.

Figure 2. Total phase function at 480 nm as a function of the particle concentration. Progressing from bottom to top on the left of the graph, c_p/c_w = 0, 1, 3, 10, and 100.

Figure 3. Computed dependence of K_d/c on depth at 440 nm for particle phase function "M." The three cases are, from right to left, for c_p/c_w = 0, 1.4, and 5.6, respectively.

Figure 4. K/c as a function of $1-\omega_0$. The symbol code is provided on Figure 1. Note, $1-\omega_0 = a/c$.

Figure 5. $\langle K\rangle/c$ as a function of $1-\omega_0$. The symbol code is provided on Figure 1. Note, $1-\omega_0 = a/c$.

Figure 6. K/cD_0 as a function of $1-\omega_0 F$. The symbol code is provided on Figure 1.

Figure 7. $\langle K\rangle/cD_0$ as a function of $1-\omega_0 F$. The symbol code is provided on Figure 1.

Figure 8. K/cD_0 for a particle free ocean (Rayleigh scattering). Open circles are for K/cD_0, while solid circles are for $\langle K\rangle/cD_0$.

Figure 9. D_0 as a function of σ^2. The curves from bottom to top correspond, respectively, to a completely overcast sky and to solar illumination with $\vartheta_0 = 60°$, $70°$, and $80°$.

Figure 10. Relative error (%) in $\langle K\rangle_B$ as a function of the relative concentration of particles.

Figure 11. $\langle K\rangle$ at 480 nm as a function of c for particle phase function "M." The lower and upper lines are for $\vartheta_0 = 0°$ and $60°$, respectively, the center line is for an overcast sky.

Figure 12. $\langle K\rangle/D_0$ as a function c at 480 nm. The points are Monte Carlo simulations for various values of ϑ_0, the line is a least-squares fit to the points with $c_p > c_w$.

Table 1: Absorption and Scattering Coefficients of Pure Sea Water.

λ (nm)	b_w (m^{-1})	a_w (m^{-1})	ω_w
440	0.0049	0.0145	0.253
480	0.0034	0.0176	0.162
550	0.0019	0.0638	0.029

Table 2: Model values of ω_p and ω_w.

λ (nm)	ω_p	ω_w
440	0.86	0.253
480	0.88	0.162
550	0.93	0.029

Table 3: D_0 just beneath the sea surface.

ϑ_0	440 nm	480 nm	550 nm	$1/\cos\vartheta_{0w}$
0°	1.0343	1.0267	1.0185	1.0000
20°	1.0737	1.0652	1.0553	1.0346
25°	1.0880	1.0768	1.0669	1.0544
30°	1.1050	1.0995	1.0933	1.0787
40°	1.1580	1.1540	1.1487	1.1415
60°	1.2855	1.2925	1.2993	1.3154
80°	1.2841	1.3105	1.3457	1.4838
Diffuse	1.1969	1.1969	1.1969	

Table 4: Computed D_0 and diffuse attenuation coefficients at 480 nm and $\vartheta_0 = 60°$ as a function of the surface roughness parameter σ.

σ	D_0	K/c	K/cD_0	$\langle K\rangle/c$	$\langle K\rangle/cD_0$
0.0	1.293	0.2624	0.2029	0.2914	0.2254
0.1	1.306	0.2632	0.2015	0.2924	0.2261
0.2	1.333	0.2733	0.2050	0.2954	0.2285
0.3	1.373	0.2833	0.2063	0.2999	0.2319

Table 5: The true $\langle K \rangle_w$ and the extrapolated value of $\langle K \rangle_w / D_0$ in m^{-1} for the three wavelengths.

	440 nm	480 nm	550 nm
$\langle K \rangle_w$	0.0182	0.0202	0.0652
$\langle K \rangle_w / D_0$	0.0178	0.0202	0.0667

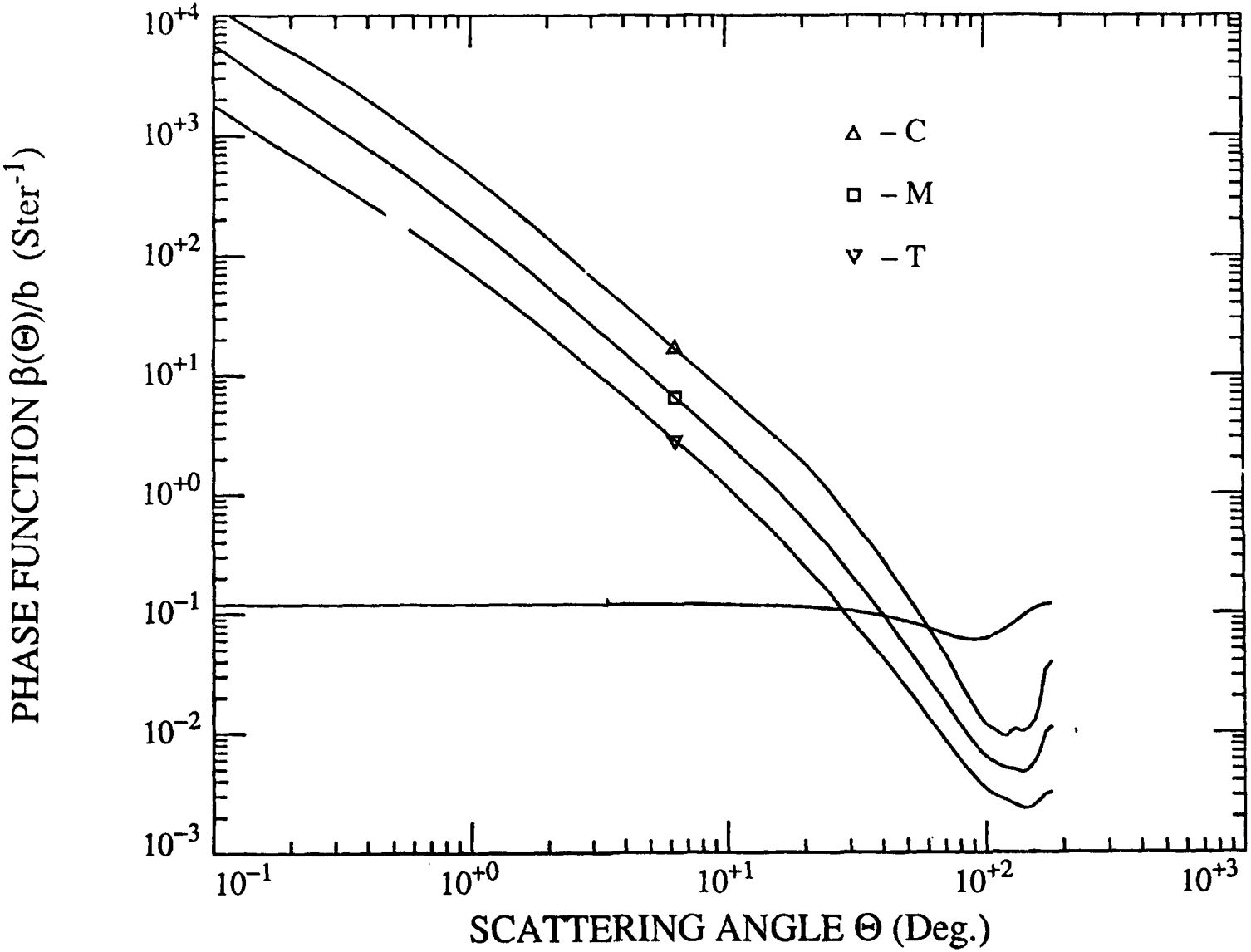

Figure 1. Phase functions for particles and water. To facilitate plotting, phase functions "M" and "C" have been multiplied by 2 and 4, respectively.

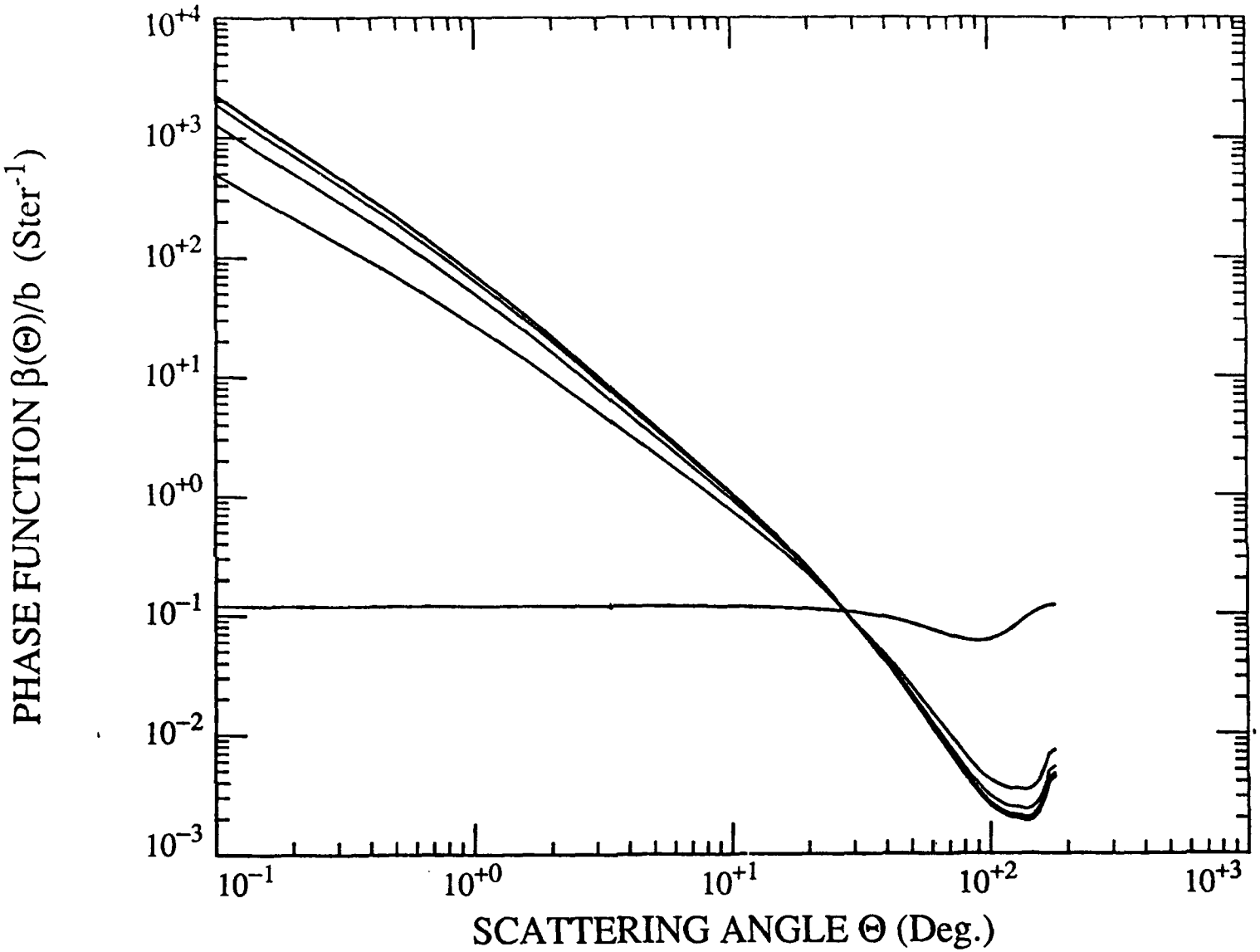

Figure 2. Total phase function at 480 *nm* as a function of the particle concentration. Progressing from bottom to top on the left of the graph, c_p/c_w = 0, 1, 3, 10, and 100.

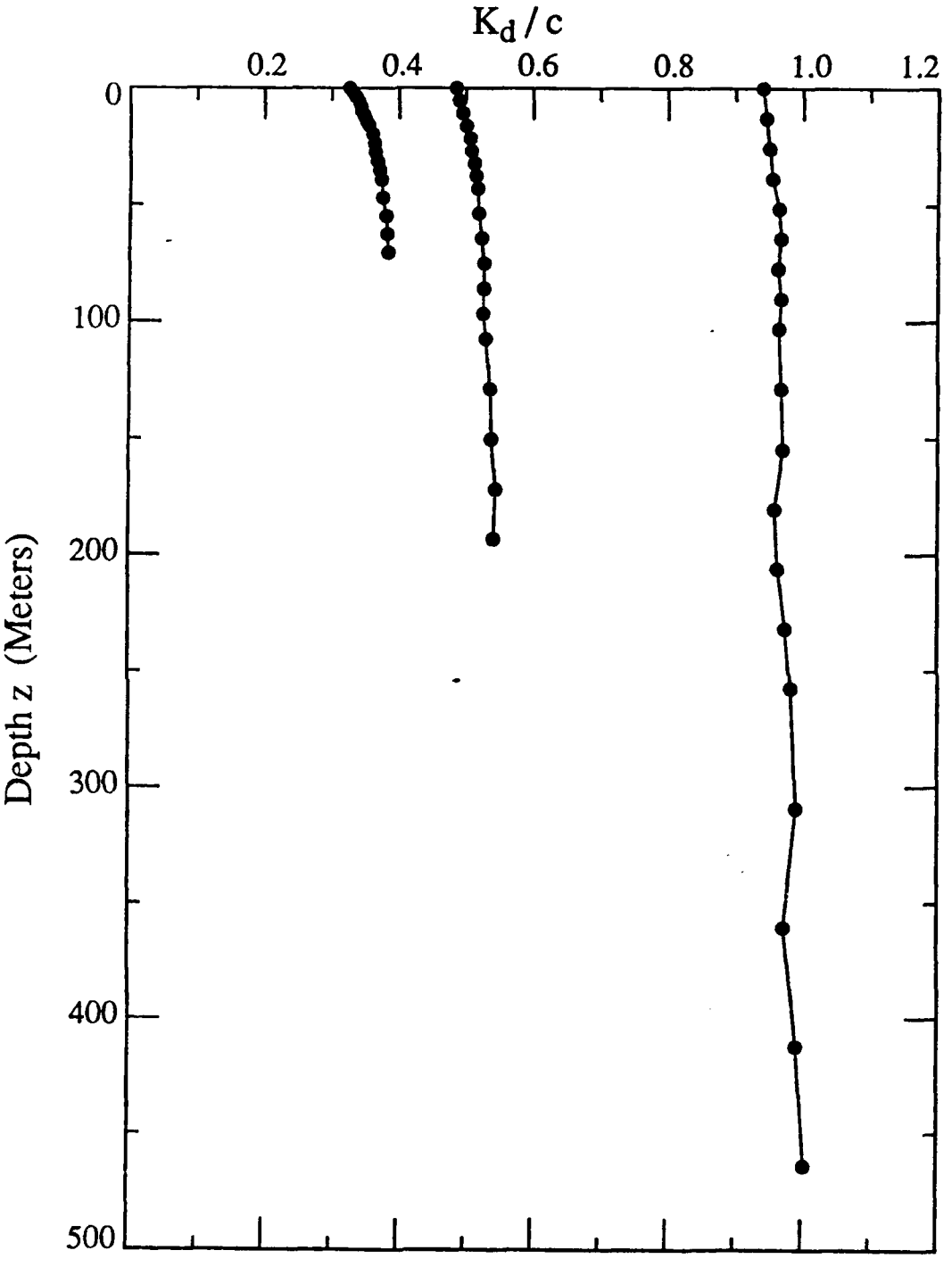

Figure 3. Computed dependence of K_d/c on depth at 440 nm for particle phase function "M." The three cases are, from right to left, for c_p/c_w = 0, 1.4, and 5.6, respectively.

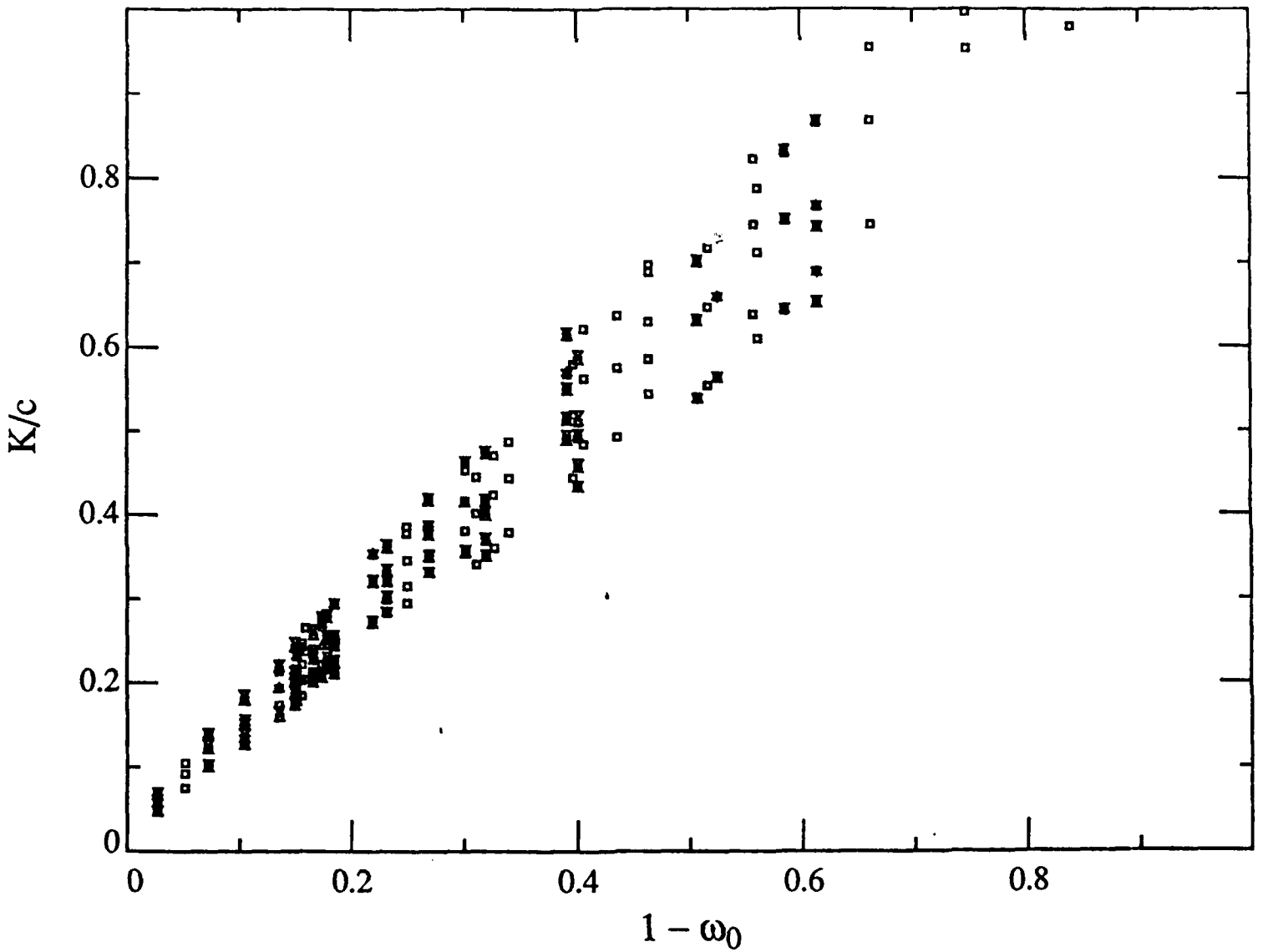

Figure 4. K/c as a function of $1-\omega_0$. Note that $1-\omega_0 = a/c$.
The symbol code is provided on Figure 1.

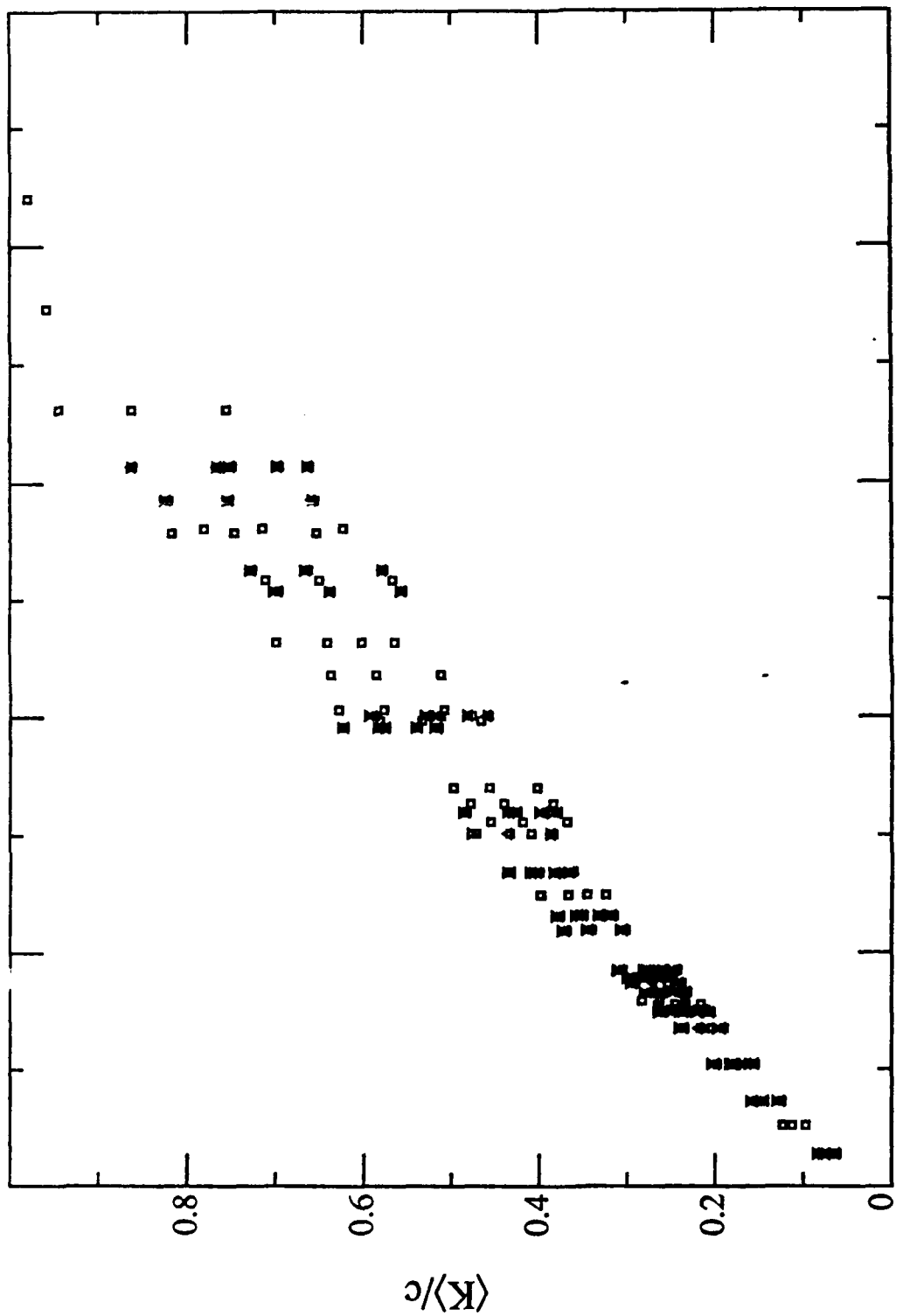

Figure 5. $\langle K \rangle/c$ as a function of $1 - \omega_0$. Note that $1 - \omega_0 = a/c$.
The symbol code is provided on Figure 1.

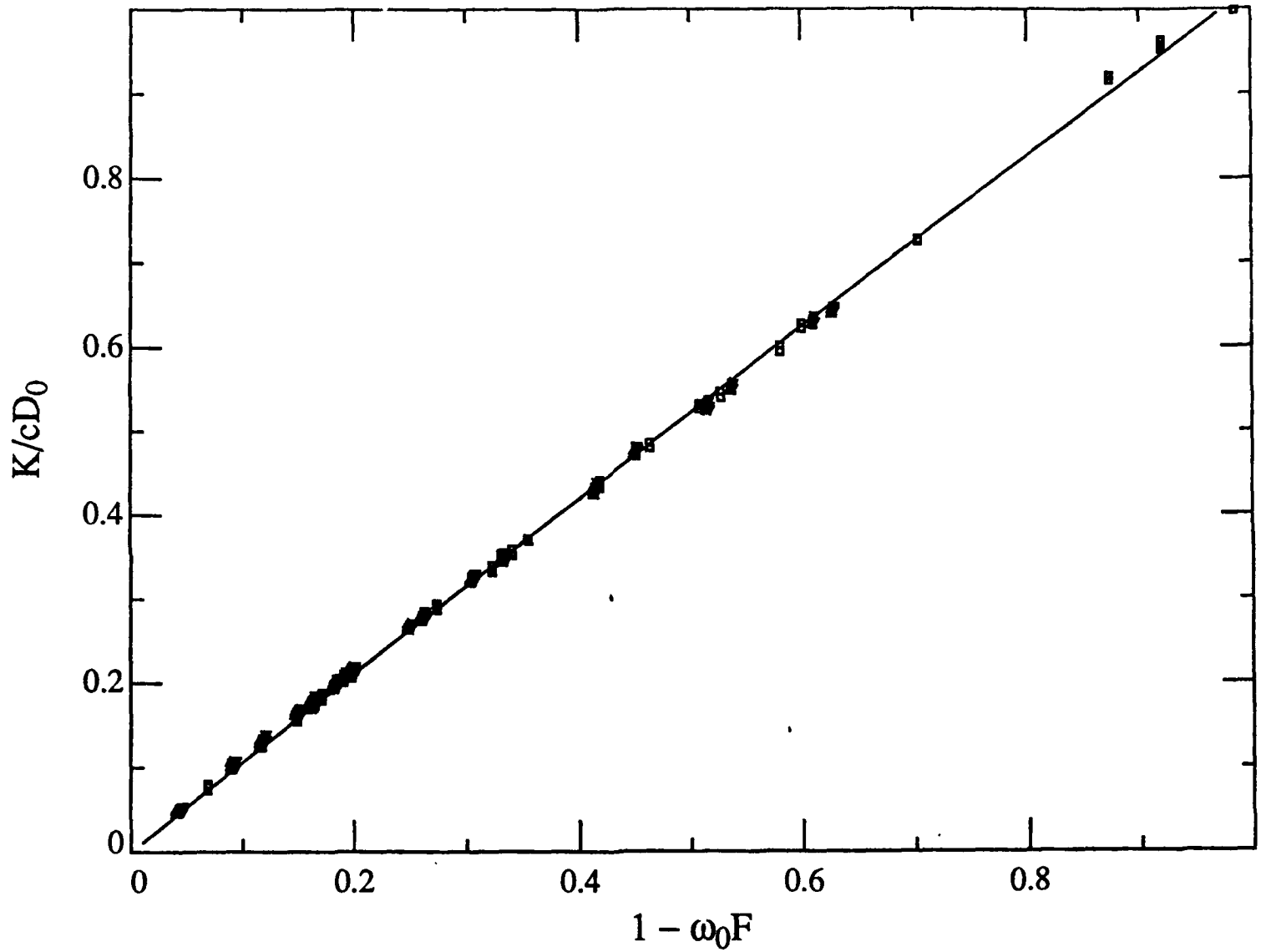

Figure 6. K/cD_0 as a function of $1-\omega_0 F$.
The symbol code is provided on Figure 1.

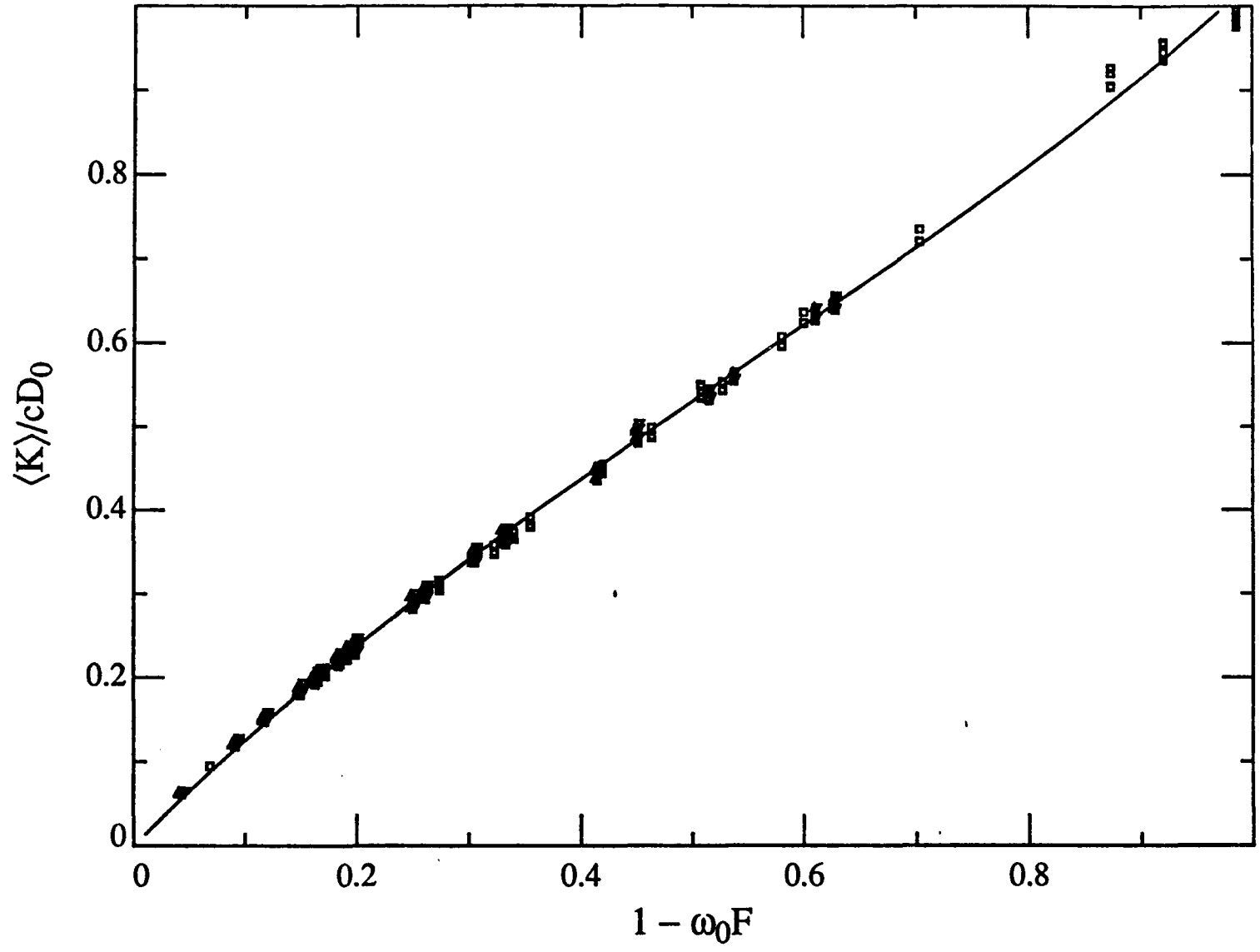

Figure 7. $\langle K \rangle / cD_0$ as a function of $1 - \omega_0 F$.
The symbol code is provided on Figure 1.

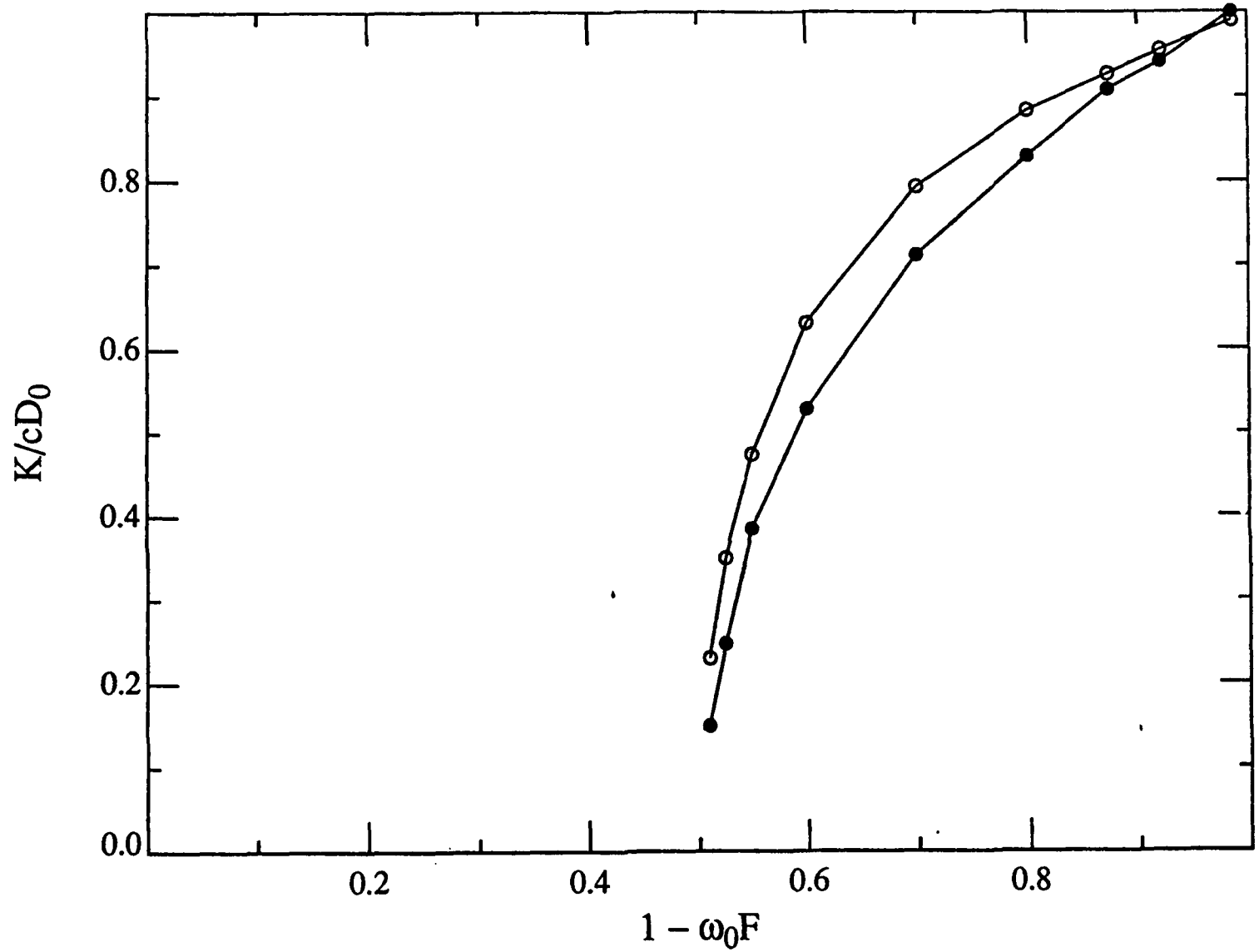

Figure 8. K/cD_0 for a particle free ocean (Rayleigh scattering). Open circles are for K/cD_0, while solid circles are for $\langle K \rangle / cD_0$.

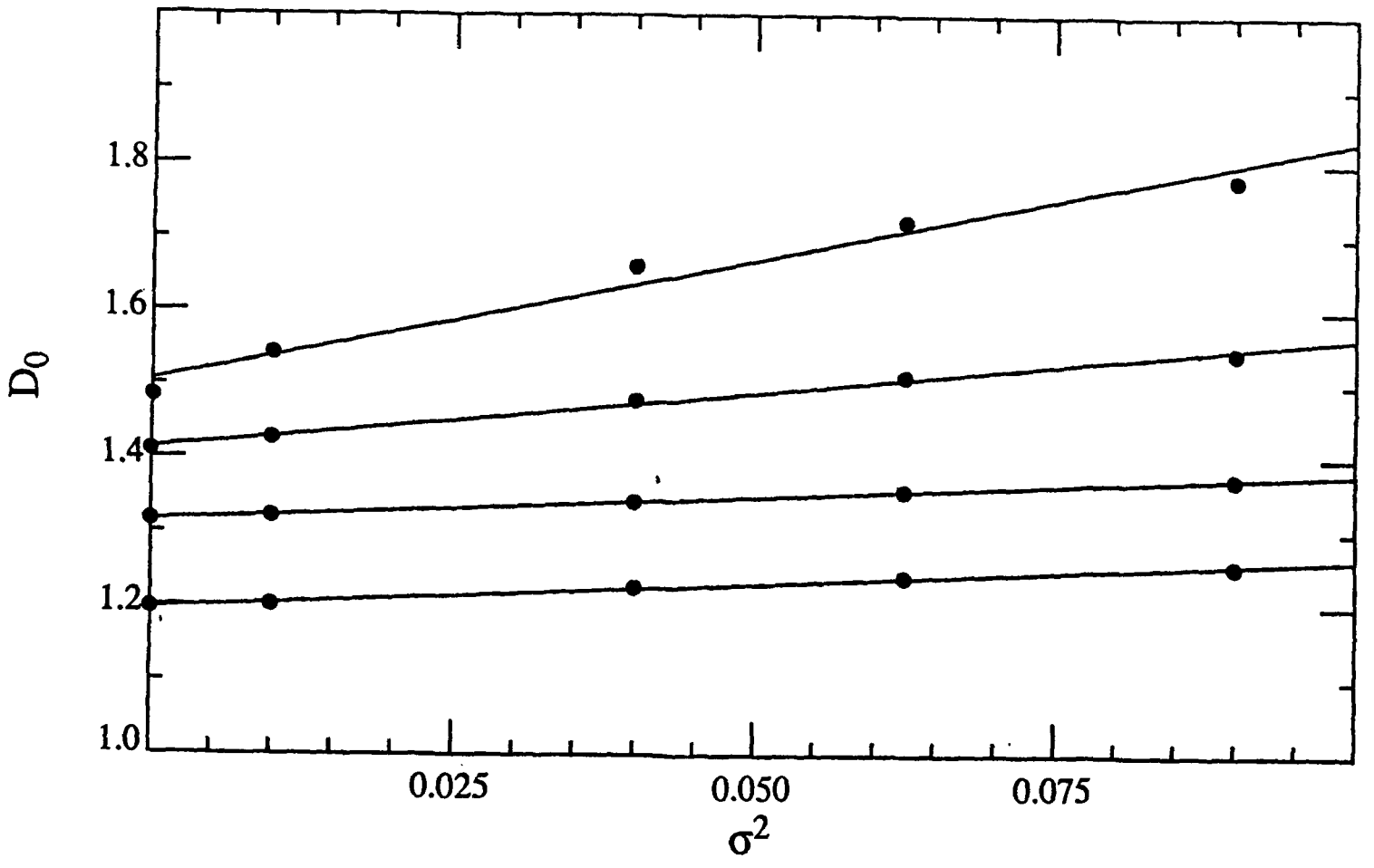

Figure 9. D_0 as a function of σ^2. The curves from bottom to top correspond, respectively, to a completely overcast sky and to solar illumination with $\vartheta_0 = 60°$, $70°$, and $80°$.

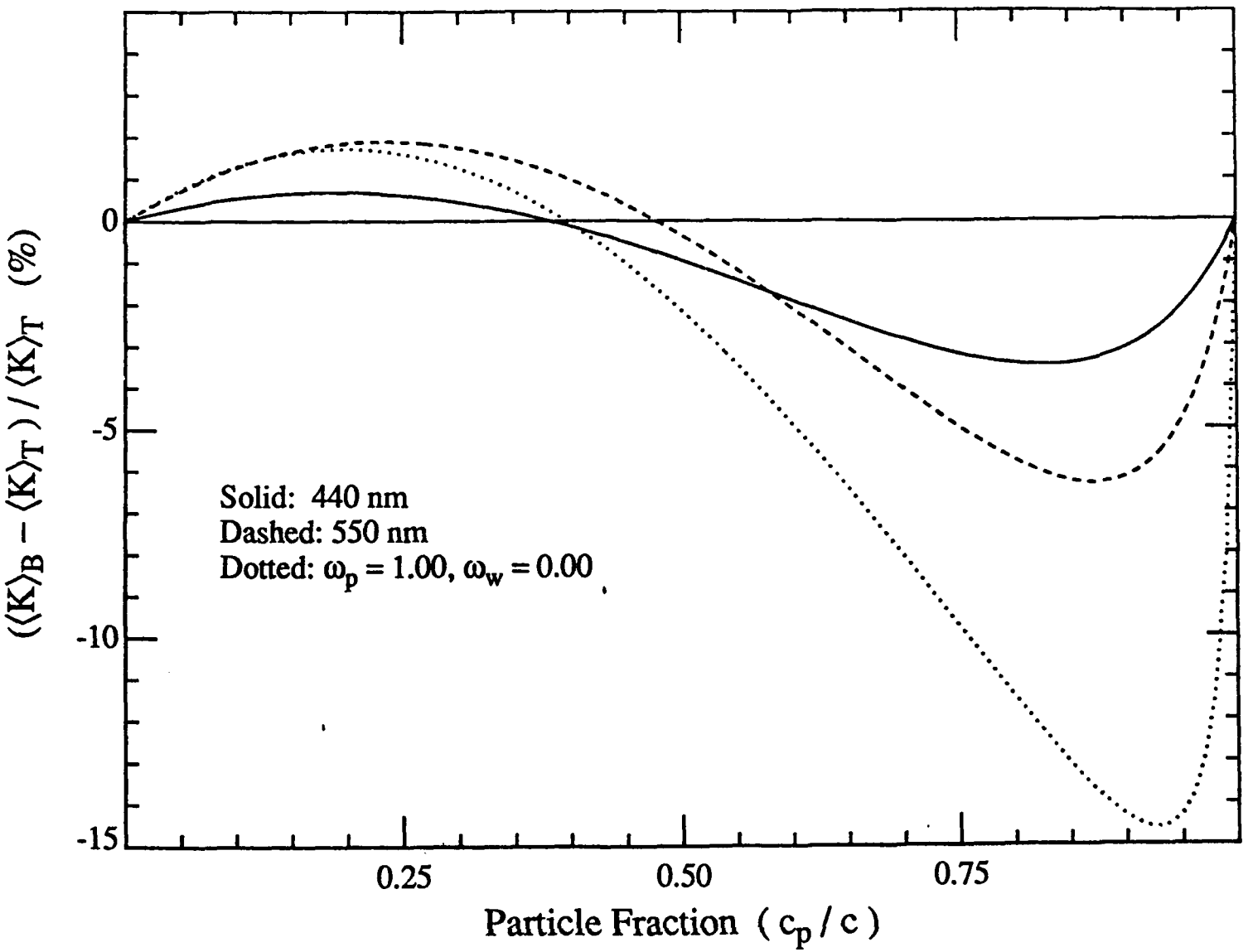

Figure 10. Relative error (%) in $\langle K \rangle_B$ as a function of the relative concentration of particles.

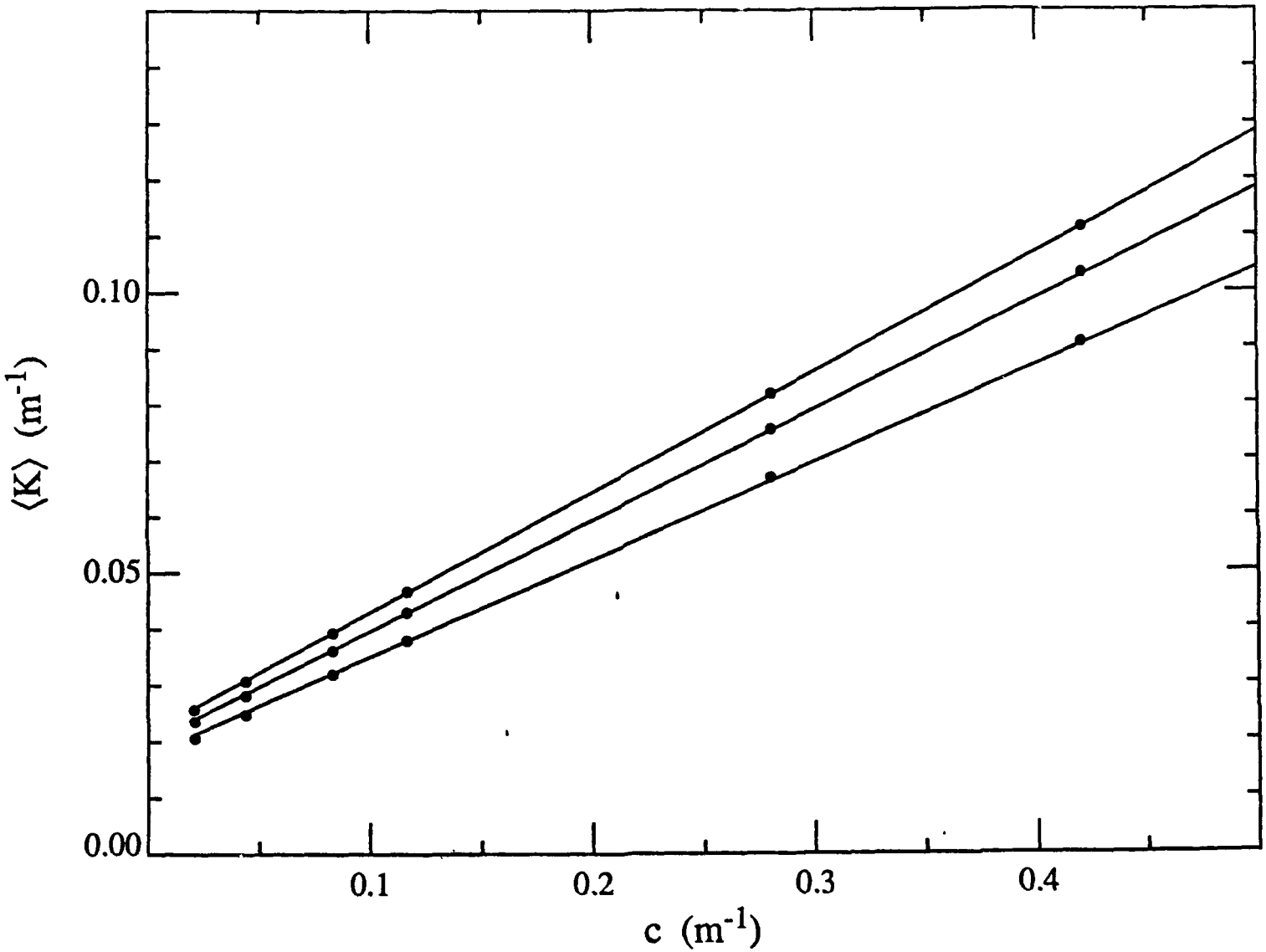

Figure 11. $\langle K \rangle$ at 480 nm as a function of c for particle phase function "M."
The lower and upper lines are for $\vartheta_0 = 0°$ and $60°$, respectively, the center line is for an overcast sky.

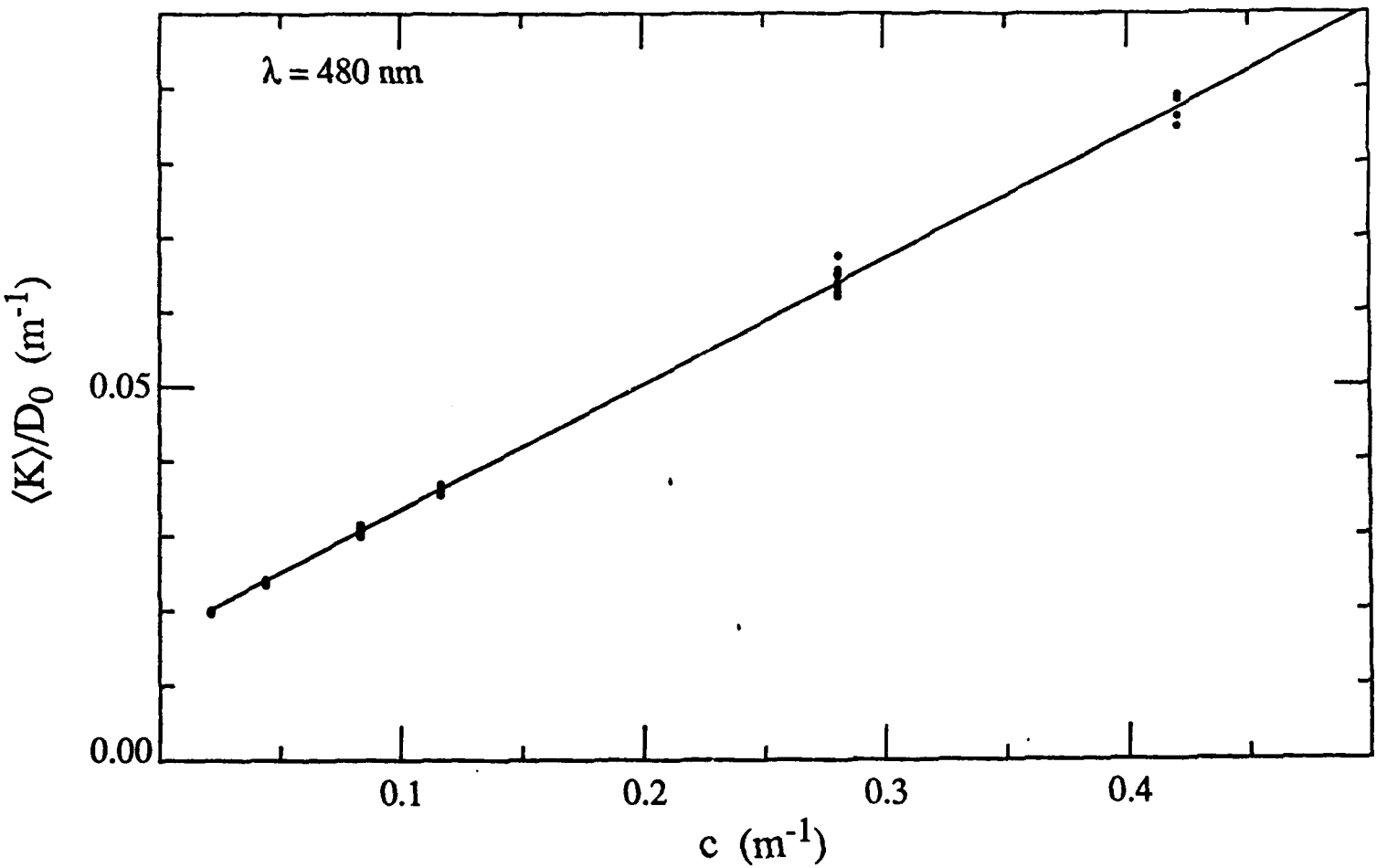

Figure 12. $\langle K \rangle / D_0$ as a function c at 480 nm. The points are Monte Carlo simulations for various values of ϑ_0, the line is a least-squares fit to the points with $c_p > c_w$.

Appendix 4

H.R. Gordon, Dependence of the Diffuse Reflectance of Natural Waters on the Sun Angle, *Limnology and Oceanography* (Submitted).

Running head: Dependence of diffuse reflectance on sun angle

Dependence of the diffuse reflectance of natural waters on the sun angle

by

Howard R. Gordon
Department of Physics
University of Miami
Coral Gables, FL 33124

(Submitted to *Limnology and Oceanography*)

Acknowledgement

This work received support from the Office of Naval Research under Contract N00014-84-K-0451 as part of the Biowatt Program and from the National Aeronautics and Space Administration under grant NAGW-273.

List of Symbols

Symbol	Name	Units
a	absorption coefficient	m^{-1}
α	scattering angle	
b	scattering coefficient	m^{-1}
$\beta(\alpha)$	volume scattering function	$m^{-1}Ster^{-1}$
c	attenuation coefficient $(a+b)$	m^{-1}
D_0	downwelling distribution function $(\omega_0 = 0)$	
e_f, e_b	phase function parameters	
$E_d(z)$	downwelling irradiance at z	W/m^2nm
$E_u(z)$	upwelling irradiance at z	W/m^2nm
K_d	attenuation coefficient for E_d	m^{-1}
m	refractive index of water	
μ, φ	integration variables	
μ_w	$\cos \vartheta_{0w}$	
$P(\alpha)$	scattering phase function (β/b)	$Ster^{-1}$
$R(D_0)$	diffuse reflectance at D_0	
$R(\vartheta_0)$	diffuse reflectance at ϑ_0	
$R(z)$	irradiance ratio (E_u/E_d) at z	
T	Fresnel transmittance of sea surface	
ϑ_0	solar zenith angle	
ϑ_{0w}	solar zenith angle below surface	
ω_0	scattering albedo (b/c)	
z	depth	m

Abstract

Through Monte Carlo simulation the variation of the diffuse reflectance of natural waters with sun angle is found to be dependent on the shape of the volume scattering function (VSF) of the medium. It is shown that single scattering theory can be used to estimate the reflectance – sun angle variation given the VSF, and conversely, the VSF can be retrieved from measurements of the variation of the reflectance with sun angle. The complex variation of reflectance with the incident illumination and surface roughness can be reduced to the variation of a single parameter: the downwelling distribution function in the absence of scattering. These observations are applicable to all but the most reflective of natural waters.

The irradiance ratio or irradiance reflectance at a depth z is defined according to $R(z) = E_u(z)/E_d(z)$, where E_u and E_d are, respectively, the upwelling and downwelling irradiances at z. When this is evaluated just beneath the sea surface it is referred to as the diffuse reflectance and indicated by R. R is interesting because it is relatively easy to measure, e.g., *absolute* calibration of the irradiance meter is not required, and it is used in the theory of ocean color remote sensing (Gordon and Morel 1983). In a series of Monte Carlo simulations of the transport of optical radiation in the ocean Gordon, Brown and Jacobs (1975) computed R for a homogeneous ocean as a function of the inherent optical properties of the water, the absorption coefficient a, the scattering coefficient b and the volume scattering function $\beta(\alpha)$, using scattering phase functions $[P(\alpha) = \beta(\alpha)/b]$ measured by Kullenberg (1968) in the Sargasso Sea. In a limited number of cases $R(\vartheta_0)$, the diffuse reflectance as a function of the solar zenith angle ϑ_0, was also studied. It was concluded that $R(\vartheta_0)$ was a very weak function of ϑ_0 – varying by less than 20% for $0° \leq \vartheta_0 \leq 60°$. Later, Kirk (1984) presented a similar Monte Carlo study (using phase functions measured by Petzold (1972) in San Diego Harbor) which showed a variation in $R(\vartheta_0)$, over the same range of angles, of much as 50%. This difference is far greater than what might be expected due to differences in the computational procedure and thus requires explanation. If it can be verified that neither computation is in error, differences in the results can only lie in the fact that different scattering phase functions were used in the computations. In fact, Jerlov (1976, page 149) states that the variation of R with ϑ_0 "is a consequence of the shape of the scattering function", but provides no quantitative demonstration of the claim. Also, even for $\vartheta_0 = 0$, Plass, Kattawar and Humphreys (1981) have already shown that R depends on the shape of the scattering phase function, contrary to the conclusion of Gordon, Brown and Jacobs (1975), Kirk (1984), and Morel and Prieur (1977) that R depends on the phase function principally through the backscattering coefficient b_b given by

$$b_b = 2\pi b \int_{\pi/2}^{\pi} P(\alpha) \sin\alpha \, d\alpha;$$

however, they employed phase functions that differed considerably from those observed in natural waters in order to demonstrate the dependence.

To investigate quantitatively the influence of the scattering phase function on the diffuse reflectance, I have recalculated R using standard Monte Carlo techniques and also using a new backward Monte Carlo code developed for another purpose (Gordon 1985). The results of the new computations are in complete agreement with the old, i.e., when the Petzold (1972) phase function is used the results from either code agree well with Kirk (1984) and when the Kullenberg (1968) phase function is used the results agree with Gordon, Brown and Jacobs (1975). This suggests the computations of both Kirk (1984) and Gordon, Brown and Jacobs (1975) were correct and that the difference is in fact due to the specific phase functions used in the two studies. It also suggests that the shape of the variation of R with ϑ_0 can provide some information about $\beta(\alpha)$. In what follows, it is shown that, given $\beta(\alpha)$, the single scattering approximation can be used to specify the variation of R with ϑ_0, and conversely, given $R(\vartheta_0)$, it is possible to invert the process and estimate $\beta(\alpha)$.

Let the ocean be illuminated by the direct solar beam. Then, if ϑ_{0w} is the solar zenith angle observed beneath the sea surface, i.e., $m \sin \vartheta_{0w} = \sin \vartheta_0$, where m is the refractive index of water, in the single scattering approximation the diffuse reflectance is given by

$$R(\vartheta_0) = \frac{1}{c} \int_0^{2\pi} d\varphi \int_0^1 d\mu \frac{\mu}{\mu + \mu_w} \beta(\alpha), \tag{1}$$

where $\cos \alpha = -\mu\mu_w + \sqrt{(1-\mu^2)(1-\mu_w^2)} \cos \varphi$, and $\mu_w = \cos \vartheta_{0w}$. This expression is valid for $b \ll a$, and provides a direct link between $R(\vartheta_0)$ and $\beta(\alpha)$ in this limit. Gordon (1973) has shown that, for a medium that scatters strongly in the forward direction, the validity of Equation 1 can be extended somewhat by replacing c by $a + b_b$. Physically this corresponds to replacing c by the value of the downwelling irradiance attenuation coefficient (K_d) that would be measured just beneath the surface of the medium (with the sun at the zenith), and it is called the quasi-single scattering approximation (QSA). Typically for the ocean $b_b \ll b$, and the QSA holds for much larger values of b/a (or equivalently $\omega_0 \equiv b/(a+b)$) than the single scattering approximation. With the sun at the zenith, Gordon (1973) found the the QSA reproduced Monte Carlo computations of R to within 0.5% for $\omega_0 < 0.6$ and 12% for $\omega_0 < 0.85$. Thus, one can expect Equation 1 to predict the variation of R with sun angle, even for rather large values of ω_0. The efficacy of Equation 1 in this respect is examined by comparison with exact (Monte Carlo) computations carried out using two scattering phase functions: "KC" , the Kullenberg (1968) phase function measured at 460 nm in the Sargasso Sea and used by Gordon, Brown and Jacobs (1975); and "T", the mean of the three particle phase functions measured in turbid water at 530 nm by Petzold (1972) and

used in the Kirk (1984) computations. These are shown in Figure 1 along with phase function for molecular (Rayleigh) scattering of pure water. The resulting comparison between Equation 1 and the Monte Carlo (M.C.) computations is presented in Figure 2, where it is seen that the analytical computation of $R(\vartheta_0)/R(0)$ agrees with the Monte Carlo computations with a maximum error of $< 5\%$ for $\omega_0 = 0.8$ and $\lesssim 10\%$ for $\omega_0 = 0.9$. The general increase in R with ϑ_0 is due to the fact that the minimum scattering angle for photons to be redirected to the surface increases with ϑ_0 according to $\alpha = \pi/2 - \vartheta_{0w}$. Since $P(\alpha)$ increases rapidly with decreasing α for $\alpha < \pi/2$ (Figure 1), portions of the phase function which are larger than those for $\pi/2 < \alpha < \pi$ increasingly contribute to R as ϑ_0 increases. This is particularly evident for phase function T for which there is a strong contrast in the values of $P(\alpha)$ above and below $\alpha = \pi/2$. In the case of scattering by pure sea water (not shown), i.e., Rayleigh scattering, the analytical computation has a maximum error of $\lesssim 0.5\%$ for the largest value of ω_0 encountered in the ocean (~ 0.3 near 400 nm).

It is seen that for $\omega_0 = 0.8$, there is a clear trend for the multiple scattering computations of $R(\vartheta_0)/R(0)$ to be above the single scattering results. This is due to the fact that at each scattering event after the first, some photons can scatter through progressively smaller angles and still be redirected toward the surface. Since $P(\alpha)$ increases with decreasing α for $\alpha \lesssim \pi/2$, multiple scattering should increase $R(\vartheta_0)/R(0)$ above the single scattering result when photons can scatter a few times before being absorbed. Since phase function T is larger at very small scattering angles than KC (25% of the scattering events for T have $\alpha \leq 1°$, compared to 5% for KC), the effect is larger for KC. For larger values of ω_0, this effect disappears because photons scatter many times before reaching the surface and the information concerning the direction at which the photon entered the water becomes lost. Thus, for small ω_0 the exact value of $R(\vartheta_0)/R(0)$ should be close to that given by Equation 1; however, as ω_0 increases, $R(\vartheta_0)/R(0)$ will initially increase above the single scattering value and then eventually decrease below it as $\omega_0 \rightarrow 1$.

The near-agreement between $R(\vartheta_0)/R(0)$ and that predicted by single scattering (or more correctly, QSA) indicates that measurements of $\beta(\alpha)$ over the appropriate range of angles, $41° \lesssim \alpha \leq 180°$, can be used to predict the dependence of R on ϑ_0; however, measurement of $\beta(\alpha)$ over this entire range is not necessary. Gordon (1976) showed that b_b could be accurately determined without knowing the full scattering function. This is accomplished by fitting measurements of β at only

three angles, $\alpha = 45°$, $90°$, and $135°$, to an analytic equation first used by Beardsley and Zaneveld (1969):

$$\beta(\alpha) = \frac{\beta(90°)}{(1 - e_f \cos\alpha)^4 (1 + e_b \cos\alpha)^4}, \tag{2}$$

where e_f and e_b are adjustable parameters. The fits of phase functions T and KC to Equation 2 are shown as the solid lines in Figure 3. The fit is excellent for scattering between about 40° and 160°, correctly reproducing the significant variation around 90°. However, Equation 2 is a very poor approximation at scattering angles less than 25°–30° and is in error by a factor of 10^3 or more near 0°. For Rayleigh scattering (not shown), Equation 2 provides an excellent fit for all scattering angles. Computation of $R(\vartheta_0)/R(0)$ using Equation 1 (single scattering) and the fits of the phase function to Equation 2 agree with those using Equation 1 and the actual phase functions with an error of less than 2%. On this basis I conclude that measurement of $\beta(45°)$, $\beta(90°)$, and $\beta(135°)$ are sufficient to describe the variation of R with ϑ_0. It is, of course, of interest to know if the process above can be inverted, i.e., given $R(\vartheta_0)/R(0)$ is it possible to estimate $\beta(\alpha)$? To examine this question, I have assumed that $R(\vartheta_0)$ is measured (in this case *simulated* by Monte Carlo) at 10° increments from 0 to 89°. This "data" is then fit to Equation 1, with $\beta(\alpha)$ given by Equation 2, using a nonlinear least-squares technique to determine the unknown parameters e_f and e_b. The resulting derived phase functions for $\omega_0 = 0.8$ (dashed curves) and 0.9 (chain dashed curves) are presented in Figure 3. In reality, the above procedure can only provide $P(\alpha)/P(90°)$; however, in Figure 3 we have normalized $P(\alpha)$ to obtain the correct value of b_b, i.e., so that the true $P(\alpha)$ and the inverted $P(\alpha)$ would yield the same value of $R(0)$. Clearly, in this restricted case, i.e., measurement of $R(\vartheta_0)$ for the full domain of ϑ_0, the general shape of $\beta(\alpha)$ for $60° - 70° \lesssim \alpha \leq 180°$ can be retrieved from measurements of $R(\vartheta_0)$.

The conclusions in this note are based on simulations of an idealized ocean, i.e., a flat, homogeneous ocean with $\omega_0 \leq 0.9$ in the absence of the atmosphere. How applicable are they to a real ocean? From the analysis of Gordon (1987) one expects $\omega_0 \leq 0.9$ in natural waters except in intense plankton blooms (in the green) or regions with a high concentration of nonabsorbing suspended particles, e.g., white sand, in the water. The only effect of the atmosphere is to add a quasi-diffuse component (skylight) to the irradiance incident on the sea surface. If dE_d is the irradiance incident on the surface with zenith angles between ϑ and $\vartheta + d\vartheta$, the reflectance is easily computed to be

$$R = \frac{\int_0^{\pi/2} R(\vartheta) T(\vartheta) (dE_d/d\vartheta)\, d\vartheta}{\int_0^{\pi/2} T(\vartheta) (dE_d/d\vartheta)\, d\vartheta},$$

where $T(\vartheta)$ is the Fresnel transmittance (air to water) of the surface for an incident angle of ϑ. For a totally diffuse incident irradiance (incident *radiance* independent of viewing direction) $dE_d/d\vartheta \propto \sin 2\vartheta$ and R normalized to $R(\vartheta_0 = 0)$ is approximately that given by Equation 1 for $\vartheta_0 = 40°$ in agreement with Monte Carlo simulations. Similarly, the effect of replacing the flat surface with a rough surface is to render the incident light field *beneath* the surface more diffuse. However, in contrast with a flat ocean, ϑ_{0w} can exceed the critical angle, $\sin^{-1}(1/m)$, when the surface is rough. For large ϑ_0 large values of ϑ_{0w} are possible, and these photons can can be redirected toward the surface through highly probable small angle scattering. Thus, in the absence of skylight $R(\vartheta_0)$ will in general be larger in an ocean ruffled by the wind than for a flat ocean. Monte Carlo simulations using a surface described by the Cox and Munk (1954) slope distribution characteristic of a 7.2 m/s wind speed with phase function T and $\omega_0 = 0.8$ showed slight ($< 2\%$) increases in $R(\vartheta_0)/R(0)$ over the smooth ocean case for $\vartheta_0 = 40°$ and 60° and increases of 7 and 18% for $\vartheta_0 = 70°$ and 80°, respectively. Thus the effect of surface waves on the validity of $R(\vartheta_0)/R(0)$ computed from Equation 1 is small for $\vartheta_0 \lesssim 60 - 70°$.

It would be useful if the effect on R of variations in ϑ_0, the amount of skylight in the incident irradiance, and the surface roughness could be explained by the variation of a single parameter. The key to finding such a parameter lies in a recent set of Monte Carlo simulations (Jerome, Bukata and Burton 1988) showing that $R(\vartheta_0)/R(0) = 1/\cos\vartheta_{0w}$. Although the present computations only have the property that $R(\vartheta_0)/R(0) \approx k/\cos\vartheta_{0w}$, where k is a constant, the value of k is approximately unity when the same phase function used by Jerome, Bukata and Burton (1988) is employed. The values of k for phase functions KC and T are approximately 0.85 and 1.15, respectively. These observations are more interesting when it is realized that if the illumination incident on a flat ocean is in the form of a parallel beam from the sun, the downwelling distribution function — the downwelling scalar irradiance divided by the downwelling irradiance (Preisendorfer 1961) — just beneath the surface in the *absence* of scattering, D_0, is exactly $1/\cos\vartheta_{0w}$. In cases with parallel beam illumination of a flat ocean, as well as situations with more complex illumination, D_0 has been used to remove the geometrical properties of the incident light field from the downwelling irradiance attenuation coefficient (Gordon 1989, Gordon, Brown and Jacobs 1975), in effect normalizing the coefficient to that which would be measured in the absence of the atmosphere with the sun at the zenith. Thus, it is natural to ask if D_0 might be used to simplify the analysis of $R(\vartheta_0)/R(0)$ in more complex situations. Clearly, the simplest procedure for trying to extend the analysis to more complex situations is to plot $R(\vartheta_0)/R(0)$ as a function of D_0, i.e., to replace the $1/\cos\vartheta_{0w}$ used

by Jerome, Bukata and Burton (1988) by its more general equivalent, D_0. Thus far, in addition to an incident beam of parallel irradiance on a flat surface, we have discussed two other incident distributions (beneath the surface): a distribution resulting from wind induced surface roughness; and a distribution resulting from uniform radiance incident above a flat surface. In the case the wind-ruffled surface described earlier, a separate computation was carried out to determine D_0 and the resulting values of $R(D_0)/R(1)$ are plotted against D_0 in Figure 4 (symbols with $+$'s) along with the results taken from Figure 2. Note that in each case, the simulated values of $R(D_0)/R(1)$ are linearly related to D_0, and that the rough ocean cases fall with excellent accuracy along the same lines as their flat ocean counterparts. Simulations carried out with totally diffuse incident irradiance falling on a flat ocean (symbols with $\times$'s in Figure 4) show that the same linear relationship is satisfied in this case as well.

These results show that for a given ω_0 and scattering phase function, $R(D_0) = kD_0R(1)$, i.e., the variation of R with the incident illumination and the surface roughness can be completely explained through their effect on D_0. [An accurate scheme for estimating D_0 from simple irradiance and wind speed measurements is provided in Gordon (1989).] The parameter k depends mostly on the scattering phase function, and for $\omega_0 \lesssim 0.9$ it can be computed using the single scattering approximation. In sum, the main conclusion of this note — that single scattering can be used to characterize the variation of R with the incident radiance distribution — should be applicable to a real ocean if highly reflective waters ($\omega_0 > 0.9$) are avoided.

References

Beardsley, G. F. and J. R. V. Zaneveld 1969. Theoretical Dependence of the Near-Asymptotic Apparent Optical Properties on the Inherent Optical Properties of Sea Water. Jour. Opt. Soc. Amer. 59: 373–377.

Cox, C. and W. Munk 1954. Measurements of the Roughness of the Sea Surface from Photographs of the Sun's Glitter. Jour. Opt. Soc. of Am. 44: 838–850.

Gordon, H. R. 1973. Simple Calculation of the Diffuse Reflectance of the Ocean. Applied Optics 12: 2803–2804.

———— 1976. Radiative Transfer in the Ocean: A Method for Determination of Absorption and Scattering Properties. Applied Optics 15: 2611–2613.

———— 1985. Ship Perturbation of Irradiance Measurements at Sea 1: Monte Carlo Simulations. Applied Optics 23: 4172–4182.

———— 1987. A Bio-Optical Model Describing the Distribution of Irradiance at the Sea Surface Resulting from a Point Source Imbedded in the Ocean. Applied Optics 26: 4133–4148.

———— 1989. Can the Lambert-Beer Law Be Applied To the Diffuse Attenuation Coefficient of Ocean Water?. Limnology and Oceanography (Submitted).

Gordon, H. R., O. B. Brown and M. M. Jacobs 1975. Computed Relationships Between the Inherent and Apparent Optical Properties of a Flat Homogeneous Ocean. Applied Optics 14: 417–427.

Gordon, H. R. and A. Y. Morel 1983. Remote Assessment of Ocean Color for Interpretation of Satellite Visible Imagery: A Review, Springer-Verlag. 114 pp.

Jerlov, N. G. 1976. Marine Optics, Elsevier. 231 pp.

Jerome, J. H., R. P. Bukata and J. E. Burton 1988. Utilizing the Components of Vector Irradiance to Estimate the Scalar Irradiance in Natural Waters. Applied Optics 27: 4012–4018.

Kirk, J. T. O. 1984. Dependence of relationship between inherent and apparent optical properties of water on solar altitude. Limnology and Oceanography 29: 350–356.

Kullenberg, G. 1968. Scattering of light by Sargasso Sea water. Deep Sea Research 15: 423–432.

Morel, A. and L. Prieur 1977. Analysis of Variations in Ocean Color. Limnology and Oceanography 22: 709–722.

Petzold, T. J. 1972. Volume Scattering Functions for Selected Natural Waters, Scripps Institution of Oceanography, Visibility Laboratory, San Diego, CA. 92152, SIO Ref. 72–78.

Plass, G. N., G. W. Kattawar and T. J. Humphreys 1981. Calculations of Radiative Transfer in the Ocean., IAMAP Third Scientific Assembly, 17-28 August, Hamburg, FDR.

Preisendorfer, R. W. 1961. Application of Radiative Transfer Theory to Light Measurements in the Sea. Union Géodésique et Géophysique Internationale 10: 11–30.

Figure Captions

Figure 1. Phase functions used in the present study.

Figure 2. R as a function of ϑ_0. Dots are for $\omega_0 = 0.8$, open circles for $\omega_0 = 0.9$. The solid curves are the result of the single scattering approximation (Eq. 1). Upper curve is for phase function "T", lower for "KC."

Figure 3. Phase functions "KC" (upper) and "T" (lower). The dots are the true values. The solid lines are fits with Eq. 2 using $P(\alpha)$ evaluated at $\alpha = 45°, 90°$, and $135°$. The dashed and chain dashed curves are the result of inverting Eq. 1 for $\omega_0 = 0.8$ and 0.9, respectively.

Figure 4. R as a function of D_0. Dots are for $\omega_0 = 0.8$, open circles for $\omega_0 = 0.9$. Symbols with $+'$s are for a rough surface. Symbols with $\times'$s are for a diffuse incident irradiance. The solid curves are the result of the single scattering approximation (Eq. 1). Upper curve is for phase function "T," lower for "KC."

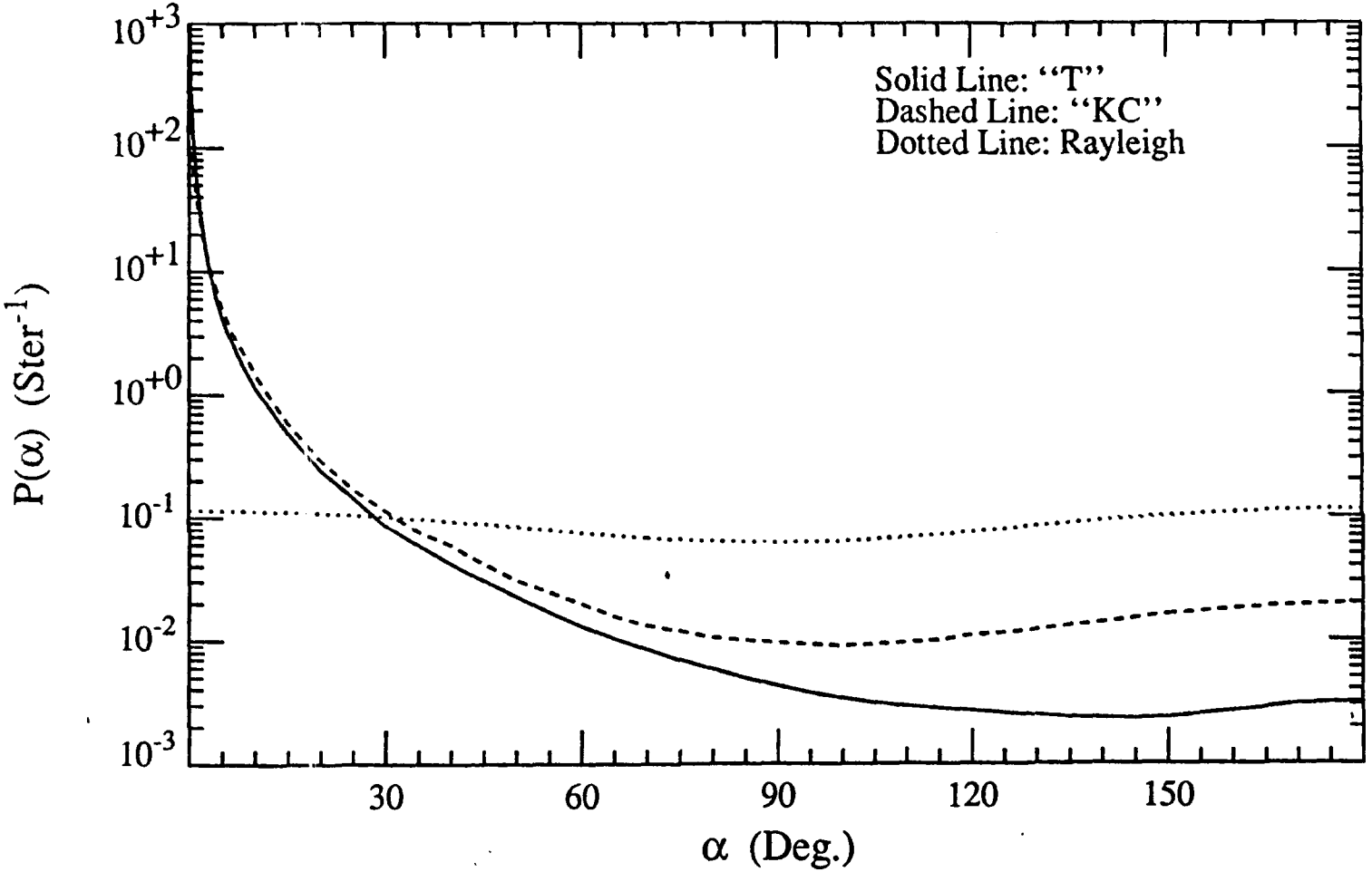

Figure 1. Phase functions used in the present study.

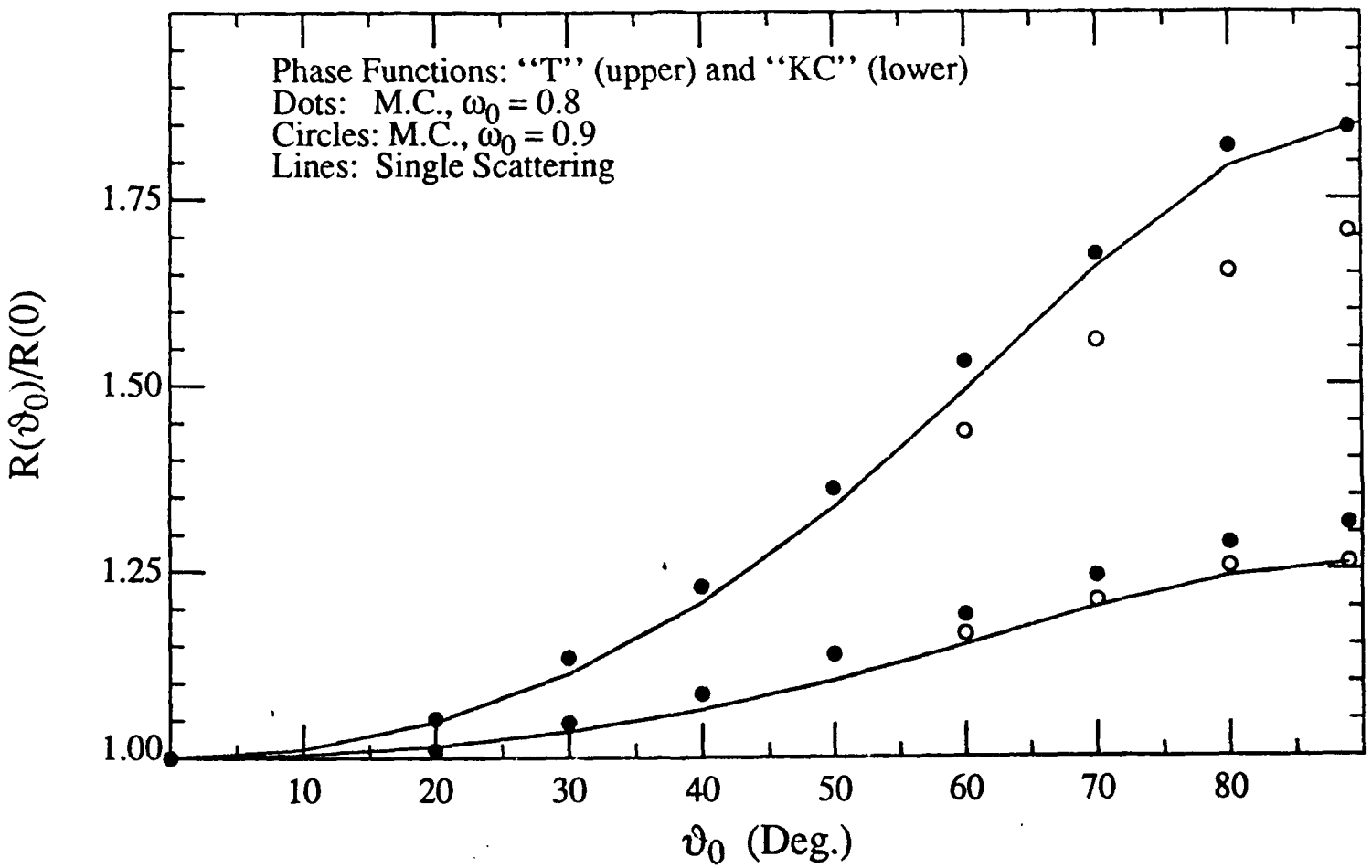

Figure 2. R as a function of ϑ_0. Dots are for $\omega_0 = 0.8$, open circles for $\omega_0 = 0.9$. The solid curves are the result of the single scattering approximation (Eq. 1). Upper curve is for phase function "T", lower for "KC."

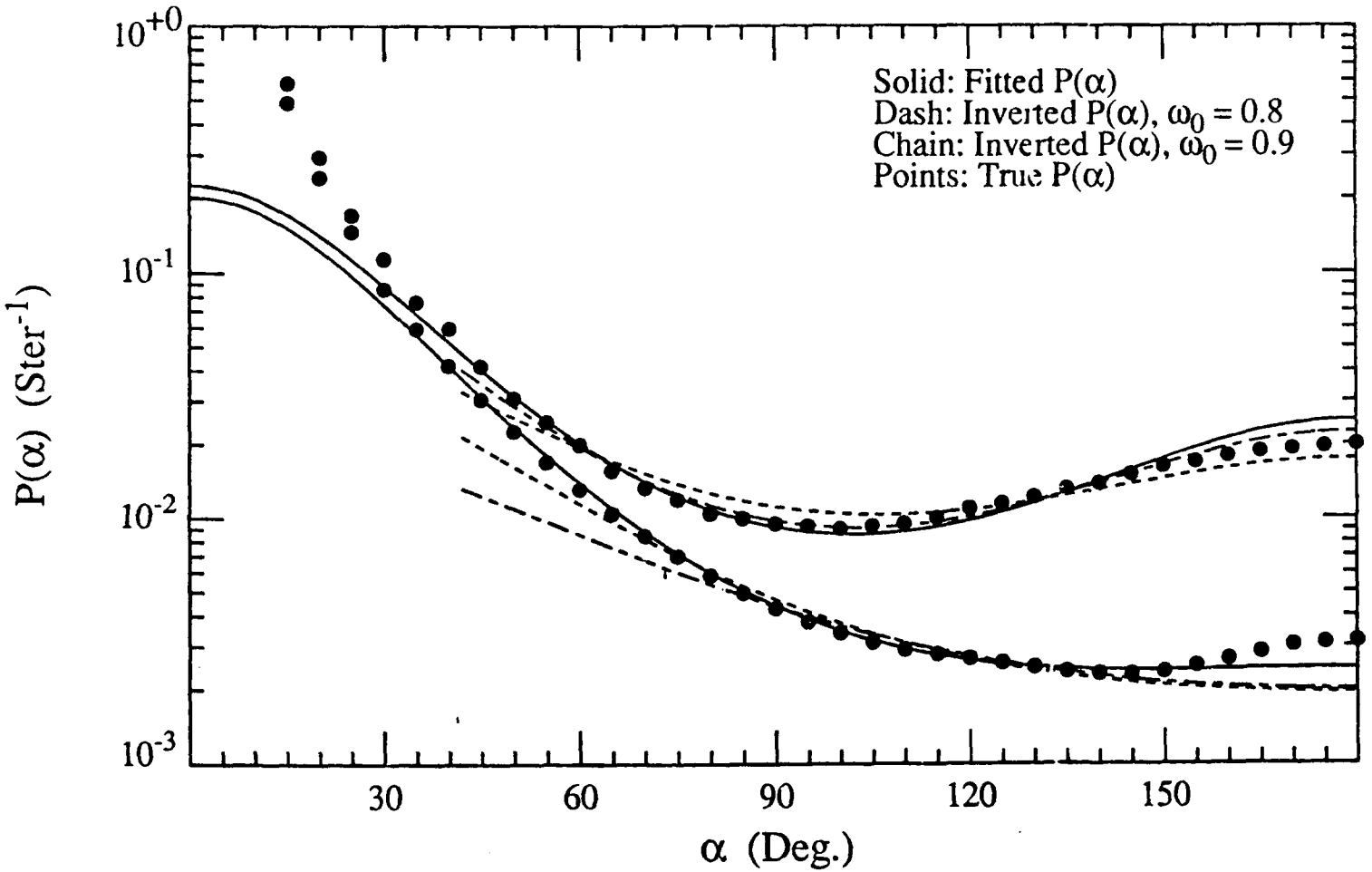

Figure 3. Phase functions "KC" (upper) and "T" (lower). The dots are the true values. The solid lines are fits with Eq. 2 using $P(\alpha)$ evaluated at $\alpha = 45°$, $90°$, and $135°$. The dashed and chain dashed curves are the result of inverting Eq. 1 for $\omega_0 = 0.8$ and 0.9, respectively.

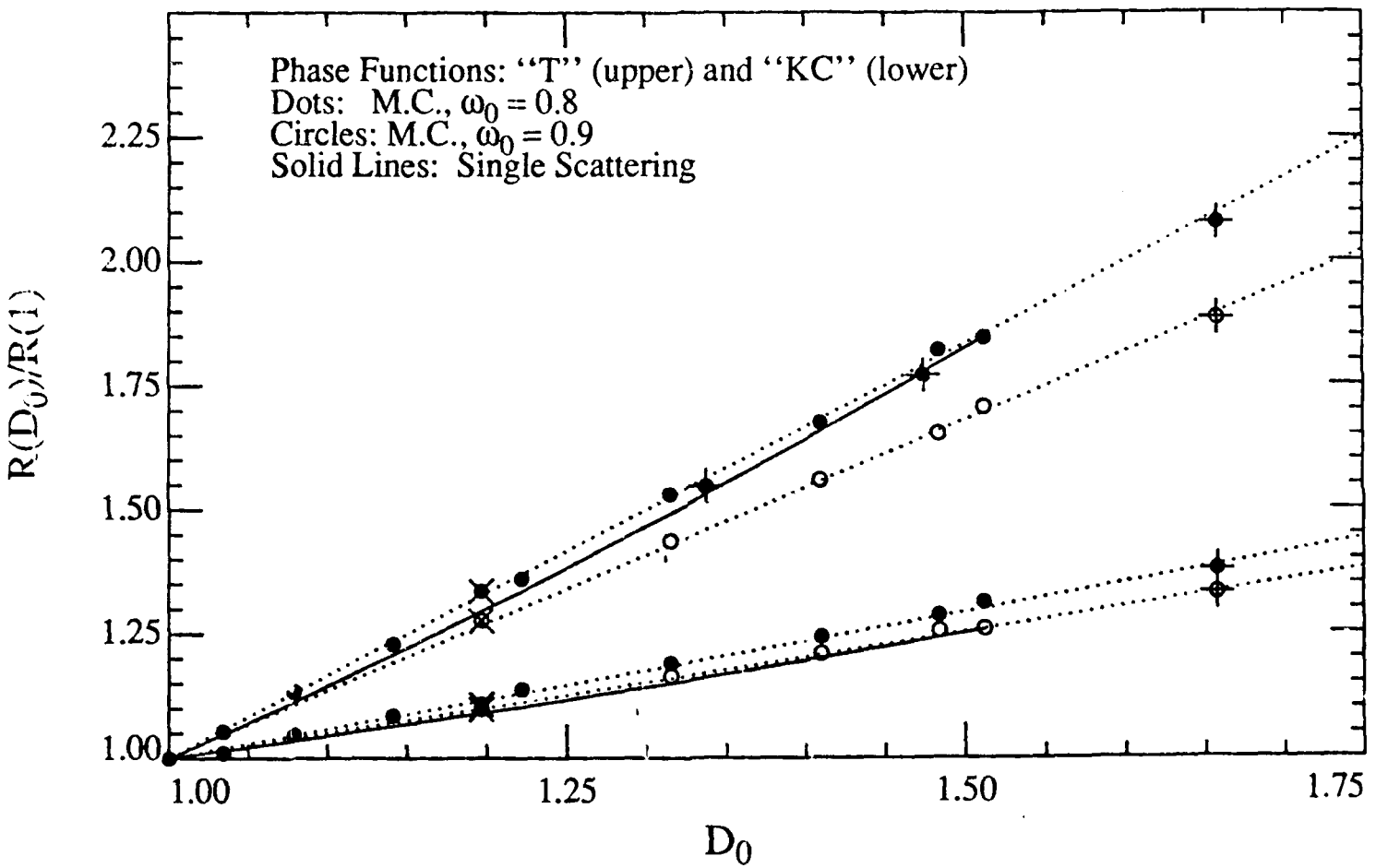

Figure 4. R as a function of D_0. Dots are for $\omega_0 = 0.8$, open circles for $\omega_0 = 0.9$. Symbols with +'s are for a rough surface. Symbols with ×'s are for a diffuse incident irradiance. The solid curves are the result of the single scattering approximation (Eq. 1). Upper curve is for phase function "T," lower for "KC."

Appendix 5

H.R. Gordon and D.J. Castaño, The Coastal Zone Color Scanner Atmospheric Correction Algorithm: Influence of El Chichón, *Applied Optics*, **27**, 3319–3321 (1988).

Reprinted from Applied Optics, Vol. 27 page 3319, August 15, 1988

Coastal Zone Color Scanner Atmospheric Correction: Influence of El Chichon

Howard R. Gordon and Diego J. Castaño

University of Miami, Physics Department, Coral Gables, Florida 33124.
Received 25 November 1987.
0003-6935/88/163319-04$02.00/0.

In a recent paper[1] we investigated the effects of multiple scattering on the Coastal Zone Color Scanner (CZCS)[2-4] atmospheric correction. As a measure of the efficacy of the correction algorithm, we defined the residual error at 443 nm in the correction algorithm $\Delta L_a(443)$, when the water leaving radiance was known in the other three bands (520, 550, and 670 nm), according to

$$\Delta L_a(443) = L_t(443) - L_r(443) - t(443)L_w(443) - \epsilon(443,670)\frac{F_0(443)}{F_0(670)}[L_t(670) - L_r(670)],$$

where $L_t(\lambda)$, $L_r(\lambda)$, and $L_w(\lambda)$ are, respectively, the total radiance observed by the sensor at the wavelength λ, the radiance due to Rayleigh scattering in the atmosphere, and the radiance exiting the sea surface from beneath; $t(\lambda)$ is the diffuse transmittance of the atmosphere, and $F_0(\lambda)$ is the extraterrestrial solar irradiance. $\epsilon(443,670)$ is the so-called atmospheric correction parameter that is determined from

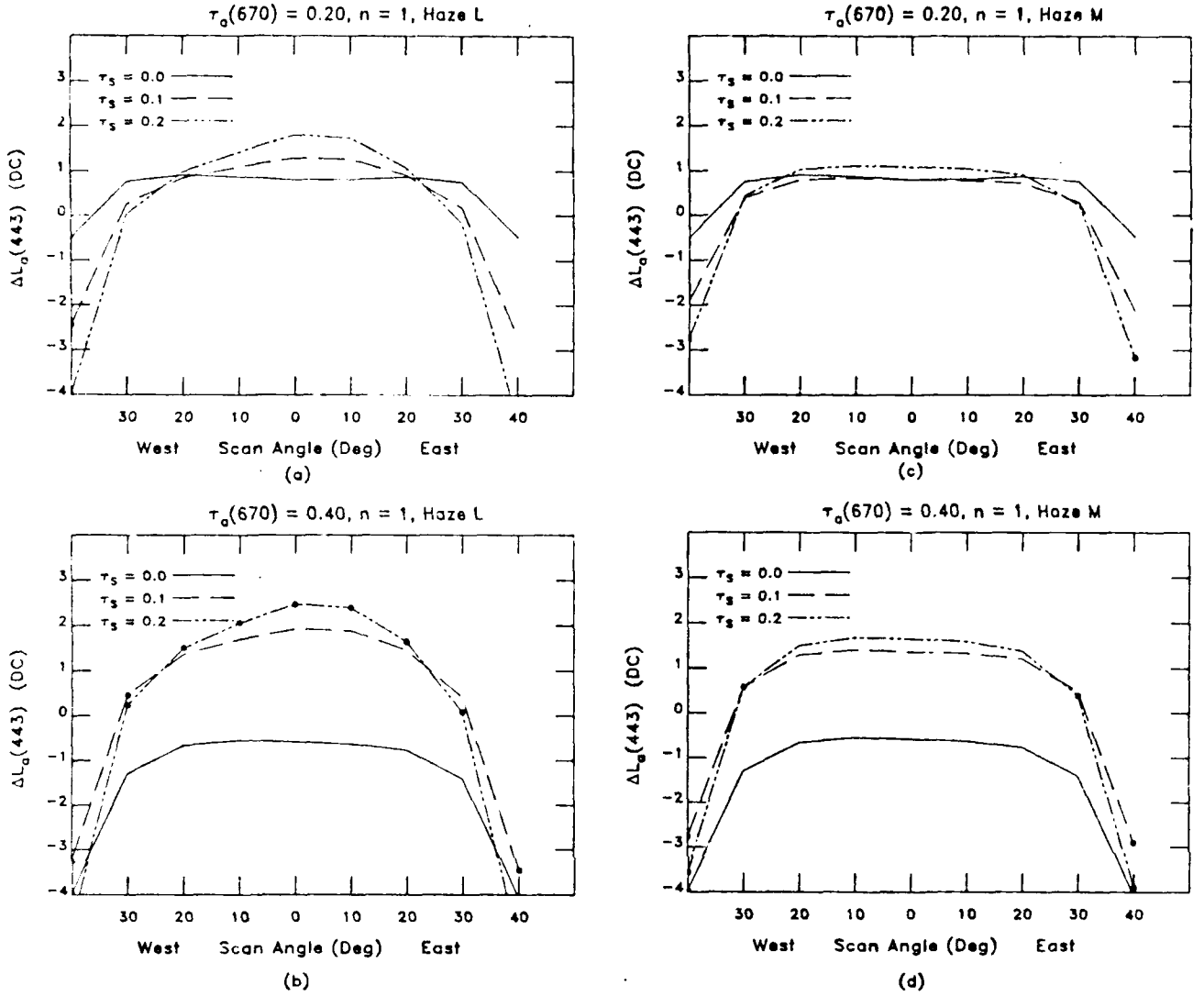

Fig. 1. Error in the recovered aerosol radiance at 443 nm (in digital counts) across the CZCS scan for Orbit 2217 as a function of the stratospheric aerosol concentration (τ_s) and phase function: (a) $\tau_a(670) = 0.2$ with the Haze L phase function in the stratosphere; (b) $\tau_a(670) = 0.4$ and Haze L in the stratosphere; (c) $\tau_a(670) = 0.2$ and Haze M in the stratosphere; (d) $\tau_a(670) = 0.4$ and Haze M in the stratosphere.

spectral variation of the radiance resulting from aerosol scattering in the atmosphere and is approximately the ratio of the aerosol optical thickness at 443 to that at 670 nm. For a perfect atmospheric correction, $\Delta L_a(443) = 0$; for an acceptable atmospheric correction $\Delta L_a(443) \lesssim 2$ DC, where 1 DC (digital counts) is the radiance corresponding to the digitization interval (one part in 256) of $L_t(\lambda)$. At 443 nm, 1 DC $\approx$ 0.045 mW/cm^2 μm sr. We computed $\Delta L_a(443)$ for the CZCS orbit as a function of the scan angle and the aerosol optical thickness in the red and found that the simple expediency of using the standard algorithm,[5] which was justified on the basis of single scattering, computing the molecular scattering contribution by correctly accounting for multiple scattering, and reducing the satellite-derived value of $\epsilon(443,670)$ by 5%, reduced $\Delta L_a(443)$ to below the 1–2 DC level for most atmospheres and viewing situations. In those computations the aerosol was largely confined to the troposphere. However, the eruption of the volcano El Chichon during 28 Mar.–4 Apr. 1982 was known to have introduced a significant quantity of aerosol into the stratosphere.[6] Since radiative transfer in the atmosphere is not insensitive to the vertical distribution of the components, and since CZCS viewed the ocean through the El Chichon aerosol layer for a significant portion of its life (1978–1986), we believed it would be useful to extend the computations to include the effect of an El Chichon-like aerosol layer on CZCS atmospheric correction. We present the results of these simulations in this Letter.

The tropospheric model follows that used previously,[1] i.e., a stratified atmosphere with both the Rayleigh and aerosol scattering, each decreasing exponentially with altitude, but with different scale heights. Approximately 90% of the aerosol is confined to a layer of 2 km in thickness near the sea surface, with ~80% of the Rayleigh scattering molecules above the aerosol. To simulate the effects of the El Chichon stratospheric aerosol, a homogeneous layer of arbitrary optical thickness τ_s and phase function is added at the top of the atmosphere. The tropospheric and stratospheric aerosols both scatter according to two-term Henyey-Greenstein[7] (TTHG) phase functions. Two aerosol models are used in the computations. The first approximates marine aerosol

phase functions given by Quenzel and Kastner.[8] The TTHG parameters for this phase function, which we shall refer to as Haze M, are $\alpha = 0.983$, $g_1 = 0.82$, and $g_2 = -0.55$. The second phase function is an approximation developed by Kattawar[7] for the Deirmendjian Haze L distribution[9] with a refractive index of 1.55, used to represent continental-type aerosols. Its parameters are $\alpha = 0.9618$, $g_1 = 0.7130$, and $g_2 = -0.7598$. In our simulations, the marine aerosol model is always used for the tropospheric phase function. Interestingly, this phase function does not differ significantly in the backward hemisphere from that proposed for the El Chichon stratospheric aerosol by King[6] based on extinction measurements.[10,11] Thus, in one set of simulations, the stratospheric aerosol phase function is also approximated by the marine aerosol model. In a second set of simulations the Haze L phase function is used for the stratospheric aerosol. Haze L differs considerably from King's model, scattering approximately an order of magnitude more at scattering angles Θ near 180°. Haze L probably represents the maximum scattering near $\Theta = 180°$ for realistic aerosol models. It was included to provide contrast to King's model. The tropospheric aerosol optical thickness is assumed to vary with wavelength according to $\tau_a(\lambda) = (670/\lambda)^n \tau_a(670)$, where $n = 0$ or 1, while the stratospheric aerosol optical thickness is assumed to be independent of wavelength.[10,11] The small effects of ozone are ignored.

Computations for the four orbital scenarios studied earlier[1] were carried out with the stratospheric aerosol layer in place. A sample of the computations is given in Fig. 1, which provides $\Delta L_a(443)$ at nine positions across the CZCS scan[12] as a function of $\tau_a(670)$ and τ_s for orbit 2217. The computed $\Delta L_a(443)$ values are for $\tau_a(670) = 0.20$ and 0.40, $n = 1$, and $\tau_s = 0$, 0.10, and 0.20. Using the standard definition of visible range, i.e., $3.912/b(550)$, where $b(550)$ is the total scattering coefficient at the surface at 550 nm, a $\tau_a(670)$ of 0.20 with $n = 1$ corresponds to a horizontal visible range at the surface of ~15.4 km while 0.40 corresponds to 7.9 km. The Haze L phase function has been used for the stratospheric aerosol in Figs. 1(a) and (b), while Figs. 1(c) and (d) are for the Haze M phase function. The symbol ● at a computed point indicates that the total radiance at the CZCS was greater than the saturation radiance (256 DC) at 670 nm. As the aerosol concentration increases, the sensor tends to saturate because of the contribution by Rayleigh scattering at large scan angles. At these points no atmospheric correction is possible in practice because the total radiance at the sensor at 670 nm is unknown.

Figures 1 show the effect of the vertical distribution of the aerosol on $\Delta L_a(443)$. Comparing the $\tau_s = 0.20$ curve in (c) [$\tau_a(670) = 0.20$] and $\tau_s = 0$ in panel (d) [$\tau_a(670) = 0.40$] reveals an ~1.5-DC difference in $\Delta L_a(443)$; however, these curves correspond to the same total aerosol optical thickness [$\tau_a(670) + \tau_s = 0.40$], and both aerosols are characterized by the same phase function (Haze M). The only difference between the two curves is that in (c) half of the aerosol is near the bottom of the atmosphere and half of the aerosol is at the top of the atmosphere, while in (d) all the aerosol is near the bottom of the atmosphere.

The immediate and most important conclusion to be drawn from Fig. 1 is that, except near the edges of the scan, in those situations where the sensor does not saturate at 670 nm the error in the atmospheric correction algorithm in the presence of the stratospheric aerosol is <1–2 DC. This observation is also applicable to the other viewing scenarios examined earlier,[1] with the exception of Orbit 3226 with Haze L in the stratosphere. The strong backscattering associated with Haze L comes into play in this orbit where almost direct backscattering is observed near the center of the scan ($\Theta \approx 174.5°$). This causes the sensor to saturate even near the scan center with τ_s as low as 0.10 when $\tau_a(670) = 0.40$ and at several points along the scan when $\tau_a(670) = 0.20$. When the sensor does not saturate near the center of the scan the error is <3 DC for $\tau_a(670) = 0.20$ and 4 DC for $\tau_a(670) = 0.40$. When the Haze M phase function is used in the stratosphere in Orbit 3226, a pattern similar to that in Figs. 1(c) and (d) is found; however, for $\tau_a(670) = 0.40$ and $\tau_s = 0.20$ the error is slightly larger than 2 DC. It is interesting to note that the addition of the stratospheric aerosol actually improves the correction in some cases. For example, Figure 11(c) in Ref. 1 shows that near the scan center of Orbit 2381 the error is approximately −1.5 DC in the absence of a stratospheric aerosol, while our calculations (not presented) reveal that with the addition of a stratospheric aerosol with $\tau_s = 0.2$ this error is reduced to about −0.25 DC.

Finally, we note that the presence of the aerosol layer will decrease the scene contrast over what would be observed if it were all in the troposphere, because adjacency effects,[13] i.e., the atmospheric scattering of photons leaving the surface from pixels other than the one under examination, are a strong function of the vertical distribution of the aerosol. However, because of the small reflectance of the ocean and the generally low contrast of ocean scenes, this effect is believed to be unimportant for CZCS.[14]

In summary, the computations presented here suggest that the addition of an El Chichon-like aerosol layer in the stratosphere has very little effect on the basic CZCS atmospheric correction algorithm. The main influence of the additional stratospheric aerosol is to increase the total radiance exiting the atmosphere and thereby increase the probability that the sensor will saturate. In the absence of saturation the correction algorithm should perform as well as in the absence of the stratospheric layer.

This work received support from the National Aeronautics and Space Administration under grant NAGW-273 and contract NAS5-28798 and the Office of Naval Research under contract N00014-84-K-0451.

References

1. H. R. Gordon and D. J. Castano, "The Coastal Zone Color Scanner Atmospheric Correction Algorithm: Multiple Scattering Effects," Appl. Opt. **26**, 2111 (1987).
2. W. A. Hovis *et al.*, "Nimbus 7 Coastal Zone Color Scanner: System Description and Initial Imagery," Science **210**, 60 (1980).
3. H. R. Gordon, D. K. Clark, J. L. Mueller, and W. A. Hovis, "Phytoplankton Pigments Derived from the Nimbus-7 CZCS: Initial Comparisons with Surface Measurements," Science **210**, 63 (1980).
4. H. R. Gordon and A. Y. Morel, *Remote Assessment of Ocean Color for Interpretation of Satellite Visible Imagery: A Review* (Springer-Verlag, New York, 1983), 114 pp.
5. H. R. Gordon, D. K. Clark, J. W. Brown, O. B. Brown, R. H. Evans, and W. W. Broenkow, "Phytoplankton Pigment Concentrations in the Middle Atlantic Bight: Comparison Between Ship Determinations and Coastal Zone Color Scanner Estimates," Appl. Opt. **22**, 20 (1983).
6. W. R. Bandeen and R. S. Fraser, *Radiative Effects of the El Chichon Volcanic Eruption: Preliminary Results Concerning Remote Sensing*, Tech. Memo. 84959 (NASA, Goddard Space Flight Center, Greenbelt, MD, Dec. 1982).
7. G. W. Kattawar, "A Three-Parameter Analytic Phase Function for Multiple Scattering Calculations," J. Quant. Spectrosc. Radiat. Transfer **15**, 839 (1975).
8. H. Quenzel and M. Kastner, "Optical Properties of the Atmosphere: Calculated Variability and Application to Satellite Remote Sensing of Phytoplankton," Appl. Opt. **19**, 1338 (1980).

9. D. Deirmendjian, *Electromagnetic Scattering on Spherical Polydispersions* (Elsevier, New York, 1969), 290 pp.
10. J. DeLuisi, E. Dutton, B. Mendonca, and M. King, "Some Radiative Characteristics of the El Chichon Dust Cloud Deduced From Solar Radiation Measurements at Mauna Loa, Hawaii," EOS Trans. Am. Geophys. Union **63**, 897 (1982).
11. J. J. DeLuisi, E. G. Dutton, K. L. Coulson, T. E. DeFoor, and B. G. Mendonca, "On Some Radiative Features of the El Chichon Volcanic Stratospheric Dust Cloud and a Cloud of Unknown Origin Observed at Mauna Loa," J. Geophys. Res. **88**, 6769 (1983).
12. One scan line of the CZCS contains 1968 pixels corresponding to a rotation of the scan mirror through a total angle of 78.72°.
13. J. Otterman and R. S. Fraser, "Adjacency Effects on Imaging by Surface Reflection and Atmospheric Scattering: Cross Radiance to Zenith," Appl. Opt. **18**, 2852 (1979).
14. P. Y. Deschamps, M. Herman, J. Lenoble, D. Tanre, and M. Viollier, "Atmospheric Effects in Remote Sensing of Ground and Ocean Reflectances," in *Remote Sensing of Oceans and Atmospheres*, A. Deepak, Ed. (Academic, New York, 1980), pp. 115–147.

Appendix 6

H.R. Gordon and D.J. Castaño, Aerosol Analysis with the Coastal Zone Color Scanner: A Simple Method for Including Multiple Scattering Effects, *Applied Optics* **28** 1320–1326 (1989).

Aerosol analysis with the Coastal Zone Color Scanner: a simple method for including multiple scattering effects

Howard R. Gordon and Diego J. Castaño

For measurement of aerosols over the ocean, the total radiance L_t backscattered from the top of a stratified atmosphere which contains both stratospheric and tropospheric aerosols of various types has been computed. A similar computation is carried out for an aerosol-free atmosphere yielding the Rayleigh scattered radiance L_r. The difference $L_t - L_r$ is shown to be linearly related to the radiance L_{as}, which the aerosol would produce in the single scattering approximation. This greatly simplifies the application of aerosol models to aerosol analysis by satellite since adding to, or in some way changing, the aerosol model requires no additional multiple scattering computations. In fact, the only multiple computations required for aerosol analysis are those for determining L_r, which can be performed once and for all. The computations are explicitly applied to Band 4 of the CZCS, which, because of its high radiometric sensitivity and excellent calibration, is ideal for studying aerosols over the ocean. Specifically, the constant A in the relationship $L_{as} = A^{-1}(L_t - L_r)$ is given as a function of position along the scan for four typical orbital-solar position scenarios. The computations show that L_{as} can be retrieved from $L_t - L_r$ with an average error of no more than 5–7% except at the very edges of the scan.

I. Introduction

There is considerable interest in the global distribution of aerosols because of their role in climate and biogeochemical cycling.[1] Because our knowledge of aerosol concentrations in remote areas, particularly over the oceans, is very limited due to the paucity of measurements, there has been considerable effort directed toward estimating aerosol concentration and other properties using earth-orbiting satellites.[2-9]

As a result of the potential success promised by the earlier investigations, NASA included aerosol radiance as one of four standard output products from the Nimbus-7 Coastal Zone Color Scanner (CZCS).[10] The CZCS is a scanning radiometer which views the ocean in six coregistered spectral bands, five in the visible and near IR (443, 520, 550, 670, and 750 nm, labeled Bands 1, 2, 3, 4, and 5, respectively) and a thermal IR band (10.5–12.5 μm, Band 6). The sensor has an active scan of 78° centered on nadir and a field of view of 0.0495°, which from a nominal height of 955 km produces a ground resolution of 825 m at nadir. The satellite is in a sun-synchronous orbit with ascending node near local noon. The sensor is equipped with provision for tilting the scan plane ±20° from nadir in 2° increments along the satellite track to minimize the influence of direct sun glint. The purpose of the CZCS experiment was to provide estimates of the near surface concentration of phytoplankton pigments (the sum of the concentrations of chlorophyll *a* plus phaeophytin *a*) and total seston by measuring the spectral radiance backscattered out of the ocean.[11] The radiance backscattered from the atmosphere and sea surface (specular reflection) is typically at least an order of magnitude larger than the desired radiance scattered out of the water. Therefore, the CZCS has very high radiometric sensitivity. Over much of the world's ocean, the radiance backscattered out of the water in Band 4 is below the sensitivity limit of the sensor and can, therefore, be taken to be zero. Thus, this combination—a very sensitive and well-calibrated scanning radiometer viewing a target (the ocean) which is essentially black—makes the CZCS an ideal tool for oceanic aerosol studies. Also, we shall see that studying aerosols with CZCS imagery is relatively inexpensive from a computational standpoint since the required quantity is already generated at the first step in the atmospheric correction procedure.[12,13]

At present the scheme for analysis of satellite imagery for aerosols, as applied to NOAA's Advanced Very High Resolution Radiometer (AVHRR) by Griggs,[4] involves the computation of the expected radiance at the sensor as a function of the aerosol concentration for various viewing angles and solar zenith and azimuth angles. The computations are then placed in a look-up table, and aerosol concentration (optical thickness) is determined from the radiance measurements and sun-viewing geometry. This requires a model of the optical properties of the aerosol. The model was chosen to reproduce previous measurements made with

The authors are with University of Miami, Physics Department, Coral Gables, Florida 33124.

Received 15 July 1988.
0003-6935/89/071320-07$02.00/0.

Landsat 2 over the ocean at San Diego, CA.[2] In some cases it may be desirable to use a different model of the aerosol, e.g., the aerosol may be known to be principally composed of Saharan dust,[7] or the spectral variation of backscattering may suggest a particular size frequency distribution.[14] This, however, requires an extensive set of computations for each new aerosol model. In this paper we present a scheme for studying aerosols with CZCS which circumverts having to do any radiative transfer computations involving the properties of the aerosol.

II. Computation of the Aerosol Radiance

The atmospheric correction algorithm for CZCS imagery has been described in considerable detail previously[13,15] and is not discussed here. Limiting our interest to CZCS Band 4 at 670 nm and noting that the water is essentially black in this band,[16] i.e., the water-leaving radiance represents <1 digital count from the sensor, the single scattering approximation allows on to partition the total radiance at the sensor L_t into a component due to Rayleigh (r) scattering L_{rs} and a component due to aerosol a scattering L_{as}:

$$L_t = L_{rs} + L_{as}. \tag{1}$$

L_{rs} and L_{as} are given by

$$L_{xs} = \omega_x \tau_x F_0' p_x(\theta_-,\theta_+)/4\pi\cos\theta_v, \tag{2}$$

where

$$p_x(\theta_-,\theta_+) = P_x(\theta_{x-}) + [\rho(\theta) + \rho(\theta_v)]P_x(\theta_+),$$

$$\cos\theta_{x\pm} = \pm\cos\theta_0\cos\theta - \sin\theta_0\sin\theta\cos(\phi - \phi_0).$$

θ_0 and ϕ_0 are, respectively, the zenith and azimuth angles of a vector from the point on the sea surface under examination (pixel) to the sun, and likewise θ and ϕ are the zenith and azimuth angles of a vector from the pixel to the sensor. $\rho(\theta)$ is the Fresnel reflectance of the interface for an incident angle θ, $P_x(\theta)$ is the scattering phase function of component x ($x = r$ or a), ω_x is the single scattering albedo of x ($\omega_r = 1$), and τ_x is the optical thickness of x ($\tau_r = 0.044$). F_0' is the instantaneous extraterrestrial solar irradiance F_0 reduced by two trips through the ozone layer,

$$F_0' = F_0\exp[-\tau_{0z}(1/\cos\theta + 1/\cos\theta_0)],$$

where τ_{0z} is the ozone optical thickness. The term involving θ_- in Eq. (2) provides the contribution due to photons which are backscattered from the atmosphere without interacting with the sea surface. The term involving θ_+ accounts for those photons which are scattered in the atmosphere toward the sea surface (sky radiance) and then specularly reflected from the surface into the field of view of the sensor [$\rho(\theta)$ term] as well as photons which are first specularly reflected from the sea surface and then scattered by the atmosphere into the field of view of the sensor [$\rho(\theta_0)$ term]. Clearly, L_{as} is directly related to the optical properties of the aerosol through $\omega_a p_a(\theta,\theta_0)$ and the aerosol column concentration through τ_a. Given the optical properties of aerosol, its mass concentration can be estimated from L_{as}. Unfortunately, because of multiple scattering, Eq. (1) is incorrect and must be replaced by[13,17]

$$L_t = L_r + L_a + C^{R,P}, \tag{3}$$

where L_r and L_a are the multiple scattered counterparts of L_{rs} and L_{as}, respectively, and $C^{R,P}$ accounts for the interaction between Rayleigh and aerosol scattering. $C^{R,P}$ can be either positive or negative and in fact can even sign along a CZCS scan line.[13] There is no way to retrieve L_a from the other terms in Eq. (3) because $C^{R,P}$ is unknown. Furthermore, even if L_a could be determined, unlike L_{as}, it is not simply related to τ_a, ω_a, and $p_a(\theta,\theta_0)$. Since L_{as} has a simple interpretation it seems desirable to be able to extract it from L_t or at least to relate it to quantities extracted from L_t. In this paper we use radiative transfer theory to compute L_t and L_r ($L_r = L_t$ when $\tau_a = 0$) including all orders of multiple scattering in the scalar approximation, i.e., polarization is ignored. Then the difference $L_t - L_r$ is formed and compared with L_{as}. We will show that L_{as} can be retrieved from $L_t - L_r$ across the CZCS scan in a manner that is relatively insensitive to the (in general unknown) scattering phase function of the aerosols and thus derive a quantity L_{as} which can be directly related to aerosol models without having to pass through the transfer equation.

III. Atmospheric Model and Computations

The atmospheric model follows that used in Gordon and Castaño.[13] Briefly, it consists of a stratified atmosphere with the Rayleigh scattering coefficient b_r decreasing exponentially with altitude z according to a scale height H_r and the aerosol coefficient b_a also decreasing exponentially with altitude with a scale height H_a, i.e.,

$$b_x = b_x^0\exp(-z/H_x), \tag{4}$$

where x and r or a, and H_r and H_a are taken to be 9.2 and 1 km, respectively.[18] Assuming no absorption, the Rayleigh and aerosol optical thicknesses are given by

$$\tau_x = b_x^0 H_x.$$

Thus ~90% of the aerosol is confined to a layer of 2-km thickness near the sea surface with ~80% of the Rayleigh scattering molecules above the aerosol. This should be typical of oceanic aerosols generated at the sea surface and confined for the most part to the marine boundary layer[19] and naturally generated continental aerosols.[20] To account for the possibility of stratospheric aerosol layers, e.g., created by volcanic activity, a homogeneous aerosol layer of arbitrary optical thickness τ_s and phase function $P_s(\theta)$ is placed at the top of the atmosphere. The tropospheric and stratospheric aerosols scatter according to a two-term Henyey-Greenstein phase function

$$P_x(\theta) = \alpha f(\theta,g_1) + (1-\alpha)f(\theta,g_2), \tag{5}$$

where

$$f(\theta,g) = \frac{(1-g^2)}{(1+g^2-2g\cos\theta)^{3/2}}, \quad (6)$$

and $x = a$ or s. Three aerosol models are used in the computations. The first approximates marine aerosol phase functions given by Quenzel and Kastner.[21] It has been used by Sturm[22] for atmospheric correction of CZCS imagery and for ocean color sensitivity analyses. The parameters in Eqs. (5) and (6) are $\alpha = 0.983$, $g_1 = 0.82$, and $g_2 = -0.55$. The second is a two-term Henyey-Greenstein approximation developed by Kattawar[23] to the Deirmendjian Haze L distribution[24] with a refractive index of 1.55 and is used to represent continental-type aerosols. Its parameters are $\alpha = 0.9618$, $g_1 = 0.7310$, and $g_2 = -0.7598$. The third is a two term Henyey-Greenstein approximation to the Deirmendjian Haze C distribution with a slope parameters $\nu = 3.5$ and a refractive index of 1.50. Its parameters are $\alpha = 0.9618$, $g_1 = 0.7130$, and $g_2 = -0.50$. These three phase functions are shown in Fig. 1, where the Haze L case has the largest backscattering ($\Theta = 180°$), Haze C the intermediate backscattering, and the marine aerosol model has the lowest backscattering. In most cases the aerosol is assumed to be nonabsorbing; however, a few cases with $\omega_a = 0.9$ have also been examined.

The ocean is assumed to be flat and totally absorbing; i.e., all photons tha penetrate the surface are absorbed. The transport equation is solved by the method of successive orders of scattering (see, e.g., Ref. 25), and the results are then transformed into CZCS scan coordinates. The computations for a given atmosphere, i.e., a given set P_a, P_s, τ_a, τ_s, and τ_r, are first carried out to compute L_t. Then τ_a and τ_s are set to zero, and the transport equation is again solved to determine L_r. In this manner $L_t - L_r$ can be found for a given atmosphere–orbital geometry scenario.

A total of four orbital scenarios is examined, two with no sensor tilt and two with a forward tilt of 20°. These scenes are listed by orbit number in Table I. Orbit 130 corresponds to fall in the Gulf of Mexico, while Orbit 2381 corresponds to spring–fall viewing near the Arctic Circle (Iceland). These are typical of orbits for which the sensor is operated in the nontilted mode. Such operation is marginal for Orbit 130, which shows some evidence of sun glitter near the center of the scan in the southern portion of the Gulf. The other two orbits 2217 and 3226 correspond to viewing in the spring and summer in the Middle Atlantic Bight, where the low solar zenith angle necessitates tilting the scan forward to avoid the sun glitter. The geometry of Orbit 3226 was similar to that which existed for the CZCS validation study presented by Gordon *et al.*[15] The variation in the local solar zenith angle across the scan (column 6 in Table I) is surprisingly small, considering that the scan swath is ~1600 km on the ground in the untilted mode and 2400 km with a tilt of 20°. In contrast for the tilted scan, θ_0 at the western edge is significantly larger than for the rest of the scan. The nominal value of θ_0 used in the computations for each orbit is given in column 7. The local viewing angle θ

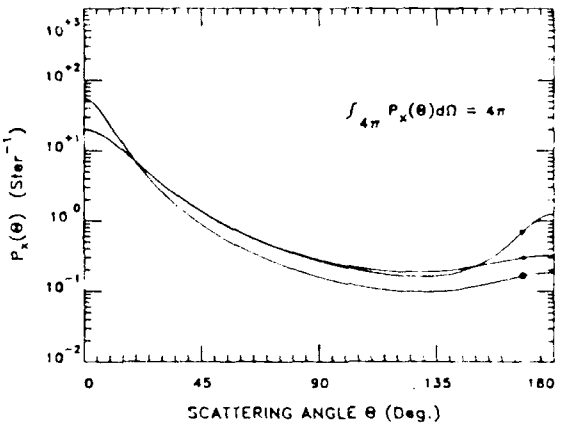

Fig. 1. Aerosol phase functions used in the study: ▼, Haze L; ▲, Haze C; ●, marine aerosol model.

varies between 0° at the center of the scan and ~66° at the edges of the scan in the untilted cases and between 23.16 and 61.01° in the cases with a 20° tilt. Thus in the tilted mode the sensor views the ocean through an air mass that changes by nearly a factor of 2 over the scan.

IV. Results

First, consider cases for which there is no aerosol in the stratosphere, i.e., $\tau_s = 0$. We computed $L_t - L_r$ and L_{as} for the three aerosol phase functions in Fig. 1, the orbital geometries listed in Table I, and four aerosol optical thicknesses, $\tau_a = 0.05, 0.20, 0.40$, and 0.60. A τ_a of 0.20 is somewhat more turbid than the V23 (23-km visibility) model used by Viollier *et al.*,[17,26] while $\tau_a = 0.60$ is approximately the same value used in their V5 (5-km visibility) model. Since our Haze C phase function corresponds to that used by Deschamps *et al.*,[17] our results for that phase function should span the range of their computation, i.e., surface visibilities down to ~5 km.

In our preliminary analysis of the resulting computations we discovered that orbits with similar sensor tilts produced similar relationships between $L_t - L_r$ and L_{as}. Thus in our presentation we combine Orbits 130 and 2381 with a tilt of zero and Orbits 2217 and 3226 with a tilt of 20°. Figures 2 and 3 provide L_{as} as a function of $L_t - L_r$ at the center of the CZCS scan for the untilted and tilted orbitals, respectively. The units for the radiances are CZCS Gain 1 digital counts

Table I. Scenes Examined in the Present Study[a]

Orbit	Tilt	Lat.[b]	Long.[b]	Day/Yr	θ_0	θ_0 (Nominal)
130	0	28	−86.1	306/1978	42.4–43.9	43.0
2381	0	66	−22.9	104/1979	58.0–58.8	58.3
2217	20	38	−62.2	92/1979	37.7–39.3[c]	39.0
3226	20	38	−64.4	165/1979	19.1–22.7[d]	22.3

[a] All angles are in degrees.
[b] Lat. and long. refer to the suborbital latitude and longitude at nadir.
[c] 40.9 at the western edge of the scan.
[d] 25.4 at the western edge of the scan.

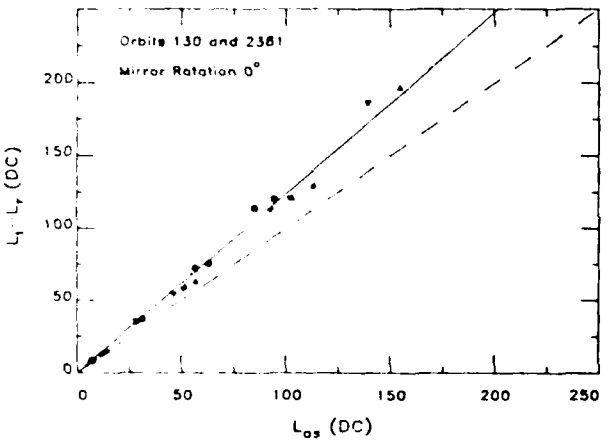

Fig. 2. L_{as} as a function of $L_t - L_r$ at the center of the scan for the nontilted orbits with the aerosol restricted to the troposphere. ●, ▼, and ▲ refer, respectively, to the marine aerosol, Haze L, and Haze C.

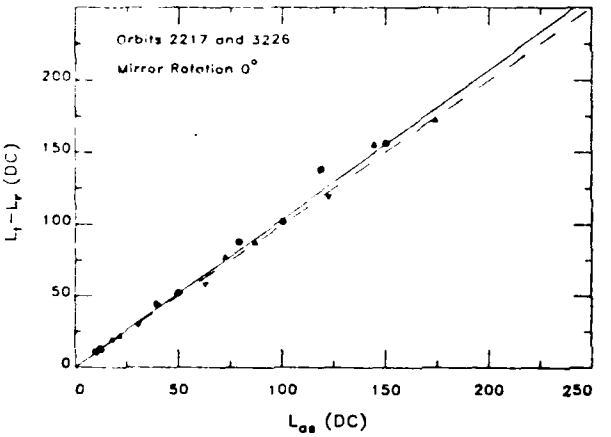

Fig. 3. L_{as} as a function of $L_t - L_r$ at the center of the scan for the tilted orbits (tilt = 20°) with the aerosol restricted to the troposphere. ●, ▼, and ▲ refer, respectively, to the marine aerosol, Haze L, and Haze C.

(DC), where 1 DC = 0.01103 mW/cm^2 μm sr. Recalling that the output signal of the CZCS is 8-bit digitized aboard the spacecraft, the maximum sensor output is 255 DC. For the geometries shown, $L_r \approx 50 \rightarrow 75$ DC, so $L_t - L_r$ must be less than ~175–200 DC to prevent sensor saturation. Computations for which $L_t \geq 255$ DC have been omitted from the analysis, since, although correct, they do not correspond to observable situations for the present CZCS. The most striking feature of Figs. 2 and 3 is the strong linearity between $L_t - L_r$ and L_{as} regardless of the scattering phase function chosen to represent the aerosols or the solar zenith angle associated with the viewing situation. In Figs. 4 and 5 a similar presentation is made for a scan mirror position so that the sensor is viewing a ground position 246 pixels from the eastern edge of the scan.[27] Note that the linearity of the $L_r - L_t$ vs L_{as} relationship still appears valid. However, the slope is larger than at the scan center. Also, for the tilted orbits (Figs. 3 and

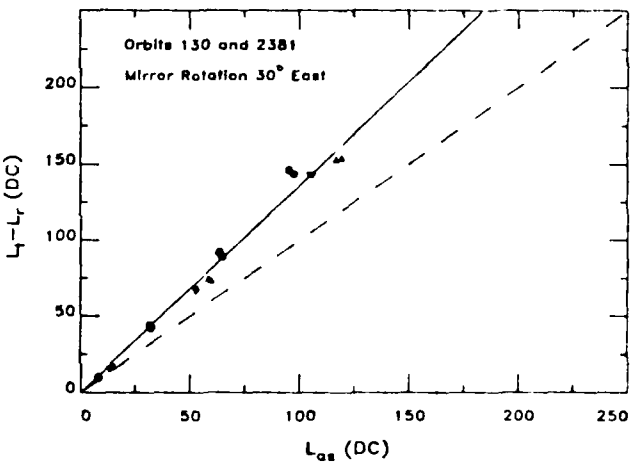

Fig. 4. L_{as} as a function of $L_t - L_r$ at a position located 246 pixels from the eastern edge of the scan (a scan mirror rotation angle of 30°). The sensor is in the untilted mode, and the aerosol is restricted to the troposphere. ●, ▼, and ▲ refer, respectively, to the marine aerosol, Haze L, and Haze C.

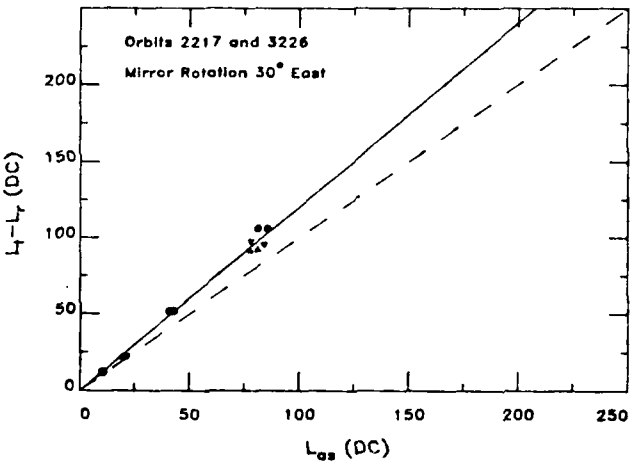

Fig. 5. L_{as} as a function of $L_t - L_r$ at a position located 246 pixels from the eastern edge of the scan (a scan mirror rotation angle of 30°). The sensor is in the tilted mode (tilt = 20°), and the aerosol is restricted to the troposphere. ●, ▼, and ▲ refer, respectively, to the marine aerosol, Haze L, and Haze C.

5) the $L_t - L_r$ values appear to be smaller near the eastern edge than at the center of the scan. This illusion is caused by the fact that three points with $L_{as} > 100$ DC in Fig. 3 have caused the sensor to saturate at the edge and are, therefore, not plotted on the figure. This saturation is due to an increase in L_r from ~75 DC at the center to ~120 DC at the position in question near the eastern edge of the scan. For the untilted orbits (Figs. 2 and 4) L_r is a much weaker function of position along the scan, and the above effect does not occur with the values of τ_a used here ($\tau_a \leq 0.60$). For the tilted orbits the Haze L phase function ▼ with its strong scattering near 180° saturates the instrument with τ_a as low as 0.40.

One normally expects multiple scattering to increase L_a over the corresponding L_{as}; i.e., if multiple scatter-

ing computations were carried out for the aerosols alone ($\tau_r = 0$), we would expect $L_a > L_{as}$. This is clearly the case in Figs. 2, 4, and 5; however, in Fig. 3, the scan center for the tilted orbits, $L_t - L_r \approx L_{as}$. This is the result of the $C^{R,P}$ term in Eq. (3). Gordon and Castaño[13] have computed $C^{R,P}$ at 443 nm (Band 1) across the CZCS scan for Orbit 2217 for all three aerosol phase functions and $\tau_a = 0.05$ and 0.20. They find that $C^{R,P} > 0$ at all scan angles for the marine aerosol model, $C^{R,P}$ is slightly negative near the scan center and positive elsewhere for the Haze C model, and $C^{R,P}$ is large and negative near the scan center and slightly positive near the scan edges for the Haze L model. $C^{R,P}$ for Band 4 will in general be less than for Band 1. However, they are qualitatively similar so we can expect the same, albeit weaker, behavior in Band 4. Equation (3) shows that when $C^{R,P}$ is negative, it has the tendency to cancel the increase in L_a over L_{as} resulting from multiple scattering. Thus in Fig. 3 the marine aerosol ● and the Haze C ▲ points tend to fall above the line $L_t - L_r = L_{as}$, while the Haze L points ▼ tend to fall below the line. Since $C^{R,P}$ is positive for all three phase functions when the mirror rotation angle is 30° east, this anomalous behavior is not seen in Fig. 5. It is interesting to note that Orbits 130 (tilt = 0°) and 2217 (tilt = 20°) have nearly the same solar zenith angle (43 and 39°, respectively) across the scan, but the dependence of L_{as} on $L_t - L_r$ is significantly different. This is also a manifestation of the $C^{R,P}$ effect. Thus the L_{as} vs $L_t - L_r$ relationship is seen to depend on the sensor tilt as well as the solar zenith angle and the position in the scan.

To see if the linearity of the $L_t - L_r$ vs L_{as} is affected by the addition of stratospheric aerosols, e.g., from a volcano such as El Chichón, several sets of computations have been carried out for cases with $\tau_s \neq 0$. Specifically, the marine aerosol model was used for the tropospheric phase function and two values of τ_a were used—0.20 and 0.40. Two models were used for the stratospheric aerosol: the marine aerosol phase function and the Haze L phase function. The values used for τ_s were 0.10 and 0.20. This yields twenty computations of $L_t - L_r$ for each orbit or a total of forty computations for each sensor tilt. The total aerosol optical thickness of the atmosphere is now $\tau_a + \tau_s$. L_{as} is computed by summing the stratospheric and tropospheric contributions in Eq. (2), i.e.,

$$L_{as} = [\omega_a \tau_a P_a(\theta,\theta_0) + \omega_s \tau_s P_s(\theta,\theta_0)] \frac{F_0'}{4\pi \cos\theta}. \quad (7)$$

As before both aerosols are taken to be nonabsorbing. The results of these computations are presented in Figs. 6–9, which are directly comparable with Figs. 2–5 for $\tau_s = 0$. In Figs. 6–9 the symbol ♦ refers to cases where $\tau_s \neq 0$; however, for clarity the two stratospheric aerosol phase functions have not been differentiated on the figures. Also, to try to examine the effect of particle absorption on the $L_t - L_r$ vs L_{as} relationships, three computations for a mildly absorbing ($\omega_a = 0.90$) marine aerosol in the troposphere ($\tau_s = 0$) were carried out for Orbit 2217 (tilt = 20°). These are indicated by the symbol + on the appropriate figures. Comparison of the corresponding figures from the two sets (2–5 and 6–9) show that the $L_t - L_r$ vs L_{as} relationship is nearly unaltered by the presence of stratospheric or mildly absorbing tropospheric aerosols.

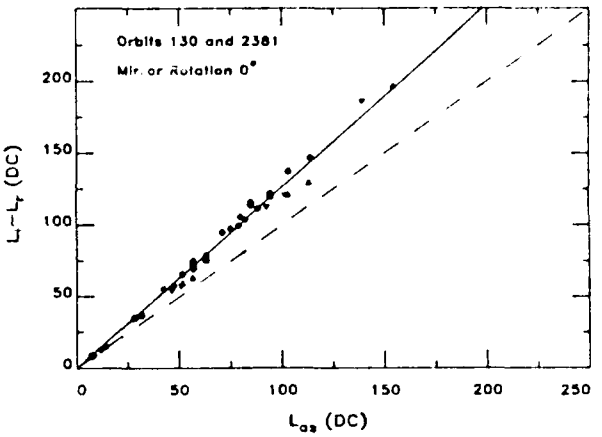

Fig. 6. L_{as} as a function of $L_t - L_r$ at the center of the scan for the nontilted orbits. Aerosols are located in both the troposphere and the stratosphere. ●, ▼, and ▲ refer, respectively, to the marine aerosol, Haze L, and Haze C, restricted to the troposphere. ♦ refers to cases with aerosols in both the troposphere and the stratosphere, i.e., $\tau_s \neq 0$.

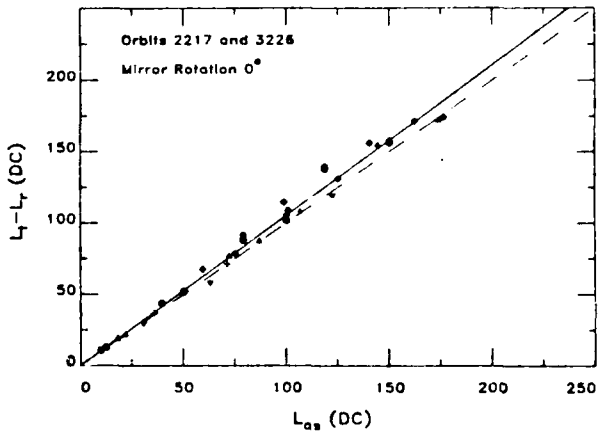

Fig. 7. L_{as} as a function of $L_t - L_r$ at the center of the scan for the tilted orbits (tilt = 20°). Aerosols are located in both the troposphere and stratosphere. ●, ▼, and ▲ refer, respectively, to the marine aerosol, Haze L, and Haze C, restricted to the troposphere. ♦ refers to cases with aerosols in both the troposphere and stratosphere, i.e., $\tau_s \neq 0$, and + refers to cases for which the tropospheric aerosol has $\omega_0 = 0.9$.

We have generated $L_t - L_r$ and L_{as} for the tropospheric–stratospheric aerosol combinations in Figs. 6–9 at nine equally spaced points along the CZCS scan. These correspond to mirror rotation angles starting 40° west of the subsatellite track (−40°) and continuing every 10° to 40° east of the subsatellite track (+40°). At each scan angle we fit L_{as} by least squares to the linear relationship

$$AL_{as} = (L_t - L_r) \quad (8)$$

and determine A. The corresponding values of A, the

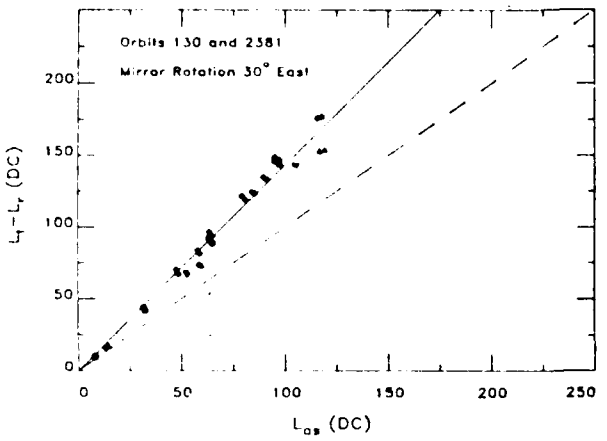

Fig. 8. L_{as} as a function of $L_t - L_r$ at a position located 246 pixels from the eastern edge of the scan (a scan mirror rotation angle of 30°). The sensor is in the untilted mode. Aerosols are located in both the troposphere and stratosphere. ●, ▼, and ▲ refer, respectively, to the marine aerosol, Haze L, and Haze C restricted to the troposphere. ♦ refers to cases with aerosols in both the troposphere and stratosphere, i.e., $\tau_s \neq 0$.

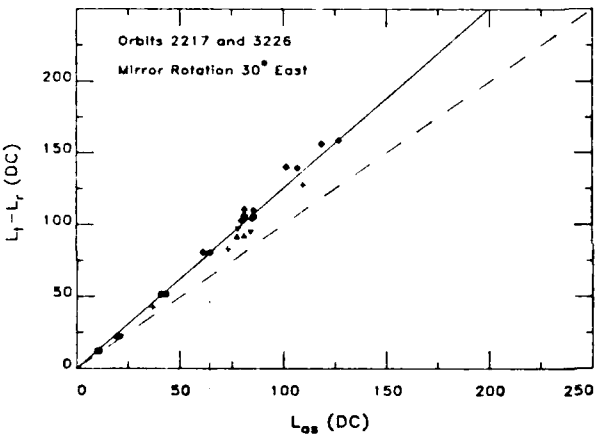

Fig. 9. L_{as} as a function of $L_t - L_r$ at a position located 246 pixels from the eastern edge of the scan (a scan mirror rotation angle of 30°). The sensor is in the tilted mode (tilt = 20°). Aerosols are located in both the troposphere and stratosphere. ●, ▼, and ▲ refer, respectively, to the marine aerosol, Haze L, and Haze C restricted to the troposphere. ♦ refers to cases with aerosols in both the troposphere and stratosphere, i.e., $\tau_s \neq 0$, and + refers to cases for which the tropospheric aerosol has $\omega_0 = 0.9$.

number of data points used in the determination of A, and the average % error in the computed L_{as} (given $L_t - L_r$), ΔL_{as}, defined by

$$\Delta L_{as} = \left| \frac{L_{as}(\text{true}) - L_{as}(\text{fit})}{L_{as}(\text{true})} \right| \times 100\%,$$

are provided in Table II. It is seen that Eq. (8) can provide L_{as} from $L_t - L_r$ to within ~5–8% except at the very edges of the scan. [Note that in the case of the tilted orbits the apparent improvement in the fit at angles of ±40° over that for ±30° is due to the fact that considerably fewer points have been used in the fit, because points were dropped due to saturation ($L_t >$ 255 DC) and do not represent a truly improved linear relationship.] Thus, in Eq. (2) the combination ($\omega_a \tau_a p_a + \omega_s \tau_s p_s$) can be estimated along the CZCS scan line from the Rayleigh removed radiance $L_t - L_r$. $L_t - L_r$ is computed in the first step of the atmospheric correction procedure and is one of the four standard derived products produced from CZCS imagery by NASA.[10] The combination ($\omega_a \tau_a p_a + \omega_s \tau_s p_s$) is generally all that can be determined directly from CZCS. To proceed further other information or an aerosol model is required.[28] For example, one may know from lidar observations that $\tau_s \approx 0$. Then, assuming the tropospheric aerosol is nonabsorbing, a model of the aerosol type, e.g., marine, Haze L, Haze C, yields the optical thickness τ_a at each pixel. It is important to note that the various aerosol models can be applied directly to a derived quantity ($\omega_a \tau_a p_a + \omega_s \tau_s p_s$) without the necessity for further radiative transfer computations. Thus the analysis of CZCS imagery for aerosol concentration etc. can be carried out completely in the single scattering approximation, even in an atmosphere with a total optical thickness as high as 0.644 (the largest value used in our computations). This considerably simplifies the analysis.

In search of a simple straightforward way of extending these results to other sensor tilts and sun angles, we tried to relate A to the phase angle of the observation, i.e., θ_- in Eq. (2). The results showed that a coarse, marginally useful, relationship exists between A and θ_-: $A = 1 + 0.00733\theta_-$, where θ_- is in degrees. This relationship predicted values of A for an intermediate tilt (12°) with a maximum error of ~7%; however, for a tilt angle of 20° and a fixed phase angle the error it induced in A could be as much as −7 and +10% on the eastern and western sides of the scan, respectively.

V. Summary

For measurement of aerosls over the ocean, we computed the total radiance L_t backscattered from the top of a stratified atmosphere which contains both stratospheric and tropospheric aerosols of various types. A similar computation is carried out for an aerosol-free, i.e., purely Rayleigh scattering, atmosphere yielding the Rayleigh radiance L_R. The difference $L_t - L_R$ is then shown to be linearly related to the radiance L_{as},

Table II. Linear Regression Estimates of the Coefficient A in Eq. (8) as a Function of the Mirror Rotation Angle α. ΔL_{as} is the Average Error in L_{as} in Percent and N is the Number of Points Used in the Individual Regressions

α	Tilt = 0°			Tilt = 20°		
(deg)	A	ΔL_{as}	N	A	ΔL_{as}	N
−40	1.511	7.2	31	1.331	6.3	18
−30	1.432	7.2	36	1.362	7.2	31
−20	1.358	6.9	36	1.218	6.1	37
−10	1.307	6.8	37	1.105	5.1	34
0	1.262	5.7	38	1.053	4.5	32
10	1.297	6.8	37	1.074	4.6	30
20	1.348	6.9	36	1.139	5.5	32
30	1.429	7.4	36	1.253	6.0	27
40	1.505	7.4	31	1.291	5.7	17

which the aerosol would produce in the single scattering approximation. This greatly simplifies the application of aerosol models to aerosol analysis by satellite since adding to, or in some way changing, the aerosol model requires no additional multiple scattering computations. In fact, the only multiple scattering computations required for aerosol analysis are those for determining L_r, which can be performed once and for all.[29]

The computations have been explicitly applied to Band 4 of the CZCS, which, because of its high radiometric sensitivity and excellent calibration, is ideal for studying aerosols over the ocean. Specifically, the constant A in the relationship $L_{as} = A^{-1}(L_t - L_r)$ is given as a function of position along the scan for four typical orbital–solar position scenarios. For the two values of the sensor tilt angle examined (comprising ~60% of the imagery acquired by CZCS during its first year in operation), L_{as} can be retrieved from $L_t - L_r$ with an average error of no more than 5–7% except at the edges of the scan.

This work received support from the National Aeronautics and Space Administration under grant NAGW-273 and contract NAS5-28798 and the Office of Naval Research under contract N00014-84-K-0451.

References

1. "Earth Observing System: Science and Mission Requirements Working Group Report," NASA Tech. Memo. 86129 (Aug. 1984).
2. M. Griggs, "Measurements of the Aerosol Optical Thickness Over Water Using ERTS-1 Data," J. Air Pollut. Control Assoc. **25,** 622 (1975).
3. Y. Mekler, H. Quenzel, G. Ohring, and I. Marcus, "Relative Atmospheric Aerosol Content from Erts Observations," J. Geophys. Res. **82,** 967 (1977).
4. M. Griggs, "AVHRR Measurements of Atmospheric Aerosols Over Oceans," NOAA National Environmental Satellite Service, Final Report contract MO-A01-78-00-4092 (Nov. 1981).
5. M. Griggs, "Satellite Measurements of Tropospheric Aerosols," NASA Contract. Rep. 3459 (Aug. 1981).
6. M. Griggs, "AVHRR Aerosol Ground Truth Experiment," NOAA National Environmental Satellite Service, Final Report contract NA-83-SAC-00106 (Jan. 1984).
7. R. S. Fraser, "Satellite Measurement of Mass of Sahara Dust in the Atmosphere," Appl. Opt. **15,** 2471 (1976).
8. P. Koepke and H. Quenzel, "Turbidity of the Atmosphere Determined From Satellite: Calculation of Optimum Viewing Geometry," J. Geophys. Res. **84,** 7847 (1979).
9. P. Koepke and H. Quenzel, "Turbidity of the Atmosphere Determined From Satellite: Calculation of Optimum Wavelength," J. Geophys. Res. **86,** 9801 (1981).
10. W. A. Hovis, "The Nimbus-7 Coastal Zone Color Scanner (CZCS) Program," in *Oceanography from Space*, J. R. F. Gower, Ed. (Plenum, New York, 1981) pp. 213–225.
11. H. R. Gordon and A. Y. Morel, *Remote Assessment of Ocean Color for Interpretation of Satellite Visible Imagery: A Review* (Springer-Verlag, New York, 1983).
12. H. R. Gordon, "Removal of Atmospheric Effects from Satellite Imagery of the Oceans," Appl. Opt. **17,** 1631 (1978).
13. H. R. Gordon and D. J. Castaño, "The Coastal Zone Color Scanner Atmospheric Correction Algorithm: Multiple Scattering Effects," Appl. Opt. **26,** 2111 (1987).
14. H. R. Gordon, "Some Studies of Atmospheric Optical Variability in Relation to CZCS Atmospheric Correction," NOAA National Environmental Satellite and Data Information Service, Final Report Contract NA-79-SAC-00714 (Feb. 1984).
15. H. R. Gordon, D. K. Clark, J. W. Brown, O. B. Brown, R. H. Evans, and W. W. Broenkow, "Phytoplankton Pigment Concentrations in the Middle Atlantic Bight: Comparison between Ship Determinations and Coastal Zone Color Scanner Estimates," Appl. Opt. **22,** 20 (1983).
16. H. R. Gordon and D. K. Clark, "Clear Water Radiances for Atmospheric Correction of Coastal Zone Color Scanner Imagery," Appl. Opt. **20,** 4175 (1981).
17. P. Y. Deschamps, M. Herman, and D. Tanre, "Modeling of the Atmospheric Effects and its Application to the Remote Sensing of Ocean Color," Appl. Opt. **22,** 3751 (1983).
18. L. Elterman, "Vertical Attenuation Model with Eight Surface Meteorological Ranges 2 to 13 Kilometers," AFCRL, Bedford, MA, Report AFCRL-70-0200 (Mar. 1970).
19. K. L. Davidson and C. W. Fairall, "Optical Properties of the Marine Atmospheric Boundary Layer: Aerosol Profiles," Proc. Soc. Photo-Opt. Instrum. Eng. **637,** 18 (1986).
20. K. Bullrich, "Scattered Radiation in the Atmosphere and the Natural Aerosol," in *Advances in Geophysics*, H. E. Landsberg and J. V. Mieghem, Eds. (Academic, New York, 1964), pp. 99–260.
21. H. Quenzel and M. Kastner, "Optical Properties of the Atmosphere: Calculated Variability and Application to Satellite Remote Sensing of Phytoplankton," Appl. Opt. **19,** 1338 (1980).
22. B. Sturm, "Ocean Color Remote Sensing and the Retrieval of Surface Chlorophyll in Coastal Waters Using the Nimbus-7 CZCS," in *Oceanography from Space*, J. F. R. Gower, Ed. (Plenum, New York, 1981), pp. 267–280.
23. G. W. Kattawar, "A Three-Parameter Analytic Phase Function for Multiple Scattering Calculations," J. Quant. Spectrosc. Radiat. Transfer **15,** 839 (1975).
24. D. Deirmendjian, *Electromagnetic Scattering on Spherical Polydispersions* (Elsevier, New York, 1969).
25. H. C. van de Hulst, *Multiple Light Scattering* (Academic, New York, 1980).
26. M. Viollier, D. Tanre, and P. Y. Deschamps, "An Algorithm for Remote Sensing of Water Color from Space," Boundary Layer Meteorol. **18,** 247 (1980).
27. One scan line of the CZCS contains 1968 pixels corresponding to a rotation of the scan mirror through a total angle of 78.72°. However, while the instrument field of view is 0.0495°, the pixel sample rate is 1 per 0.04°, so there is an ~25% overlap between adjacent pixels. Pixel 246 from the eastern edge of the scan corresponds to a position where the scan mirror has been rotated 30° from the subsatellite track toward the east.
28. However, over the open ocean, where the pigment concentration is sufficiently low, the water-leaving radiance (known to be <1 DC in Band 4) is known in Bands 2 and 3.[16] This may allow derivation of the above mentioned combination as a function of wavelength which could provide a means of proceeding with a reduced dependence on models or provide guidance in choosing models.
29. H. R. Gordon, J. W. Brown, and R. H. Evans, "Exact Rayleigh Scattering Calculations for use with the Nimbus-7 Coastal Zone Color Scanner," Appl. Opt. **27.** 862 (1988).